Chapter 6

Triple Hybrids

Abstract:

In this chapter we explore a new approach within the field of hybrid materials, namely, HCF-doped polypyrrole or polyaniline inserted in turn into layered V_2O_5 . That is, a novel kind of hybrid we will call I-O-I materials. The synthetic approach was based on our earlier work on the PAni/V_2O_5, PAni/HCF and PPy/HCF systems. The materials obtained were studied by means of FTIR, XRD, TGA, elemental analyses, and ICP and their electrochemical properties as insertion cathodes in rechargeable Li cells were also explored. Although their performance in the final devices fell short of our expectations, in one aspect or another, we have been able to prepare and characterize some of these hybrids successfully and present in this chapter our results.

6.1. INTRODUCTION

In chapter 5 we mentioned how the PAni/V_2O_5 (IO) hybrid system lost its initial high specific charge (280 Ah/Kg, with a C/7.5 rate) through repeated charge-discharge cycles, resulting in a stabilized value of 50-60 Ah/Kg after 100 cycles. This low specific charge value was obtained for all PAni/V_2O_5 samples, independently of their synthesis conditions, and resulting properties.

On the other hand, earlier work carried out in our group concerning the PAni/HCF (OI) hybrid system (HCF, hexacyanoferrate), showed that a stable good specific charge value was obtained for this molecular hybrid, when used as cathode material in lithium rechargeable cells (137 Ah/kg at C/15, 110 Ah/kg at C/5 charge-discharge rates) [1]. In contrast, the PPy/HCF hybrid system was also studied, but resulted only in moderated specific charge values, due to the formation of oxygenated groups (carbonyl, hydroxyl) in the polypyrrole chain [2,3].

In this context we considered the possibility to prepare triple hybrids in which all the components would be electroactive, thus aiming at higher specific charges, hoping to get reasonable cycling by achieving the doping of the conducting polymer with the molecular HCF species.

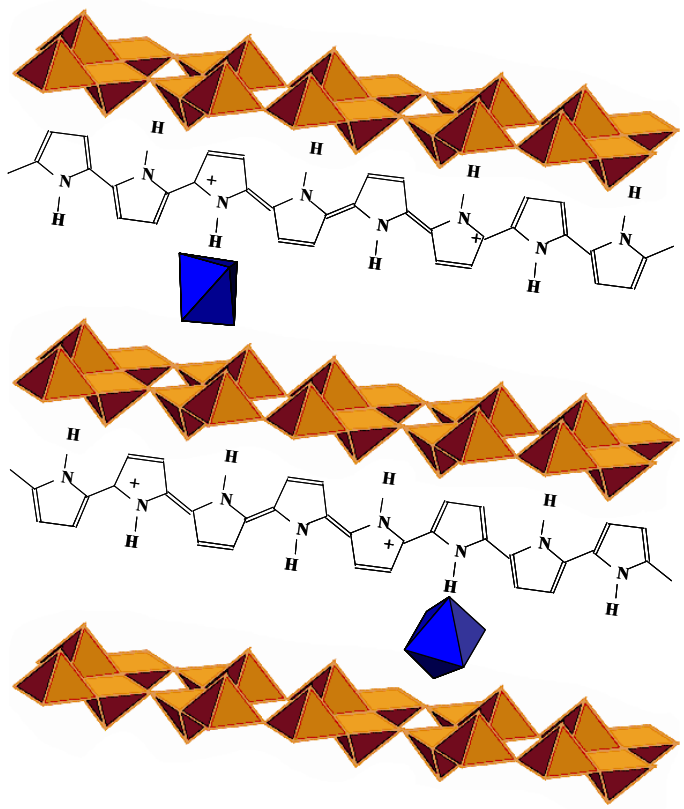

Figure 6.1.- Schematic structure of the desired triple hybrid, using polypyrrole as a conducting polymer.

This triple hybrid concept is based on the doping of the conducting polymer with $[Fe(CN)_6]^{3-}$ hexacyanoferrate (HCF), followed by its intercalation between the layers of V_2O_5. In figure 6.1 we show a schematic view of the desired structure for this triple hybrid concept. In relation to the classification of hybrid materials

proposed in chapter 1, these triple hybrids would be of the OI type considering the HCF-COP moiety, but IO considering the COP-V_2O_5 interaction, thus resulting in what we could call an IOI new class of hybrid.

It was interesting to realize that this idea was also conceived and followed by other groups in different ways. Thus, simultaneously to our work, described below, the synthesis of similar triple hybrids was attempted through different procedures. In one of them a surfactant was inserted between the layers of V_2O_5, then, according to the authors, HCF was immobilized on the surface of the hybrid instead of being intercalated [4]. This work was essentially synthetic and only cyclic voltammetry was reported. In the other report double doping of polyaniline with phosphomolybdic acid, and m-cresol was reported[5]. In contrast, our triple hybrid approach aimed from the beginning at the integration of all three electroactive species in a single bulk material.

In this chapter we will describe our syntheses of triple hybrid materials with polyaniline or polypyrrole, doped with HCF and its intercalation between the layers of V_2O_5. These synthesis were generally carried out in one-pot reactions and the resulting materials characterized by FTIR, XRD, TGA, elemental analyses, ICP, and finally tested in compact rechargeable lithium cells.

6.2. PPy/HCF/V_2O_5 TRIPLE HYBRID.

The synthesis approach used was based in a one-pot reaction leading to the simultaneous formation of the the organic (PPy) and inorganic (V_2O_5) polymers in the presence of acidic HCF.

Despite the fact that PPy-HCF hybrids were not as good as PAni-HCF, we considered the synthesis of PPy triple hybrids of interest from a basic point of view and also from an application point of view. From a basic point of view it would be of great importance to obtain the desired structure by controlling the synthesis parameters for comparative reasons, and from an application point of view, it might be interesting to see if we can accomplish the synergic effect on their performance in lithium rechargeable cells.

6.2.1. Synthesis

For PPy/HCF/V_2O_5 hybrids we carried out a series of synthesis according to the following procedure. We used in all cases a solution of 0.25 ml pyrrole risen to 50 ml with deionized water. The acid ferricyanide derivative was freshly prepared by a metathesis reaction between potassium ferricyanide ($K_3Fe(CN)_6$) solution (40 ml) and $HClO_4$ (see table VI.I for the used amounts), with precipitation of $KClO_4$ which was filtered-off, resulting in the acidic $H_3[FeCN)_6]$ solution. To this acidic HCF solution, water was added to complete a volume of 50 ml. The V_2O_5 gel was prepared as described in section 4.2 and aged for three moths previously to their use. Immediately prior to the syntheses, the gels were titrated to determine the precise amount of V(V). Then, the desired amounts of V_2O_5 were diluted with deionized water to complete a 50 ml solution. The only parameter that we varied was the molar ratio in each of the four samples synthesized (as indicated in table VI.I). The reaction took place in an ice bath for a 30 minute period, using magnetic stirring at 500 rpm, adding in 3 minutes the V_2O_5 solution to the HCF solution, and then the pyrrole solution in another 3 minutes. After the 30 minutes of synthesis, the solids formed were filtered off and separated from the yellow-greenish filtrate, washed with deionized water until no coloration came through, then collected and dried under vacuum for three days.

Table VI.I.- Molar ratio used in the synthesis of each polypyrrole triple Hybrid samples.

Sample	molar ratio (Py:V:Fe)	$K_3[Fe(CN)_6]$ + $HClO_4$	excess reagent
PyVFe1	(0.5: 1: 1)	2.37 g + 1 ml	Double amount of inorganics
PyVFe2	(0.5: 0.5: 0.5)	1.18 g + 0.5 ml	Normal
PyVFe3	(0.5: 0.5: 1)	2.37 g + 1 ml	HCF excess
PyVFe4	(0.5: 1: 0.5)	1.18 g + 0.5 ml	V_2O_5 excess

6.2.2. Basic Characterization

We carried out first FTIR analyses in order to detect characteristic vibrational modes from each of the components of the triple hybrid (PPy, V_2O_5, and HCF). In figure 6.2 we show the spectra for each of the polypyrrole triple hybrid samples indicated in table VI.I. We can detect the vibrational modes of V_2O_5 marked with red circles; the most characteristic mode of HCF marked with a diamond; and the ones belonging to the formation of polypyrrole with arrows. Bands from V_2O_5 are present at 515 cm^{-1} and 760 cm^{-1} for V-O-V vibrational modes, and at 973 cm^{-1} for V=O stretchings. The only band clearly assigned to HCF appears at 2079 cm^{-1}, and is due to the C≡N stretching. The polypyrrole bands are approximately at 1053 cm^{-1} (inner C-H plane and N-H), at 1179 cm^{-1} (ring vibration), at 1382 cm^{-1} (ring vibration with C=C/C-C and C-N contributions), and at 1555 cm^{-1} (C=C/C-C modes). We can observe also a very weak band around 1700 cm^{-1} in some samples which can be associated to C=O formation, indicating some overoxidation of polypyrrole.

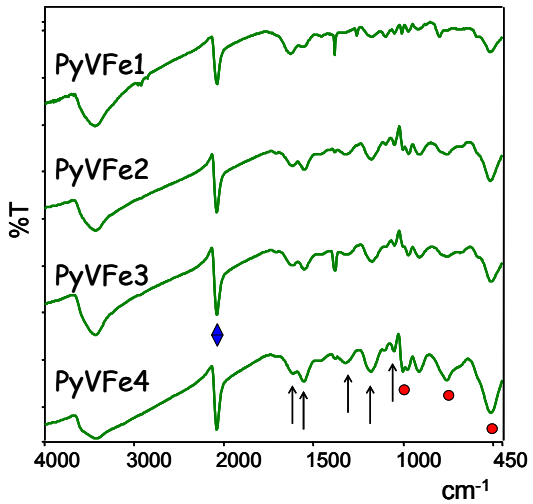

Figure 6.2.- FTIR spectra of each PPy/V_2O_5/HCF sample. The red circles indicate the vibrational modes of V_2O_5, the arrows the ones belonging to polypyrrole, and the rhomb belonging to HCF.

In addition, as part of the structure characterization, we carried out powder XRD, experiments in order to determine the possible intercalation of molecular species within the layers of V_2O_5. The layered structure of V_2O_5 as we already mention in previous chapters, is characterized by a 001 peak present at low angles, indicating the spacing between their layers. This 001

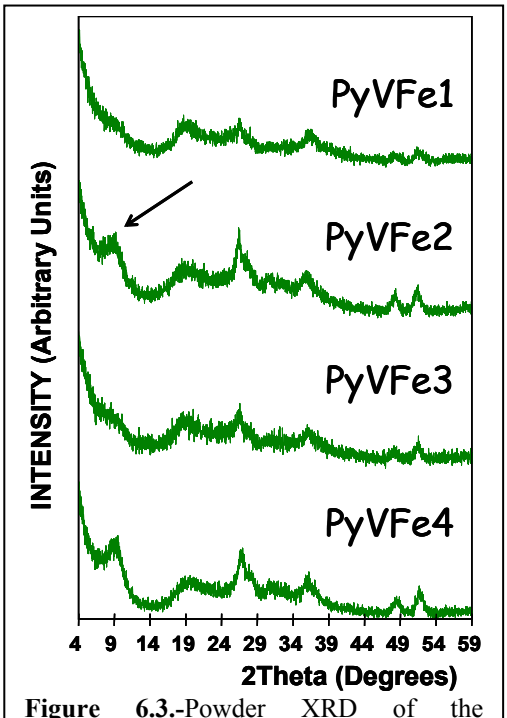

Figure 6.3.-Powder XRD of the polypyrrole triple hybrid samples

spacing is usually 11.5 Å, when one layer of water (2.8 Å) is intercalated. In figure 6.3 we can observe the diffraction patterns corresponding to the different samples of polypyrrole triple hybrids, which present poorly crystalline structures, almost amorphous (with crystallinities slightly decreasing further in the order PyVFe4>PyVFe2>PyVFe3>PyVFe1). In samples PyVFe2 and PyVFe4 we can detect a peak at low angles (ca. 2θ = 8.0º and 8.26º respectively) corresponding to a spacing of 11.0Å and 10.7Å respectively, while in the other two samples (PyVFe1 and PyVFe3) only a shoulder can be detected at ca. 8º. The net gap between slabs in samples PyVFe2 and PyVFe4 is 2.3 Å and 2.0 Å respectively, indicating that no polypyrrole was intercalated (expected expansion of 5.3 Å) nor HCF anion (expected 4 Å), but instead only water molecules as in V_2O_5 xerogels. However, polypyrrole and HCF are unambiguously present in the hybrid as indicated by FTIR. In principle this points out to a material where PPy/HCF is segregated from V_2O_5.

If we estimate the spacing that this polypyrrole triple hybrid could present if we accomplish the desired proposed structure and considering the added expansions of both, the minimum spacing to be expected would be around 18 Å appearing at 2θ= 4.9º. As a matter of fact, in all samples a shoulder peak that can be confused by the basal signal of the radiation is present at lower angles. So, we can not rule out the existence of a wider expansion between the layers of V_2O_5 and a probable formation of the triple hybrid structure.

Following the basic characterization outline, we carried out a thermogravimetric analysis (TGA) in order to determine the amount of the residual inorganic matter, and the amount of organic matter and hydration water that remains in the material. In figure 6.4 we can observe the TGA analysis carried out on our triple polypyrrole hybrid samples (2ºC/min up to 360ºC keeping the temperature for 6 hours). There are two weight losses with a characteristic structure best detected in the derivative curves (inset), one between 70-80 ºC

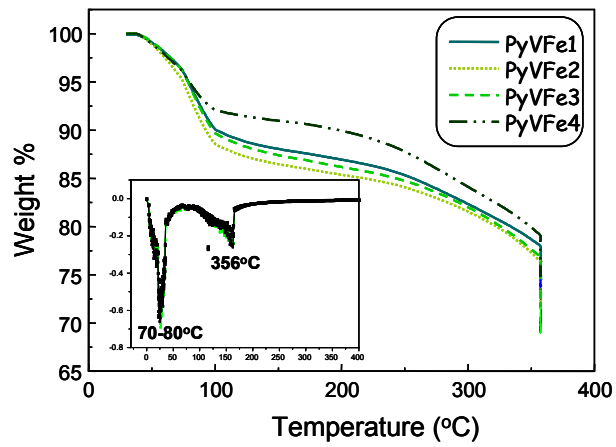

Figure 6.4.-TGA analysis of polypyrrole triple hybrids in argon, heating rate 2ºC/min up to 360ºC then isothermal for 6 hours. (derivative shown in inset)

corresponding to the hydration water, with the main loss taking place during the isothermal heating at 360°C, corresponding to the combustion of the polymer. The remaining weight percentage belongs to the inorganic part of the hybrid (HCF+V_2O_5), which resulted similar for each sample: 69.5% for PyVFe1, 69.0% for PyVFe2, 68.9% for PyVFe3, and slightly higher for PyVFe4 with a 73.7%. The stoichiometry of these polypyrrole triple hybrid samples was calculated based on elemental analyses and ICP analyses. In table VI.II we present the summarized data from these analyses and the calculated values obtained for the proposed formulas.

Table VI.II.- Summarized data of the chemical analysis to determine the respective stoichiometry of each polypyrrole triple hybrid samples.

	Py:V:Fe	%C	%N	%H	%V	%Fe	Formula	sample
Exp.	(0.5:1:1)	17.03	13.14	2.02	24.93	7.40	$(C_4H_2N)_{0.64}V_2O_5[HCF]_{0.53}3.8H_2O$	PyVFe1
Calc		17.05	13.23	2.37	25.19	7.32	FW=404.3	
Exp.	(0.5:0.5:0.5)	10.45	7.23	1.38	19.01	3.77	$(C_4H_2N)_{0.60}V_2O_5[HCF]_{0.35}10H_2O$	PyVFe2
Calc		11.18	7.68	4.54	21.65	3.91	FW=470.4	
Exp.	(0.5:0.5:1)	17.56	12.27	2.13	24.92	6.55	$(C_4H_2N)_{0.76}V_2O_5[HCF]_{0.47}4H_2O$	PyVFe3
Calc		17.46	12.44	2.57	25.28	6.51	FW=403.0	
Exp.	(0.5:1:0.5)	12.35	8.57	1.62	32.28	4.80	$(C_4H_2N)_{0.43}V_2O_5[HCF]_{0.25}2.8H_2O$	PyVFe4
Calc		12.34	8.62	2.21	32.52	4.45	FW=313.3	

6.2.3. Electrochemical Characterization

The electrochemical characterization was carried out by using the polypyrrole triple hybrid samples as cathodes in rechargeable lithium cells. Each sample was thoroughly mixed with 30% weight of super-P carbon, and the composite cathode in powder form was cycled vs. metallic lithium anodes. The charge-discharge of the cell was performed at a voltage range between 3.8-2.1V and at a slow

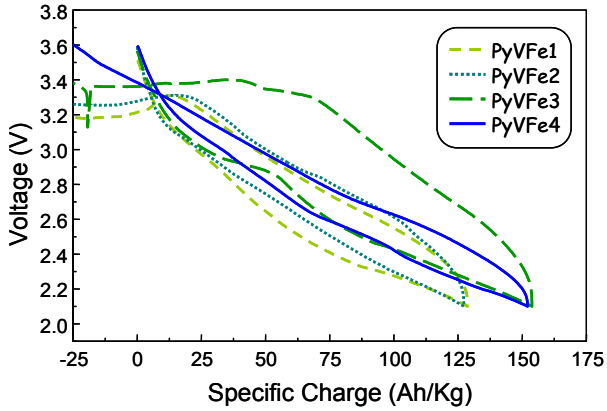

Figure 6.5.-Electrochemical characterization in reversible lithium cells of our cathodic polypyrrole hybrid samples, at a slow rate of C/40

rate of C/40. In figure 6.5 we can observe the results of these analyses. We obtained high specific charges in the initial cycle, between 125-160 Ah/Kg. The expected theoretical values (calculated for 0.33e^- per pyrrole ring, 2e^- per V_2O_5 (one per V atom) and 1e^- per Fe atom) were between 160-200 Ah/kg for the different compositions.

In general the cyclability was not very good for these materials. Thus, after five cycles, sample PyVFe1 lost 30% of its initial specific charge (129 Ah/Kg), sample PyVFe2 lost 50% of its initial specific charge (125 Ah/Kg), sample PyVFe3 lost 29% of its initial specific charge (155 Ah/Kg), and finally sample PyVFe4 lost 20% of its initial specific charge (151 Ah/Kg). However, this might have more to do with the choice of voltage limit values during recharge, since in all cases the voltage could not reach the 3.8V on recharge. This is a factor that will need to be addressed in future studies.

6.3. PAni//HCF/V_2O_5 TRIPLE HYBRID.

In past work carried out in our group relating to the PAni/HCF hybrid, it was seen that the hybrid worked very well as a cathodic material in rechargeable lithium batteries and kept a constant specific charge through cycling at a high C/5 rate (110 Ah/Kg). On the other hand, PAni/V_2O_5 hybrid resulted in a higher initial specific charge (280 Ah/Kg) at a C/6 rate, than the PAni/HCF hybrid, but after 100 cycles resulted in a low specific charge of 60 Ah/Kg.

As for the PPy triple hybrid and in parallel with it we applied the same approach to the development of a PAni/HCF/V_2O_5 triple hybrid. Furthermore, in an attempt to control de insertion of the different components into V_2O_5 , we have carried out in this PAni system a more complete series of experiments trying to optimize and detect the effect of several synthetic parameters related to the sequential addition of the various reagents.

6.3.1. Synthesis

The synthesis approach was to simultaneously form each of the components of the hybrid in a one-pot synthesis. We used in all cases a solution made of 1 ml of aniline risen to 50 ml with deionized water. The acidic ferricyanide solution was prepared as described for the PPy hybrid from the amounts of $K_3Fe(CN)_6$ indicated in table VI.III for each sample. The V_2O_5 gel was aged for three months and titrated

immediately prior to the synthesis to determine the precise amount of V(V). Then, the desired amounts of V_2O_5 were diluted with deionized water to complete a 50 ml solution. The only parameter varied was the molar ratio in each of the three samples synthesized (as indicated in table VI.III)

Table VI.III.- Molar ratio used in the synthesis of each polyaniline triple hybrid syntheses.

Sample	molar ratio (PANI:V:Fe)	$K_3[Fe(CN)_6]$ + $HClO_4$	excess reagent
PaVFe1	(3:0.5:0.5)	0.602 g + 0.2 ml	normal
PaVFe2	(3: 1: 0.5)	0.602 g + 0.2 ml	V_2O_5 - rich
PaVFe3	(3: 0.5: 1)	1.205 g +0.4 ml	HCF-rich

We set up the synthesis in an ice bath using magnetic stirring at 500 rpm, the V_2O_5 solution was added dropwise (during 3 minutes) to the HCF solution, and then the aniline solution was added to the homogeneous mixture in another 3 minutes. The reaction time was extended for 120 hours (5days). The dark solid was filtered off, and separated from an amber colored filtrate. The solids were washed with deionized water until no coloration persisted, and dried under vacuum for 3 days.

6.3.1.1. Basic Characterization

Our basic characterization started with FTIR analyses, in order to detect characteristic vibrational modes from the three components of the triple hybrid (PAni, V_2O_5, and HCF). In figure 6.6 we can observe the spectrum of each polyaniline triple hybrid sample, where we can detect the vibrational modes of V_2O_5 marked with circles; the characteristic CN stretching from HCF (marked with a diamond) and the bands indicating the formation of polyaniline (marked with arrows). The vibrational modes belonging to V_2O_5 appear at 515 cm^{-1} and 757 cm^{-1} corresponding to the V-O-V vibration, and at 981 cm^{-1} for the V=O stretching.

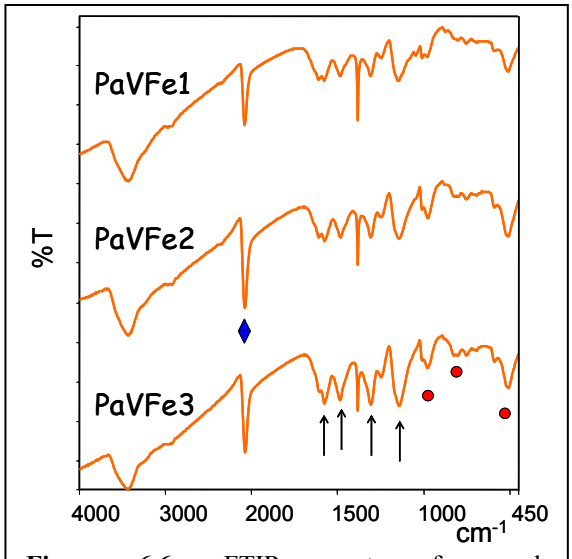

Figure 6.6.- FTIR spectra for each PAni/V_2O_5/HCF triple hybrid sample. The circles indicate the vibrational modes of V_2O_5, the arrows the ones belonging to polyaniline, and the rhomb belonging to HCF.

The C≡N stretching from HCF appears at 2079 cm^{-1}, whereas polyaniline bands are found approximately at 1147 cm^{-1} (C-H ring vibrations), at 1310 cm^{-1} (C-N of arylic secondary amine), at 1486 cm^{-1} and 1580 cm^{-1} (benzenic/quinone ring deformation).

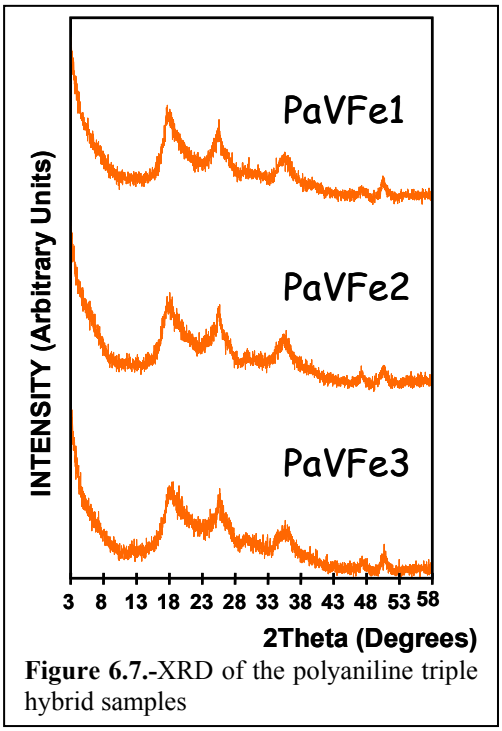

Figure 6.7.-XRD of the polyaniline triple hybrid samples

Moreover, in order to study the structure, we carried out powder XRD analyses to detect possible intercalation between the layers of V_2O_5. In figure 6.7 we show the diffraction patterns corresponding to the different samples of polyaniline triple hybrid samples. In principle, we cannot observe any apparent peak at low angles related to an intercalation. However, a weak shoulder around 5° , hardly distinguished from the background, though somewhat more clear in sample PaVFe2, hints to the presence of a spacing of ca. 17.6 Å for this hybrid.

We carried out an estimate of the structural modification to be expected upon insertion in this type of hybrids. Taking into account that polyaniline takes 5.5 Å [8] when inserted into V_2O_5 layers and that the minimum space for HCF is 4 Å, we would have in the triple hybrid structure a spacing of 18.2 Å if the expansions were additive resulting in a peak at 2θ 4.8°. With all due precautions in view of the very poorly defined shoulder, we take this agreement between our calculation and the position of the shoulder as an indication of a hybrid material with very poor crystallinity but with both PAni and HCF components inserted within V_2O_5 . A tentative conclusion that should be confirmed later with more materials and data.

TGA analyses were carried out to determine the amount of inorganic matter, organic matter and get an estimate of the hydration water in our samples. In figure 6.8 we present TGA analyses carried out for our triple polyaniline hybrid samples (2 °C/min up to 360 °C, keeping the temperature for 6 hours and 5 hours for sample PaVFe1). There are two important weight losses with a characteristic structure best detected in the derivative curves (inset), one at 55 °C corresponding to loosely bound hydration water and the other between 287-357 °C corresponding to the combustion

of the polymer. The remaining weight percentage corresponds to the inorganic part of the hybrid (HCF+V_2O_5), that for each sample is similar: 71.78% for PaVFe1, 73.09% for PaVFe2, and 75.84% for PaVFe3.

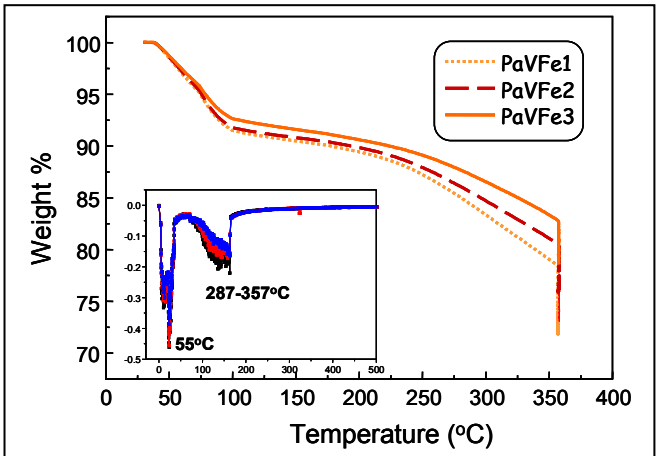

Figure 6.8.-TGA analyses of polyaniline triple hybrids, using the following program: rate 2ºC/min up to 360 ºC for 6 hours in Argon.

The stoichiometry of these polyaniline triple hybrid samples was calculated based on elemental analyses and ICP analyses. In table VI.IV we present the summarized data of these experimental analyses and the calculated values for the proposed stoichiometric formulas.

Table VI.IV.- Summarized data of the chemical analysis to determine the respective stoichiometry of each polyaniline triple hybrid samples.

	PA:V:Fe	%C	%N	%H	%V	%Fe	Formula	sample
Exp	(3:0.5:0.5)	33.50	14.68	2.54	17.84	6.79	$C_6H_4N(V_2O_5)_{0.48}[HCF]_{0.33}1.3H_2O$	**PaVFe1**
Cal		35.39	15.41	2.45	18.06	6.80	FW= 270.77	
Exp	(3:1:0.5)	28.17	14.86	2.31	19.87	7.46	$C_6H_4N(V_2O_5)_{0.75}[HCF]_{0.52}2.7H_2O$	**PaVFe2**
Cal		28.42	14.97	2.45	19.82	7.53	FW= 385.37	
Exp	(3:0.5:1)	35.22	15.03	2.61	16.66	6.73	$C_6H_4N(V_2O_5)_{0.42}[HCF]_{0.31}1.4H_2O$	**PaVFe3**
Cal		36.67	15.56	2.66	16.62	6.72	FW= 257.42	

6.3.1.2. *Electrochemical Characterization*

The electrochemical characterization was carried out by using the polyaniline triple hybrid samples as cathodes in rechargeable lithium cells. Each sample was thoroughly mixed with 30% weight of super-P carbon, and the composite powder was used as cathode vs. metallic lithium anodes. The charge-discharge cycles of the

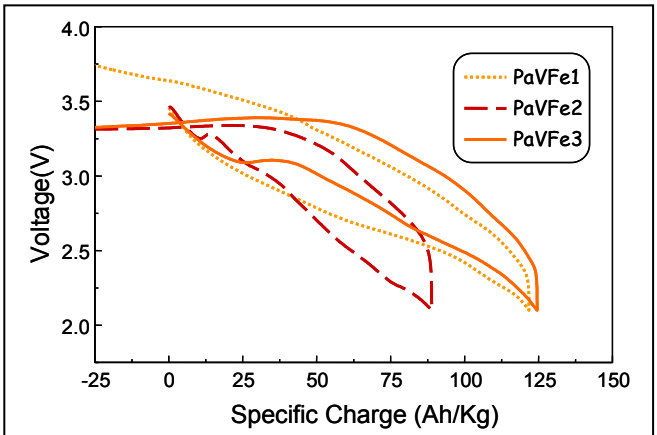

Figure 6.9.-Electrochemical characterization in rechargeable lithium cells of our polyaniline triple hybrid samples, at a slow charge-discharge rate of C/40.

cell were carried out in the voltage range of 3.8-2.1V at a slow C/40 rate. In figure 6.9 we show the results of these electrochemical analyses. We obtained good specific charges of 120.4 Ah/Kg for sample PaVFe1 (176 Ah/Kg theoretical value, expected for 1.8 e-/Li+ per formula unit), 88.7 Ah/Kg for PaVFe2 (174 Ah/Kg, for 2.5 e-/Li+ per formula unit), and 124 Ah/Kg for sample PaVFe3 (172 Ah/Kg, for 1.65 e-/Li+ per formula unit). As for PPy hybrids, the voltage could not reach the 3.8 V set for recharge and the cyclability was poor in all cases. After five cycles, sample PaVFe1 had lost 33% of its initial specific charge, sample PaVFe2 55%, and sample PaVFe3 31%.

6.3.2. Effect of the order of addition of the inorganic reagents

Due to the poor performance of polyaniline triple hybrids in lithium batteries, we carried out an attempt to optimize the synthesis parameters to study the influence in their electrochemical properties. This optimization involved the order of addition of the inorganic reagents in a series of experiments otherwise corresponding to the synthetic parameters used for sample PaVFe3, which had an electrochemical behavior closer to the theoretical behavior.

6.3.2.1. Synthesis

We used a molar ratio of Ani:V:Fe of (3:0.5:1), where in all cases, a solution of 1 ml of aniline risen to 50 ml was used, 1.205 g of $K_3[Fe(CN)_6]$ was dissolved in 40 ml of deionized water to prepare $H_3[Fe(CN)_6]$ (HCF) with 0.4 ml of $HClO_4$ and risen to 50 ml, and finally, V_2O_5 gel was titrated before the synthesis to prepare the corresponding 50 ml solution. The synthesis was carried out using a reaction time of 5 days in an ice bath with magnetic stirring at 500 rpm. We prepared two different samples. Sample VPaFe3 was carried out by first adding V_2O_5 to the aniline solution over a period of 4 minutes, mixing for 2 minutes before the addition of the HCF solution that was added in 10 minutes. Sample FePaV3 was carried out similarly, but we first added the HCF solution to Aniline during 4 minutes, mixing for 2 minutes before adding V_2O_5. It appears that the reaction with V_2O_5 is spontaneous in both cases, thereby giving a dark solid. In sample FePaV3, were we added first the HCF solution, only a faint greenish coloration was detected upon HCF addition to Aniline, but no solid was formed before V_2O_5 was added, indicating slower kinetics for the oxidative polymerization of Aniline with HCF as compared with V_2O_5.

6.3.2.2. Basic characterization

Figure 6.10 shows the FTIR spectra of samples VPaFe3 and FePaV3 triple hybrid. V_2O_5 bands appear at 515-511 and 753 cm^{-1} (V-O-V) and at 970-977 cm^{-1} (V=O stretching), the C≡N stretching from HCF at 2072 cm^{-1} and polyaniline bands in the range1143-1150 cm^{-1} (C-H of the ring), at 1306-1309 cm^{-1} (C-N of an arylic secondary amine), at 1490-1494 cm^{-1} and 1577-1580 cm^{-1} (benzenic/quinone ring deformation).

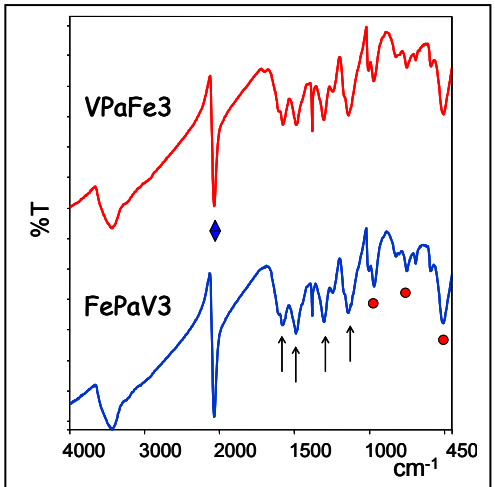

Figure 6.10.- FTIR spectra for PAni/V_2O_5/HCF samples optimized according to the order of addition of the inorganic components. The circles indicate the vibrational modes of V_2O_5, the arrows the ones belonging to polyaniline, and the rhomb belonging to HCF.

Figure 6.11 shows XRD patterns for these two samples. In this case, the shoulders present around 5° can be better detected, confirming the expansion we have discussed above and therefore confirming the insertion of PAni/HCF between the layers of V_2O_5.

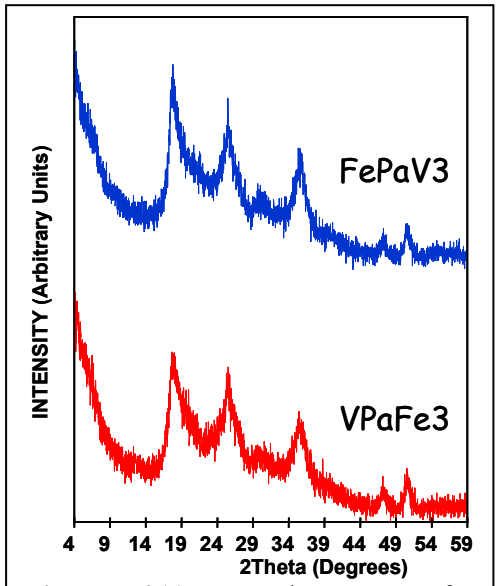

Figure 6.11.- Powder XRD for PAni/V_2O_5/HCF samples optimized according to the order of addition of the inorganic components.

Figure 6.12 shows the corresponding TGA analyses carried out in our new triple polyaniline hybrid samples (2°C/min up to 360°C for 6 hours). Loosely bound water is lost at 73 °C (inflection point) and at 360 °C takes place the combustion of the polymer, detected better in the derivative curves (inset). The remaining weight percentage belongs to the inorganic part of the hybrid (HCF+V_2O_5), 79.64% in sample FePaV3, and 78.03% in sample VPaFe3. As we can see, these new samples of polyaniline triple hybrids have similar amounts of inorganic residual. The order of addition of the inorganic components do not influence the amount of inorganic residue.

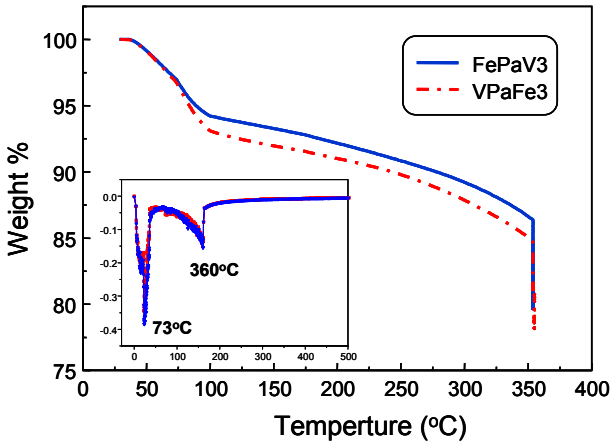

Figure 6.12.-TGA analyses of polyaniline triple hybrids, optimized according to the order of addition of the inorganic components. The followed program was using a rate 2°C/min up to 360°C for 6 hours.

The stoichiometry of these new polyaniline triple hybrid samples were calculated based on elemental analyses and ICP analyses. In table VI.IV we summarized the data of these analyses and the comparison with calculated values for the proposed stoichiometric formulas.

Table VI.V.- Summarized data of the chemical analysis to determine the respective stoichiometry of each polyaniline triple hybrid samples, optimized based on the order of addition of the inorganic's.

	PA:V: Fe	%C	%N	%H	%V	%Fe	Formula	sample
Exp.	(3:0.5:1)	35.00	14.91	2.71	16.06	6.95	$C_6H_4N\ (V_2O_5)_{0.44}[HCF]_{0.34}2H_2O$	**VPaFe3**
Cal.		34.70	15.30	2.89	16.11	6.82	FW= 278.22	
Exp.	(3:0.5:1)	35.03	14.97	2.66	14.85	5.91	$C_6H_4N\ (V_2O_5)_{0.36}[HCF]_{0.26}1.9H_2O$	**FePaV3**
Cal.		37.07	14.64	3.20	14.97	5.92	FW= 244.91	

6.3.2.3. Electrochemical Characterization

The electrochemical characterization was carried out by using the new polyaniline triple hybrid samples as lithium insertion cathodic materials in rechargeable lithium cells as detailed above. The cell was cycled between the same voltage range as before (3.8-2.1V, C/40 rate). In figure 6.13 we can observe the results of these electrochemical analyses. We obtained moderate specific charges of 84 Ah/Kg for FePaV3, and 72 Ah/Kg for sample VPaFe3. The theoretical value for these new samples is 161-166 Ah/Kg, higher than the values obtained experimentally. In this case the voltage did reach the 3.8V on recharge, thereby accomplishing the

process of cycling between the voltage limits, but values of specific charge obtained were lower than before. Sample VPaFe1 lost more specific charge through cycling than for the case of sample FePaV3 (only 10% loss after 5 cycles). These results are below the initial specific charge compared to the PAni/HCF system (137 Ah/Kg at C/15) [1],

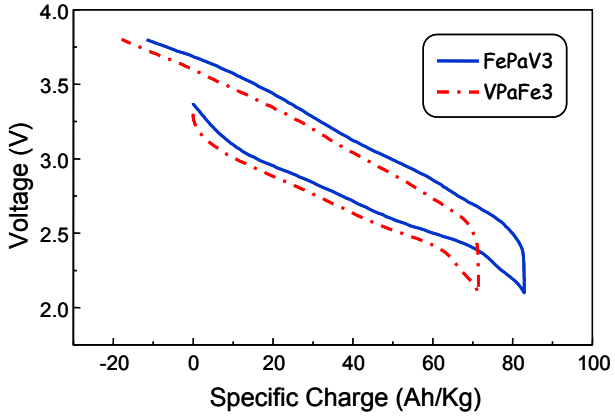

Figure 6.13.-Electrochemical characterization in rechargeable lithium cells of our cathodic polyaniline triple hybrid samples, synthesized by changing the order of addition of the inorganic components, at a slow charge-discharge rate of C/40

6.3.3. Effect of the time between the addition of the inorganic reagents

In our first optimization based on the order of addition of the inorganic components, we observed that the initial specific charge decreased, but the cyclability loss was lower for the case of sample FePaV3 (10% loss). In this sample, on which we will base our next optimization step, HCF solution was first added to aniline followed by the addition of V_2O_5 solution. In past work carried out by our group, regarding the PAni/HCF hybrid mentioned before [1], it was observed that it took time to form the solid hybrid. Based on this, we will attempt to carry out the next optimization step by first forming the PAni/HCF hybrid during extended periods of time, and then try to intercalate it between the layers of V_2O_5. In this optimization we will control the time of addition between the inorganic components, to establish its influences over their electrochemical properties.

6.3.3.1. Synthesis conditions

We used a constant molar ratio for Ani:V:Fe of (3:0.5:1) for all samples, where in all cases, a solution of 1 ml of aniline risen to 50 ml was used, 1.205 g of $K_3[Fe(CN)_6]$ was dissolved in 40 ml of deionized water to prepare $H_3[Fe(CN)_6]$ solution (HCF) with $HClO_4$ and risen to 50 ml, and finally, V_2O_5 gel was titrated before the synthesis to prepare the corresponding 50 ml solution. The synthesis was carried out using an ice bath with magnetic stirring at 500 rpm, and finally adding, first, HCF previously formed and then V_2O_5 to the aniline solution. The parameters that we varied, as we previously

Table VI.VI.- Synthetic optimization conditions for triple polyaniline hybrids, based on the time of addition between the inorganic components.

Sample	1)Reaction time with HCF	2)Reaction time with V_2O_5	Total time of synthesis
AFe1V	1 day	2 days	3 days
AFe2V	2 days	2days	4 days
AFe1V3	1 day	3days	4 days
AFe3V3	3 days	3days	6 days
AFe3V5	3 days	5days	8 days

mentioned, were the time of addition between the inorganic components, resulting in five different experiments that are summarized in table VI.V.

During the synthesis of these newer polyaniline triple hybrid samples we saw that 1 day after the addition of HCF, we had a greenish solution (AFe1V, AFe1V3). For samples where HCF was in contact with polyaniline (AFe3V3, AFe3V5) for a longer period of time, a greenish fine powder was present in the solution. In each case, when V_2O_5 was added, the reaction was spontaneous and fast, giving a rapid colour change from light translucent green to dark opaque green. After the reaction time was over, a solid was obtained in each case, and was filtered off obtaining an amber filtrate. The solid was washed with deionised water until no coloration appeared, and dried under vacuum for 3 days.

6.3.3.2. *Basic characterization*

In figure 6.14 we show the FTIR spectra of each new optimized polyaniline triple hybrid samples. V_2O_5 bands appear at 507-522 cm^{-1} and 749-757 cm^{-1} (V-O-V) and at 970-977 cm^{-1} (V=O stretching), the C≡N stretching from HCF at 2065-2072 cm^{-1} and polyaniline bands in the range of 1140-1147 cm^{-1} (C-H of the ring), at 1306-1313 cm^{-1} (C-N of an arylic secondary amine), at 1483-1494 cm^{-1} and 1577-1584 cm^{-1} (benzenic/quinone ring deformation).

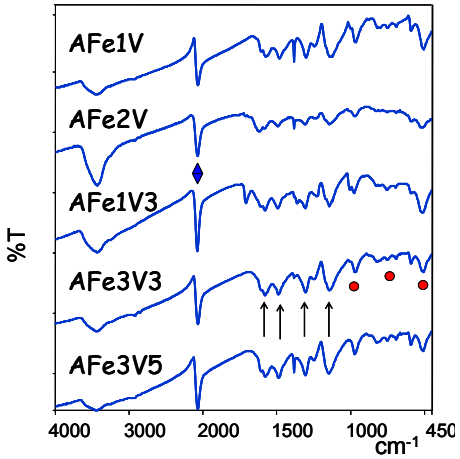

Figure 6.14.- FTIR spectra of PAni/V_2O_5/HCF samples, optimized according to the time addition between HCF and V_2O_5. The circles indicate the vibrational modes of V_2O_5, the arrows the ones belonging to polyaniline, and the rhomb belonging to HCF.

In addition, in figure 6.15 we show the diffraction patterns corresponding to these newer polyaniline triple hybrid samples. For this particular set of samples, only in the case of sample AFe1V3 a shoulder around

6° can hardly be distinguished from the background as in hybrids from section 6.3.1.1), that hints to the presence of a spacing of ca. 14.71 Å for this hybrid. This particular spacing represents only the insertion of polyaniline. This spacing is substantially smaller than the one estimated for samples FePaV3 and VPaFe3 (2θ=50°, 18Å), yet, larger than that of V_2O_5 xerogel. This could be explained if PAni and HCF are inserted within V_2O_5 but alternate along a direction perpendicular to the c crystallographic axis. In this way, the expansion expected for PAni and that for HCF would not add up to produce a double expansion but both would accommodate within this estimated 3-3.5 A expansion.

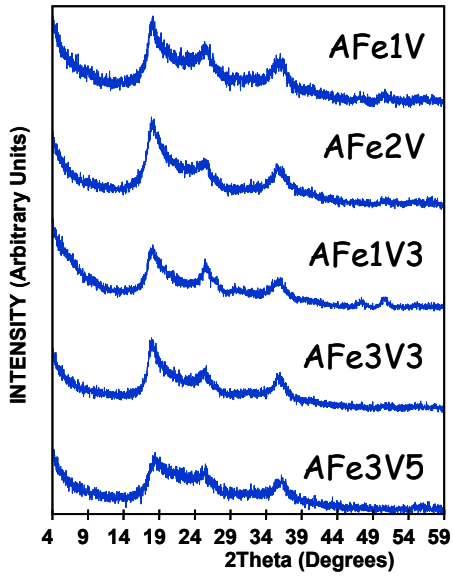

Figure 6.15.- Powder XRD for PAni/V_2O_5/HCF) samples optimized according to the time of addition between the inorganic components.

The stoichiometry of these optimized polyaniline triple hybrid samples was calculated based on elemental analyses and ICP analyses. In table VI.VI we present the data of these analyses and the calculated valued for the proposed stoichiometric formulas.

Table VI.VII.- Summarized data of the chemical analysis to determine the respective stoichiometry of each polyaniline triple hybrid samples, optimized based on the time of addition between HCF and V_2O_5.

	PA:V:Fe	%C	%N	%H	%V	%Fe	Formula	sample
Exp	(3:0.5:1)	31.49	15.45	2.47	14.54	7.83	C_6H_4N $(V_2O_5)_{0.48}[HCF]_{0.46}3.1H_2O$	**AFe1V**
Cal		31.81	15.92	3.10	14.78	7.76	FW= 330.75	
Exp	(3:0.5:1)	30.36	15.65	2.37	13.23	8.41	C_6H_4N $(V_2O_5)_{0.53}[HCF]_{0.61}4.9H_2O$	**AFe2V**
Cal		28.71	16.15	3.44	13.36	8.43	FW= 404.06	
Exp	(3:0.5:1)	33.89	14.96	2.55	16.43	6.69	C_6H_4N $(V_2O_5)_{0.48}[HCF]_{0.34}$ $2H_2O$	**AFe1V3**
Cal		34.48	15.01	2.90	16.49	6.63	FW= 277.92	
Exp	(3:0.5:1)	35.32	17.18	2.81	10.39	8.26	C_6H_4N $(V_2O_5)_{0.3}[HCF]_{0.43}3.1H_2O$	**AFe3V3**
Cal		35.33	17.19	3.52	10.47	8.23	FW= 291.65	
Exp	(3:0.5:1)	36.73	18.08	2.82	10.18	8.93	C_6H_4N $(V_2O_5)_{0.29}[HCF]_{0.47}2.9H_2O$	**AFe3V5**
Cal		35.94	18.15	3.35	10.02	8.90	FW= 294.71	

6.3.3.3. *Electrochemical Characterization*

In figure 6.16 we show the first cycles of these materials as cathodes in lithium cells set up as before (3.8-2.1V, C/40 rate). We obtained moderate specific charges between 40-92 Ah/Kg and not all the samples reached the 3.8V on recharge (AFe2V

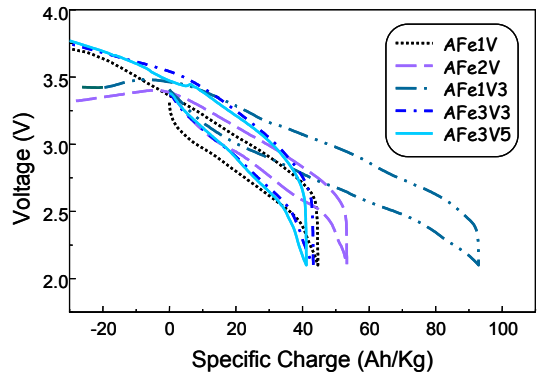

Figure 6.16.-Electrochemical characterization in rechargeable lithium cells of our polyaniline triple hybrid samples, optimized based on the time between the addition of HCF and V_2O_5, at a slow charge-discharge rate of C/40.

and AFe1V3). The remaining samples reached this potential with no difficulty, although the initial specific charge was lower. All samples lost specific charge through five charge-discharge cycles: for AFe1V, 21%; for AFe2V, only could perform 3 cycles; for AFe1V3, 13%; AFe3V3, 0%; and finally for AFe3V5, 20%. It appears that exposing aniline to HCF for longer periods of time during the synthesis results detrimental for the specific charge values obtained. The expected theoretical values of lithium uptake and specific charge (140-173 Ah/Kg) were in some cases two times above the experimental ones. We can see that the time of addition between the inorganic components, in the synthesis of the triple hybrid with polyaniline, did not result in an enhanced initial specific charge or cyclability.

We have synthesized a new class of hybrids based on the intercalation of polypyrrole and/or polyaniline doped with HCF, inserted in turn between the layers of V_2O_5. We have identified each component of the triple hybrids with FTIR analyses, their intercalation in V_2O_5 layers by powder XRD (detected only in certain cases), and their stoichiometry by elemental analyses, TGA and ICP analyses. Unfortunately, the performance of these triple hybrid materials, as prepared and measured here, is not better than the corresponding binary counterparts. Thus, their specific charges compare quite unfavorably with those from the simpler binary hybrids PAni/HCF system (137 Ah/Kg at C/15) [1] and PAni/V_2O_5 (280 Ah/Kg at C/7.5) and cyclabilities are also poor. However, we would like to stress that this work constitutes a relative success in relation to the synthetic chemistry of hybrid materials, since it is a first step in the design of novel approaches for functional hybrids of greater complexity which could also be useful for other applications as catalysts, sensors, etc.

REFERENCES

[1] Gómez-Romero, P.; Torres-Gomez, G.; *Adv. Mat.* **2000**(12), 1454.
[2] Torres-Gomez, G.; Gomez-Romero, P.; *Synth. Met.***1998**(98), 95.
[3] Torres-Gomez, G.; Skaarup, S.; West, K.; Gomez-Romero, P.; *J. Electrochem. Soc.* **2000**(147), 2513.
[4] Da Silva, L.F.; Profeti, L.P.R.; Stradiotto, R.; Oliveira, H.P.; *J. Non-Cryst. Solids* **2002**(298), 213.
[5] Pokhodenko, V.D.; Kurys, Y.I.; Posudievsky; *Synth. Met.* **2000**(113), 199.
[6] Kuwabata, S.; Masui, S.; Tomiyori, H.; Yoneyama, H.; *Electrochim. Acta* **2000**(46), 91.
[7] Torres-Gómez, G.; "*Materials Hibrids Funcionals de tipus molecular. Hexacianoferrat integrat en polymers conductors com a electrodes en bateries recarregables de liti.*."; Ed. Universitat Autonoma de Barcelona; Barcelona **2001**, 166.
[8] Kanatzidis, M.G.; Wu, C.G.; *J. Am. Chem. Soc.* **1989**(111), 4141.
[9] Cuentas-Gallegos, A.K.; Palacin, M.R.; Colomer, M.T.; Jurado, J.R.; Gómez-Romero, P.; *Bol. Soc. Esp. Ceram. Vid.* **2001**(41), 115.

Chapter 7

Vanadyl Phosphate Hybrids

Abstract:

We describe in this chapter our efforts to synthesize a new hybrid system based on conducting polymers (PAni, PPy) inserted into layered vanadyl phosphate. The characterization of the resulting materials indicated the partial decomposition of the vanadyl phosphate during synthesis. However, these materials can be used as cathodes in rechargeable Li cells, obtaining moderate specific charge values but good stability during cycling. Eventually a novel hybrid material of formula $PPy(VOPO_4)_{0.13}{\cdot}1.1H_2O$ was isolated and showed a maximum specific charge of 155Ah/Kg and very good cyclability after stabilization around values of 90-100Ah/kg after 35 cycles at 20mA/g.

7.1. INTRODUCTION

Vanadyl phosphates have been extensively studied because of their importance in selective catalysis of hydrocarbon oxidation reactions. They present several allotropic structural modifications: β- $VOPO_4$ has a tunnel structure consisting of a three-dimensional network, ε- $VOPO_4$ [1,2] which structure has yet to be determined [3] and finally a series of other polymorphs α_I, α_{II}, γ, δ, and ω-phases with layered structures [4].

Many of these compounds are synthesized via high-temperature solid state routes. But recently other synthetic methods have been explored like aqueous precipitation [5], sol-gel [6], hydrothermal [1]. and sonochemical methods [7]

Transition metal phosphates have been recently shown to be viable cathode materials for Li cells, especially where kinetic limitations to electronic conductivity can be overcome. Among the metal phosphates, olivine phase of $LiFePO_4$ or $LiCoPO_4$, have attracted great interest as cathode of Li ion rechargeable battery. [8]

Dupre et al. [9] studied the electrochemical intercalation and de-intercalation of Li into $VOPO_4$ and demonstrated the high potential plateau at 3.76 V. Therefore, vanadyl phosphate is considered as a new cathode material for Li ion rechargeable batteries. As we already mention, there are several crystal phases (seven), which differ on the connection and arrangement, of VO_6 octahedra and PO_4 tetrahedra units. The theoretical specific charge for Li intercalation into $VOPO_4$ is 165 mAh/g (1e-/V atom). However, in spite of sharing the same $VOPO_4$ formula, charge and discharge capacities are strongly dependent on the crystal phases at hand. In fact, the order of specific charge that can be obtained from these different vanadyl phosphate structures upon Li intercalation is: $\delta>\varepsilon>\alpha_I>\omega>\alpha_{II}>>\beta$. [4]

However, the phase that we will focus on in this chapter is α_I-$VOPO_4{\cdot}2H_2O$. As we already mentioned, α_I-$VOPO_4{\cdot}2H_2O$ is a layered compound, characterized by a great anisotropy of its chemical bonds. The sheets cohesion is maintained by iono-covalen bonds, while weak Van der Waals or electrostatic forces bring out the stacking up. This anisotropy is also found in the physical chemistry of this material, the large specific surface and the exchange properties of the Van der Waals gap give rise to potential applications (catalyst, electrodes, battery, ions exchanger) [10]. The water molecules can be reversibly intercalated between these layers leading to $VOPO_4{\cdot}H_2O$ (α_{II}), but at ambient conditions the dihydrate $VOPO_4{\cdot}2H_2O$ (α_I) is the stable phase. The

layered tetragonal structure of this phase has a space group P4/mmm according to R'Kha et. al. [6], but according to Tachez et. al. [11] the space group is P4/nmm, and contains two formula units per unit cell. The $(VOPO_4)_n$ layers are built of (VO_6) octahedra with a marked axial anisotropy (one short V=O and one long axial bond) which are linked together by corner sharing with (PO_4) tetrahedra, while adjacent layers are held together by weak bonding interactions. In the hydrated phase the complete coordination occurs through a $V\cdots OH_2$ bond, while in the anhydrous phases this is obtained by the formation of a loose V···O bond between atoms of adjacent layers [12,13]. Water molecules are intercalated between these layers. They lead to an increase of the *c* parameter from 4.11 Å for anhydrous $VOPO_4$, up to 6.30 Å for $VOPO_4{\cdot}H_2O$, and 7.41 Å for $VOPO_4{\cdot}2H_2O$. One water molecule is directly bonded to a vanadium ion along an axial position opposite to the V=O short bond. The other water molecules are loosely bound in between $VOPO_4$ slabs. The structure of this phase can be seen in figure 7.1. The enhancement of ionicity of (V-O) bonds by $(PO_4)^{-3}$ anion in vanadyl phosphate is expected to give way to high potential, compared to simple vanadium oxides. Moreover, the mixed ionic-electronic conducting property in hydrated $VOPO_4$ suggests a possibility for rapid insertion/extraction of small alkali metal cations such as proton or lithium ions.

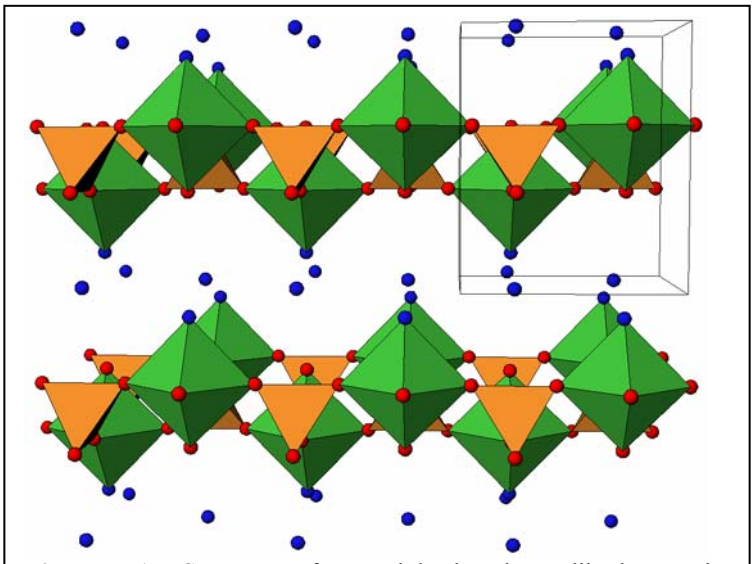

Figure 7.1.- Structure of Vanadyl phosphate dihydrate. The orange tetrahedra is the phosphate group, the green octahedra is the vanadyl group, the red circles are bonded oxygen, and the blue circles are oxygen from water.

For the synthesis of $VOPO_4 \cdot 2H_2O$, a prolonged reflux of V_2O_5 in aqueous phosphoric acid has been conventionally used since 1965 [14]. However, this method often leads to large mm-sized crystalline particles, which might have an ill-influence on its electrochemical lithium insertion kinetics. Thus, a more effective route for controlling particle size of $VOPO_4 \cdot 2H_2O$ was required to use in battery application. Currently, sonochemistry is been studied as a simple and effective method for generating novel materials with unusual properties and microstructures. Nam-Gyu Park et. al. [7] have applied this method using a high intensity ultrasonic probe to prepare $VOPO_4 \cdot 2H_2O$; and tried it as a lithium insertion cathode material obtaining specific charges values of 136 Ah/kg which are stable after 25 cycles, observing also that the insertion kinetics was remarkably insensitive to the charge-discharge rate.

On the other hand, as a host structure, $VOPO_4 \cdot 2H_2O$ is able to intercalate various guests into the interlayer space, as molecules, atoms, or ions (as we already mentioned for Li) [13]. Alternatively, conducting organic polymers (COPs) (polypyrrole, polyaniline, etc.) have also been intercalated $VOPO_4 \cdot 2H_2O$ [15-18]. In those works aniline was used among many other inserted species but did not led to a high polymerization degree [15,17]. More recently de Farias et. al. [19] obtained a higher polymerization degree resulting in a formula of $(C_6H_4N)_{1.1}VOPO_4$ of the hybrid. Alternatively, for the case of pyrrole polymerization between the layers of $VOPO_4$, when neat pyrrole was used, a lower content of polypyrrole was obtained in the final hybrid material ($(C_4H_2N)_{0.6}VOPO_4 1.5H_2O$), as compared with the contents obtained when pyrrole solutions (in ethanol) were used ($(C_4H_2N)_{1.14}VOPO_4 14H_2O$). [17] In addition, the synthesis with dissolved pyrrole resulted in an amorphous hybrid.

In this chapter we present our results regarding the formation of this type of hybrid materials, by means of an “in-situ” oxidative polymerization of pyrrole or aniline between the layers of vanadyl phosphate dihydrate, synthesized by a sonochemical method. We carried out a synthesis with higher amounts of the corresponding monomers, in order to obtain hybrids with higher amounts of polymer. Also, we carried out the corresponding basic characterization (FTIR, XRD, TGA), chemical characterization (elemental analyses, ICP), physical-chemical characterization (SEM, Conductivity measurements), and finally their electrochemical characterization as lithium insertion cathodes.

7.2. VANADYL PHOSPHATE DIHYDRATE ($VOPO_4 \cdot 2H_2O$)

In this section, we present the synthesis route and basic characterization of $VOPO_4 \cdot 2H_2O$. For the basic characterization we used FTIR analysis as a fingerprint method to detect the formation of the compound and powder XRD to confirm the formation of the layered $VOPO_4 \cdot 2H_2O$ phase.

7.2.1. Synthesis

To prepare $VOPO_4 \cdot 2H_2O$ we followed a modification of the method by Nam-Gyu Park et. al. [7], using a sonochemical technique but with a different apparatus and lower power. The synthesis was carried out as follows: a suspension of 2 g of crystalline V_2O_5 with 100 ml of deionized water and 31.5 ml of concentrated H_3PO_4 85% was placed in a closed Erlenmeyer in an ultrasound bath (Transsonic 460/H, Elma) for 3 hours. During the reaction time, we observed an increase of the temperature up to 40°C, and a color change from an off-yellow color to a light brighter yellow. After the 3 hours of synthesis, the very fine powder suspended was filtered off under vacuum using a milipore filter. The solid was washed with 10 ml of acetone and dried in the same filter overnight.

7.2.2. Basic characterization

In figure 7.2 we present the FTIR spectrum, where we assign the vibrational modes corresponding to our vanadyl phosphate, which can help us compare with the $VOPO_4 \cdot 2H_2O$ obtained by other methods [6]. We found the same vibrational modes for our $VOPO_4 \cdot 2H_2O$ (at 3428 cm^{-1}, 1620 cm^{-1}, 1086 cm^{-1}, 947 cm^{-1}, 680 cm^{-1}, and at 571 cm^{-1}), compared with the material prepared by sol-gel and sonochemistry. [6,7]. Thus, no relevant difference was detected when using the ultrasound bath instead of traditional methods.

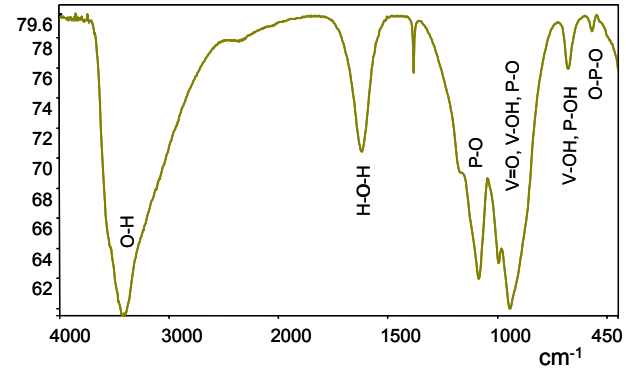

Figure 7.2.- FTIR spectrum of $VOPO_4 \cdot 2H_2O$ phase, where each stretching modes is assigned.

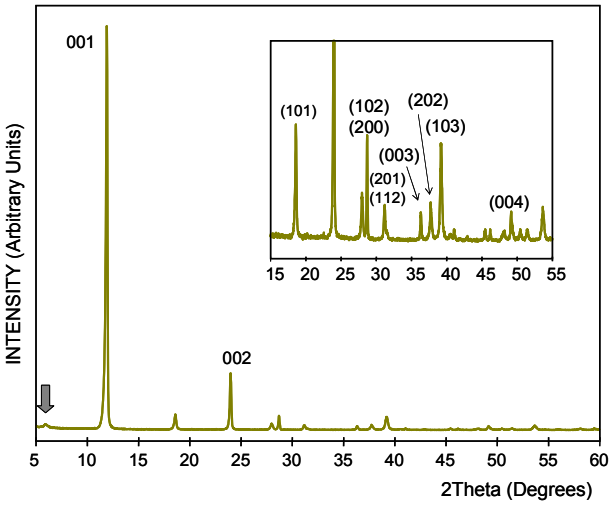

Figure 7.3.- Powder XRD of $VOPO_4{\cdot}2H_2O$ sonochemically synthesized. The planes of the structure are indicated in the diffraction pattern. The arrow indicates the peak of the superstructure.

With this in mind, we carried out the powder XRD analysis. In figure 7.3 we present the XRD diffraction pattern where we have assigned the different Miller indices based on the structure reported by Park et al.[7] (P4/nmm), thus confirming the formation of this same layered $VOPO_4{\cdot}2H_2O$ phase. The most relevant peak to consider in this diffraction pattern can be found at lower angles, which represents the 001 plane corresponding to the spacing between the layers of $VOPO_4{\cdot}2H_2O$. Our data 2θ (001) = 11.9° yield a spacing value of 7.4 Å, which is in good agreement with previous results [7]. The weak peak marked with an arrow in figure 7.3, that appears at even lower angles corresponds to a spacing of 14.7 Å, therefore indicating a doubling of the unit cell along the *c* axis, which, as far as we know, has not been reported before for this phase. This doubling could be the result of a superstructure derived from a slight distortion of the lattice. The presence of this superstructure was the only difference found between our material and the one reported by Park et. al.[7]

7.3. PPy/$VOPO_4{\cdot}2H_2O$ HYBRIDS

Hybrid materials based on polypyrrole and $VOPO_4{\cdot}2H_2O$, have been previously synthesized as we mentioned above, with a low content of polypyrrole in the resulting bulk hybrid, and in some cases leading to an amorphous phase, with no indication of polymer insertion within $VOPO_4$.

In this section we will explore different synthetic methods for PPy-$VOPO_4$ systems. Initially, we tried to use the same general approach we have used for other materials, namely, the simultaneous formation of the organic polymer and the inorganic lattice or the incorporation “in-situ” of monomers into freshly prepared

$VOPO_4$ .The main objective and control parameter for the design of these PPy/$VOPO_4$ hybrid materials and for the optimization of their synthesis will be essentially their electrochemical performance as insertion cathodes in rechargeable Li cells.

First, we will discuss the synthetic methods applied initially for the formation of PPy/$VOPO_4$ hybrids, followed by successive optimization procedures based on different synthesis parameters. Also, we will present the corresponding basic characterization, in some cases their physical-chemical characterization, as well as their electrochemical characterization as cathode material for lithium insertion batteries.

7.3.1. Comparative analysis of Synthetic Methods

In order to determine the best synthetic route, we explored four different syntheses procedures. In all cases the $VOPO_4{\cdot}2H_2O$ used was prepared by ultrasound treatment: 1) sonochemical method, using pre-formed $VOPO_4{\cdot}2H_2O$ to react with pyrrole in an ultrasound bath; 2) an in-situ sonochemical method (addition of pyrrole during the formation of $VOPO_4{\cdot}2H_2O$; 3) chemical method at room temperature (i.e. without ultrasounds); and 4) chemical method in an ice bath.

7.3.1.1. Synthesis

First of all, we carried out method 1) above by using the same ultrasound bath set-up, as mention in section (7.2.1.). The synthesis procedure was carried out as follows: 1 ml of pyrrole with 5 ml of water was arranged in a beaker with $VOPO_4{\cdot}2H_2O$ (0.9457 g) resulting in a molar ratio of Py:$VOPO_4{\cdot}2H_2O$ of (3:1), and was treated with ultrasounds for a period of 3 hours. We observed a rapid color change to black, during the synthesis. The fine black solid (E1PVP) was filtered off using a Millipore filter, washed with deionized water, collected and dried under vacuum for 3 days.

Next, we carried out the in-situ sonochemical method (2), which consisted on the formation of the hybrid during the formation of $VOPO_4{\cdot}2H_2O$ (1 g of V_2O_5, 16.93 ml of H_3PO_4 with 42 ml of deionized water). We followed the same procedure of section 7.1.1., adding the pyrrole solution (1 ml risen to 25 ml with deionized water) after 30 minutes of the $VOPO_4{\cdot}2H_2O$ synthesis, and then completing the whole 3 hours of reaction. The molar ratio used of Py:$VOPO_4{\cdot}2H_2O$ was (3:1). Before the addition of the pyrrole solution we observed a color change to light yellow, indicating the formation of $VOPO_4{\cdot}2H_2O$. Immediately after the addition of pyrrole solution, we observed a color

change to black. The very fine black solid (E2PVP) was filtered off with a Millipore filter, washed with water, and dried under vacuum for 3 days.

Finally, we carried out the chemical methods as follows: we suspended $VOPO_4 \cdot 2H_2O$ (0.9508 g) in a 50 ml $HClO_4$ solution (0.41 ml in 50 ml of deionized water), followed by the addition of a pyrrole solution (1 ml risen to 50 ml with deionized water) during 3 minutes, letting react for 5 days with magnetic stirring at 500 rpm. The molar ratio used of $Py:VOPO_4 \cdot 2H_2O:HClO_4$ was (3:1:1). These conditions were used for the synthesis carried out at room temperature (E3PVP), as well as, for the one carried out in an ice bath (E3PVP0^o). In both chemical syntheses, we observed a color change from light yellow to pale green to black when pyrrole was added. The dark solids obtained in each case were filtered off, washed with water, and dried under vacuum for 3 days.

7.3.1.2. Basic Characterization

As part of our basic characterization we carried out FTIR analyses in order to detect the formation of each of the components that constitute the hybrid material. In figure 7.4, we show the FTIR spectra for the different $PPy/VOPO_4$ samples obtained by different synthetic routes. Bands from polypyrrole are marked with arrows, and the ones from $VOPO_4 \cdot 2H_2O$ with circles. First of all, observing the spectra for samples synthesized by the ultrasound method (E1PVP and E2PVP), we could not clearly detect the set of vibrational modes belonging to polypyrrole, indicating its absence. On the other hand, in samples synthesized by the chemical method (E3PVP and E3PVP0^o) the presence of polypyrrole was confirmed. These vibrational modes are present at 788 cm^{-1} (assigned to C-H off-plane vibration), at 1043-1046 cm^{-1} (C-H and N-H in-plane vibration), at 1174-1179 cm^{-1} (ring vibrations), at 1290-1297 cm^{-1} (C-H

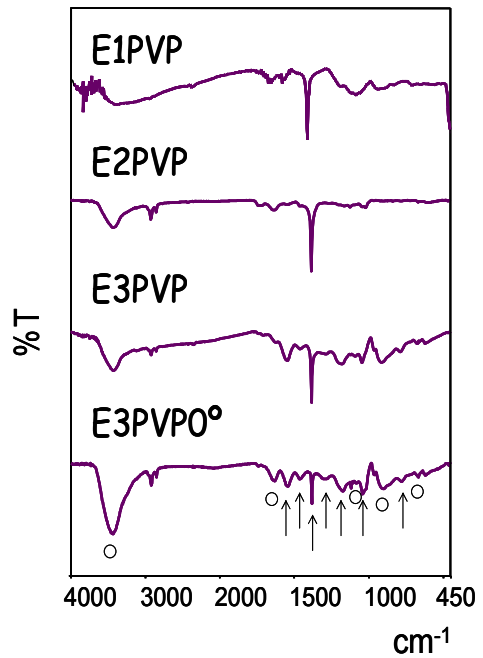

Figure 7.4.- FTIR spectra of $PPy/VOPO_4$ hybrid samples, synthesized by different methods. The arrows indicate the stretching modes of PPy present in the hybrid and the circles the ones belonging to $VOPO_4$ and H_2O.

vibrations), at 1384 cm^{-1} and 1458-1465 cm^{-1} (corresponding in both cases to C=C/C-C and C-N ring vibrations), and finally at 1542-1546 cm^{-1} (C=C/C-C stretching). In the spectra of all samples we can observe a sharp intense band at 1384 cm^{-1}, that decreases its intensity in going from samples E1PVP, E2PVP, to E3PVP, to sample E3PVP0^{o} coinciding with the formation of polypyrrole in that order. This band could point to the possible overoxidation of pyrrole, an unwanted product leading to a variety of by-products resulting from oxidative addition which have been reported to form under certain conditions during the synthesis of PPy in aqueous media [20].

On the other hand the vibrational modes of the inorganic matrix are present at 1078 cm^{-1} (weak band ν_3 asymmetric stretching for P-O), at 906 cm^{-1} (for V=O stretchings, V-OH, and ν_1 symmetric stretching for P-O, are overlapped), at 669 cm^{-1} (δ V-OH or P-OH), and the bending mode related to O-P-O at 571 cm^{-1} is weak and not clearly detected here. Finally, we find characteristic water peaks at 3432-3436 cm^{-1} for (H-O stretching), and at 1633 cm^{-1} (H-O-H bending).

Also as part of basic characterization we carried out powder XRD analyses in order to obtain structural data for our samples. With this analysis we can determine the formation or presence of specific $VOPO_4$ phases, or amorphous materials, and their intercalation properties. In figure 7.5 we show the diffraction patterns of the four synthesized PPy/$VOPO_4$ samples. At first glance, we observe the greatest difference between the first sample (using pre-formed $VOPO_4$) and the other three. Thus, the diffraction pattern from sample E1PVP (with no PPy formation according to FTIR) showed sharper peaks belonging to the crystalline α_{II}-$VOPO_4 \cdot H_2O$ phase, with apparent preferential orientation. The 001 plane that corresponds to the c spacing perpendicular to the layers is present at $2\theta=14^{o}$ (6.3 Å spacing) indicating the intercalation of only one water molecule. On the other hand, samples E2PVP, E3PVP and

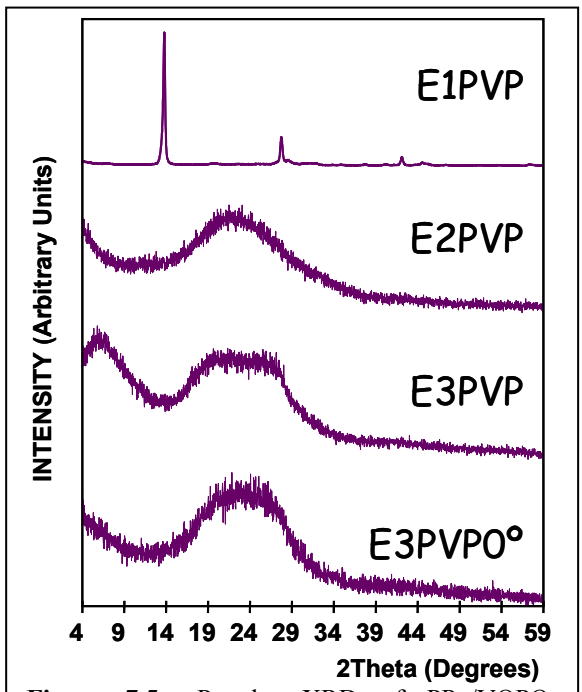

Figure 7.5.- Powder XRD of PPy/$VOPO_4$ samples synthesized with different methods.

E3PVP0^{o} with just very broad diffuse scattering peaks indicate the presence of essentially amorphous phases. Among these three samples, only E3PVP shows any sign of intercalation in the form of an otherwise very broad peak at low angles ($2\theta=5^{o}$, with a spacing of 14 Å), indicating that the formed PPy was indeed intercalated. For sample E3PVP0^{o} synthesized by the chemical method (and containing polypyrrole according to FTIR data). The lack of diffraction peaks and any long-range order indicates that polypyrrole is not intercalated in an orderly way between layers of $VOPO_4{\cdot}2H_2O$, instead it is probably segregated from $VOPO_4$ phase forming a nanocomposite amorphous hybrid.

Based on these two basic characterization techniques, we can conclude that the chemical method worked more efficiently for the incorporation of PPy into $VOPO_4$ – based materials, whether intercalated or segregated. In all cases the resulting materials are very poorly crystalline or amorphous.

7.3.1.3. Electrochemical Characterization

We carried out the electrochemical characterization in rechargeable Li cells for only the samples synthesized with the chemical method, where PPy was formed. The powder composite cathodes were fabricated by thoroughly mixing 30% weight of super-P carbon with 70% of our hybrid samples (E3PVP and E3PVP0^{o}). Thorough grinding was avoided in order to prevent the decomposition of vanadyl phosphate. The cells were assembled in the dry box and tested by using a charge-discharge current density of I=5 mA/g, between a voltage range of 2.1 V and 3.8 V. In figure 7.6 we show the first discharge-charge cycle for both samples resulting initially in low specific charge values. In the case of sample E3PVP the specific charge value was 37 Ah/Kg, and for sample E3PVP0^{o}, 41 Ah/Kg. Only in the case of sample E3PVP0^{o} the cell could be properly recharged up to 3.8 V. Thus, sample E3PVP0^{o} synthesized by the chemical method at 0^{o}C had the best synthetic conditions for the

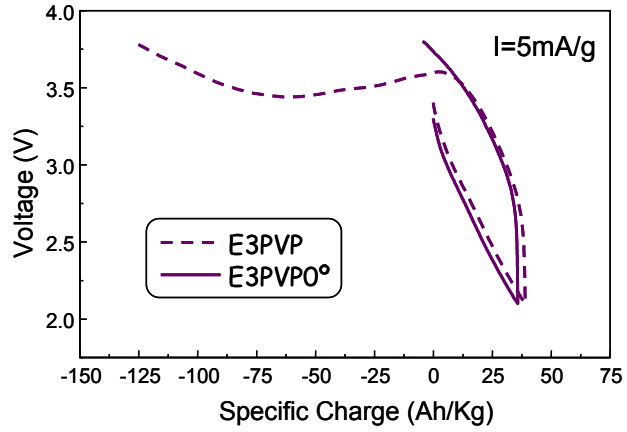

Figure 7.6.- First charge-discharge cycle for PPy/ $VOPO_4$ hybrid samples, synthesized by the chemical method at different temperatures.

formation of PPy/$VOPO_4$ hybrid with better recharge characteristics in lithium reversible cells.

7.3.2. Optimization of reaction time

From the data presented so far, sample E3PVP0^o synthesized by the chemical method at 0^{o}C in 5 days was the one that resulted in a hybrid material with better electrochemical performance compared to derivatives obtained by other synthetic routes. We carried out successive optimization procedures based on the various synthetic parameters used for the chemical synthesis (E3PVP0^o). In this section we present the optimization of the reaction time parameter, with the other conditions used for sample E3PVP0^o as the basis.

7.3.2.1. Synthesis

We carried out five experiments applying different reaction time periods as shown in table VII.I., while maintaining constant the remaining parameters. The synthesis was carried out as follows: an acidic suspension of $VOPO_4 \cdot 2H_2O$ (0.9508 g in a solution of 0.62 ml $HClO_4$ risen to 50 ml) was set-up in an ice bath with magnetic stirring at 500 rpm, and then a pyrrole solution (1 ml risen to 50 ml with deionized water) was slowly added. We used a molar ratio of pyrrole: $VOPO_4 \cdot 2H_2O$ of 3:1. When the reaction time was over, we filtered off the solids, washed them with deionized water, and dried them under vacuum for 3 days.

Table VII.I.- Reaction time applied for each sample

Sample	Reaction time
PVP34	4 days
PVP33	3 days
PVP32	2 days
PVP33h	3 hours
PVP31h	1 hour

7.3.2.2. Basic Characterization

In figure 7.7 we show the spectra for PPy/$VOPO_4$ samples synthesized by using different periods of time, where we can detect the bands assigned to polypyrrole (at 669-790 cm^{-1}, 1037-1048 cm^{-1}, 1163-1181 cm^{-1}, 1299-1318 cm^{-1}, 1384 cm^{-1}, and, at 1450-1466 cm^{-1} and 1542-1550 cm^{-1}). In addition, we can detect a weak peak at 1705 cm^{-1} (marked with a bigger arrow) only for the case of sample PVP32 (synthesized in 2 days). This band is assigned to C=O stretching, indicating over-oxidation of polypyrrole. On the other hand, vibrational modes for the inorganic matrix are detected (at 1089-1090 cm^{-1}, 890-906 cm^{-1}, 960-966 cm^{-1}, 669-678 cm^{-1}, and at 613-625 cm^{-1})

as well as bands belonging to hydration water (at 3424-3458 cm^{-1}, and 1629-1635 cm^{-1}).

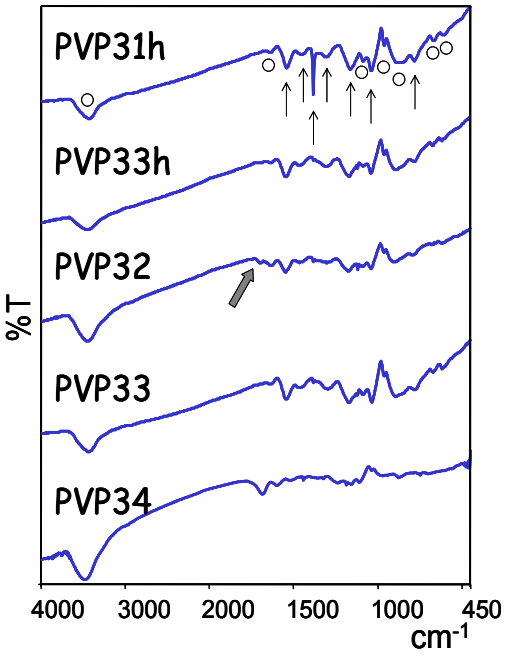

Figure 7.7.- FTIR spectra of $PPy/VOPO_4$ hybrid samples, synthesized in different reaction times. The arrows indicate the vibrational modes for PPy, and circles the ones from $VOPO_4$ and H_2O.

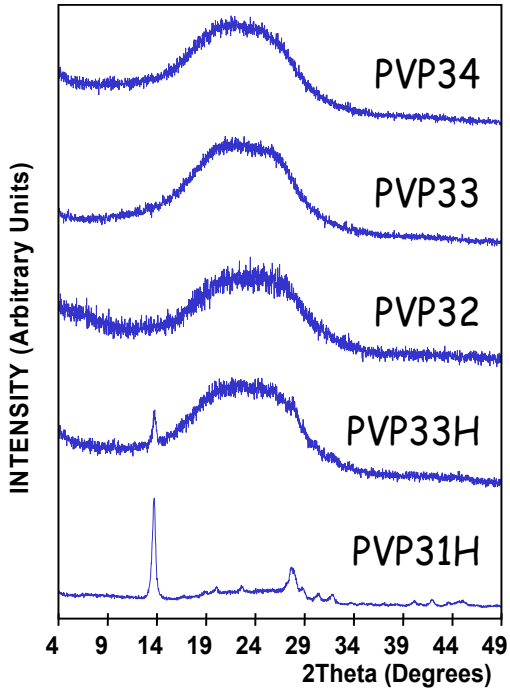

Figure 7.8.- Powder XRD of $PPy/VOPO_4$ hybrids samples, synthesized in different reaction times.

In figure 7.8 we show the diffraction patterns for this new series of $PPy/VOPO_4$ samples, where we can appreciate the evolution of crystallinity with reaction time. As the reaction time decreases, in going from samples PVP34, PVP33, PVP32, PVP33H, to PVP31H, the materials present a more crystalline profile as seen in sample PVP31H (synthesized in 1 hour), indicated by the presence of narrower peaks. In samples synthesized by using a shorter reaction time (PVP33H 3 hours, PVP31H 1 hour) a peak at $2\theta=13.7^{o}$ can be detected with a spacing of 6.4 Å. This spacing indicates the intercalation of just one water molecule, implying that polypyrrole has not been inserted in the interlayer spacing in those cases and therefore must be segregated from the inorganic matrix.

7.3.2.3. Electrochemical Characterization

We carried out the electrochemical characterization for this series of $PPy/VOPO_4$ samples in rechargeable lithium cells. The tests of our composite cathodes (30%

carbon super-P and 70% of hybrid) were carried out by using a discharge-charge current density of I=5 mA/g, between voltages of 2.1 V and 3.8 V vs. Li anodes. In figure 7.9 we show the first charge-discharge curves for all samples, where we can detect a tendency with the reaction time used during the syntheses. As the reaction time decreases (PVP34> PVP33> PVP32> PVP33H> PVP31H), the initial specific charge is increased. The highest specific charge was obtained for sample PVP31h (97 Ah/Kg) synthesized in one hour. The remaining samples resulted in specific charges of: 52 Ah/Kg for sample PVP34 (synthesized in 4 days), 53 Ah/Kg for PVP33 (synthesized in 3 days), 38 Ah/Kg for PVP32 (synthesized in 2 days), and 65 Ah/Kg for PVP33h (synthesized in 3 hours). The maintenance of the initial specific charge value essentially unchanged through 10 charge-discharge cycles indicated good reversibility properties.

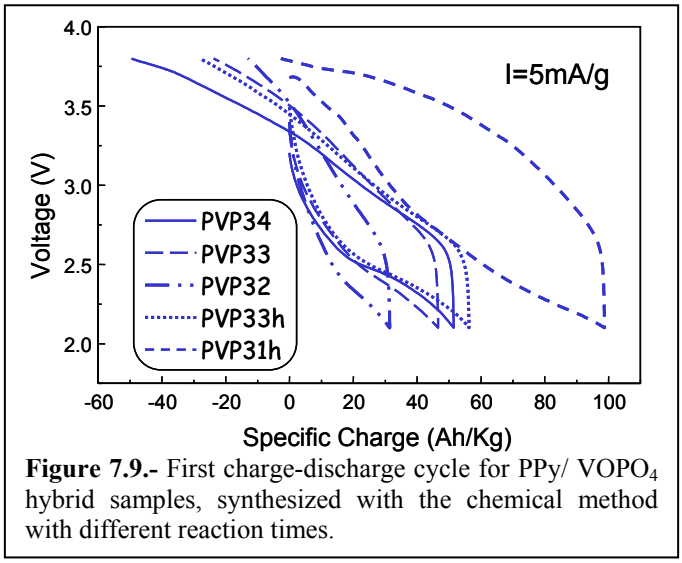

Figure 7.9.- First charge-discharge cycle for PPy/ $VOPO_4$ hybrid samples, synthesized with the chemical method with different reaction times.

Summarizing, we can conclude that by decreasing the reaction time during the synthesis, more specific charge can be obtained during discharge.

7.3.3. Optimization of the order of addition of the reagents

The next optimization step plays with the order of addition of the regents. The chemical syntheses followed for this optimization was based on parameters similar to those used in sample PVP31h (synthesized in one hour by adding the pyrrole solution to the acidic ($HClO_4$) suspension of $VOPO_4 \cdot 2H_2O$), which resulted in a PPy/$VOPO_4$ hybrid material with the highest initial specific charge so far(97 Ah/Kg). We did however modify the nominal ratio of reagents in order to avoid the use of excess pyrrole which was suspected to be detrimental.

7.3.3.1. Synthesis

We carried out three experiments varying the order of addition of the reagents, keeping constant the following factors: molar ratio of pyrrole: $VOPO_4{\cdot}2H_2O$:$HClO_4$ (1:1:1), using magnetic stirring at 500 rpm in an ice bath during 1 hour of synthesis. The samples that we synthesized were: PVP11A, where pyrrole solution (0.5 ml risen up to 50 ml with deionized water) was added to the acidic suspension of $VOPO_4{\cdot}2H_2O$ (1.42 g suspended in a solution of 0.62 ml of $HClO_4$ risen to 50 ml with deionized water); PVP11B, pyrrole/$HClO_4$ solution (0.5 ml of pyrrole risen to 50 ml with a solution consisting of 0.62 ml of $HClO_4$ risen to 50 ml with deionized water) was added to the aqueous suspension of $VOPO_4{\cdot}2H_2O$ (1.42 g in 50 ml of deionized water); and finally PVP11C, where in this case the acid was divided in two parts, one for the solution with pyrrole (0.5 ml of pyrrole risen to 50 ml with a solution consisting of 0.31 ml of acid risen to 50 ml with deionized water) and the other for the suspension of $VOPO_4{\cdot}2H_2O$ (1.42 g of vanadyl phosphate suspended in 50 ml of a solution of 0.31 ml of $HClO_4$ risen to 50 ml with deionized water). In this last sample (PVP11C) the acidic pyrrole solution was added to the acidic $VOPO_4{\cdot}2H_2O$ suspension. After the reaction time was completed (1h in all cases), we filtered off the solids, washed them with deionized water, and dried them under vacuum for 3 days.

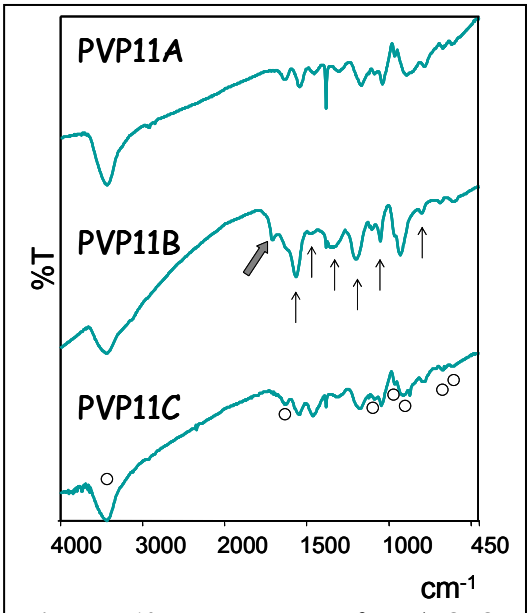

Figure 7.10.- FTIR spectra of PPy/$VOPO_4$ hybrids samples, synthesized with different addition order. The arrows indicate the vibrational modes of PPy present in the material and the circles the ones corresponding to $VOPO_4$ and H_2O.

7.3.3.2. Basic Characterization

In figure 7.10 we show the FTIR spectra for the three new PPy/$VOPO_4$ samples. We can observe that in all samples bands correspondent to polypyrrole formation are present (at 786-796 cm^{-1}, 1042-1049 cm^{-1}, 1168-1183 cm^{-1}, 1302-1320 cm^{-1}, 1382 cm^{-1}, 1458-1468 cm^{-1}, and at 1544-1551 cm^{-1}). In addition, in sample PVP11B we can detect the peak at 1703 cm^{-1} (marked with a bigger arrow) indicative of polypyrrole overoxidation (i.e C=O). On the other hand, bands of the inorganic phase are present (at 1089-1096 cm^{-1}, 898-916 cm^{-}

[1], 966 cm^{-1}, 674-681 cm^{-1}, and at 608-616 cm^{-1}). Finally, hydration water bands were detected in all samples (3427-3434 cm^{-1}, and 1635 cm^{-1}).

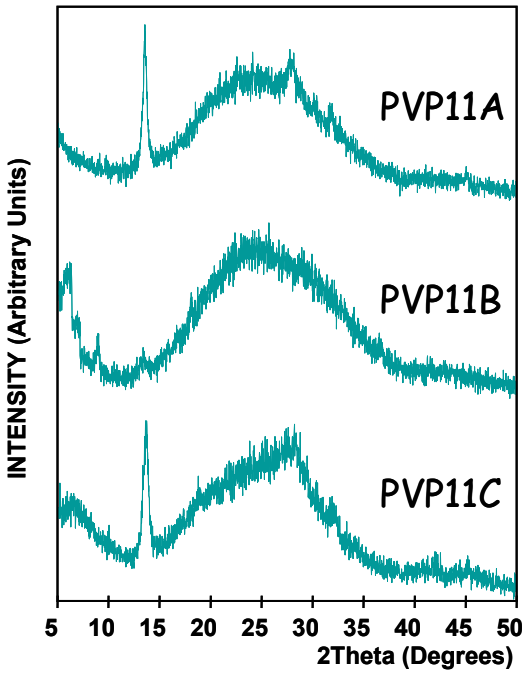

Figure 7.11.- Powder XRD of $PPy/VOPO_4$ hybrids samples, synthesized by changing the order of addition of the reagents.

In figure 7.11 we show the diffraction patterns of these three $PPy/VOPO_4$ hybrid samples. The diffraction patterns are typical of amorphous solids, where peaks corresponding to the c spacing of a crystalline phase are present. In sample PVP11A (addition of pyrrole solution to the acidic $VOPO_4 \cdot 2H_2O$ suspension), the c spacing appears at $2\theta=13.6^o$ (6.5057 Å) as a sharper peak indicating the presence of one intercalated water molecule (i.e. α_{II}-$VOPO_4 \cdot H_2O$ phase). Therefore, PPy was not intercalated in these samples, but instead was segregated from the inorganic matrix. Sample PVP11C also shows the same peak from crystalline α_{II}-$VOPO_4 \cdot H_2O$ but in addition, a much wider additional peak displaced to lower angles is observed ($2\theta=6.5^o$, 13.6 Å). A similarly wide peak is found for sample PVP11B ($2\theta=6.0^o$, 14.7 Å). Thus, we can conclude that for samples where pyrrole was first protonated (with half or a whole equivalent of $HClO_4$), before being added to the $VOPO_4 \cdot 2H_2O$ suspension, materials with PPy inserted between the layers of the inorganic matrix were obtained. Nevertheless, we have to mention that in the case of sample PVP11B, we can observe three narrower and less intense peaks at low angles that show different insertion degrees or phases.

7.3.3.3. Electrochemical Characterization

We carried out the testing in lithium cells of the $PPy/VOPO_4$ samples (30% carbon super-P and 70% hybrid) synthesized by changing the addition order of the reagents. The conditions used were using a charge-discharge current density of I=10 mA/g, between a voltage range of 2.1 V and 3.8 V. In figure 7.12, we show the first charge-discharge cycles carried out. The highest specific charge observed was for

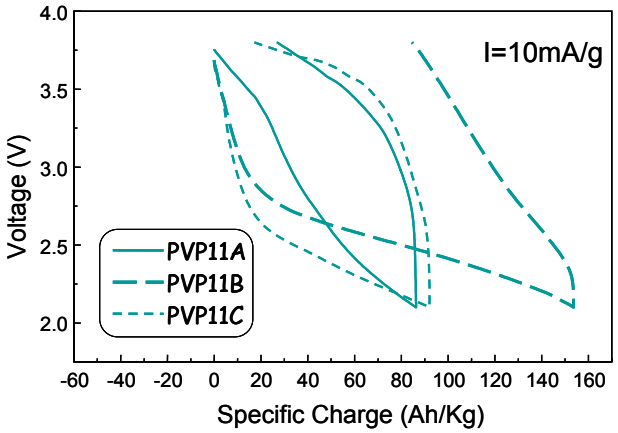

Figure 7.12.- First charge-discharge cycle for PPy/ $VOPO_4$ hybrid samples, synthesized by changing the order of addition of the reagents.

sample PVP11B of 157.23 Ah/Kg. The other two samples resulted in 86 Ah/Kg for PVP11A, and 91 Ah/Kg for PVP11C. During the recharge of the cells, the specific charge values are not completely recovered. This irreversible capacity is more pronounced precisely for sample PVP11B. On the other hand, after this first cycle the specific charge values get stabilized at lower values (for PVP11A at 65 Ah/Kg, for PVP11B at 70 Ah/Kg, and for sample PVP11C at 55 Ah/Kg).

We can conclude based on this electrochemical data that by adding first the pyrrole in its totally protonated state (with acid as in PVP11B), a hybrid results in which PPy is well formed and inserted between the layers of the inorganic phase, with a higher initial specific charge value but with a relatively large irreversible capacity. This series of experiments underscore the importance of the protonation state of pyrrole and the order of addition of reagents in this type of polymerization reactions.

7.3.4. Optimization of the $HClO_4$ molar ratio.

Despite its large irreversible capacity, sample PVP11B (where pyrrole was first protonated) was the one selected for our next parameter optimization in consideration of its higher specific charge value both before and after stabilization. In this section we have carried out the optimization based on the amount of acid used to protonate pyrrole in the synthesis.

7.3.4.1. Synthesis

We have carried out three experiments varying the molar ratio of $HClO_4$ respect to pyrrole and $VOPO_4 \cdot 2H_2O$ (see table VII.II). We kept constant the following parameters: the order of addition was carried out by first adding the acidic pyrrole solution (0.5 ml of pyrrole risen to 50 ml with the solution made with the corresponding amount of acid risen to 50 ml) to the $VOPO_4 \cdot 2H_2O$ suspension (1.42 g in 50 ml of

water) in an ice bath with magnetic stirring at 500 rpm, letting it react for 1 hour. P11c2 sample had some differences from sample P11b2, where the same amount of acid was used.

Table VII.II.- Experiments to synthesize PPy/$VOPO_4$ hybrids with different $HClO_4$ quantities.

Sample	Molar ratio ($Py:VOPO_4.2H_2O:HClO_4$)	$HClO_4$ ml in 50 ml solution
P11b15	(1:1:1.5)	0.93 ml
P11b2	(1:1:2)	1.24 ml
P11c2	(1:1:2)	1.24 ml

For sample P11c2 the total amount of acid was divided in two equal parts (as in sample PVP11C): one for the pyrrole solution (0.62 ml of $HClO_4$) and the other part for the $VOPO_4{\cdot}2H_2O$ suspension (0.62 ml of $HClO_4$). After the reaction time was completed, we filtered off the solids, washed them with deionized water, and dried them under vacuum for 3 days.

7.3.4.2. Basic Characterization

In figure 7.13 we show the spectra of the three newer PPy/$VOPO_4$ samples. Surprisingly, no PPy was formed for samples P11b2 and P11c2 (i.e. with excess acid), independently of how the acid was added. The only sample where the FTIR fingerprint of PPy is present was P11b15 (at 778 cm^{-1}, 1038 cm^{-1}, 1168 cm^{-1}, 1302 cm^{-1}, 1382 cm^{-1}, 1461 cm^{-1}, and at 1541 cm^{-1}). In addition, sample P11b15 shows the characteristic bands of the inorganic phase (at 1089 cm^{-1}, 879 cm^{-1}, 966 cm^{-1}, 670 cm^{-1}, and at 602 cm^{-1}.), and also we can detect the presence of hydration water (at 3427-3449 cm^{-1} and 1635 cm^{-1}).

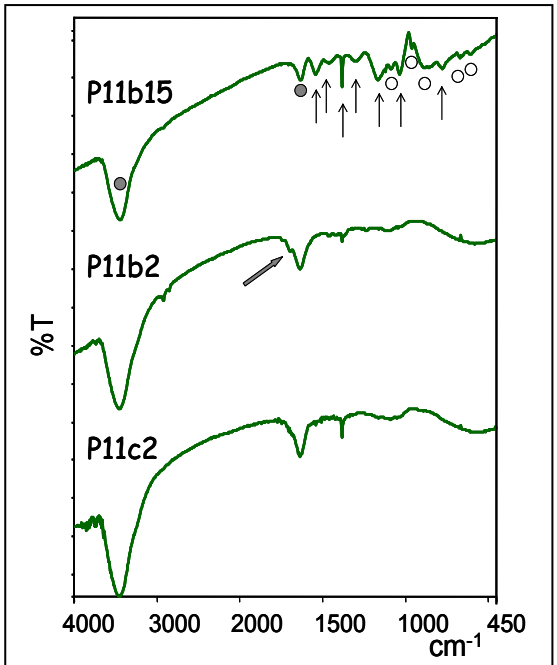

Figure 7.13.- FTIR spectra of PPy/VOPO4 hybrid samples, synthesized with different amounts of acid. The arrows indicate the bands of PPy present in the material and the circles the ones corresponding to $VOPO_4$ and H_2O.

In figure 7.14 we show the powder XRD patterns of these three samples, which are amorphous with the presence of same crystalline α_{II}-$VOPO_4{\cdot}H_2O$ phase indicated by the sharper peak at $2\theta=13.7^{o}$ (6.4 Å). Only for sample P11b15 a very broad feature close to 5º in 2theta hints the presence of PPy inserted into $VOPO_4$ slabs.

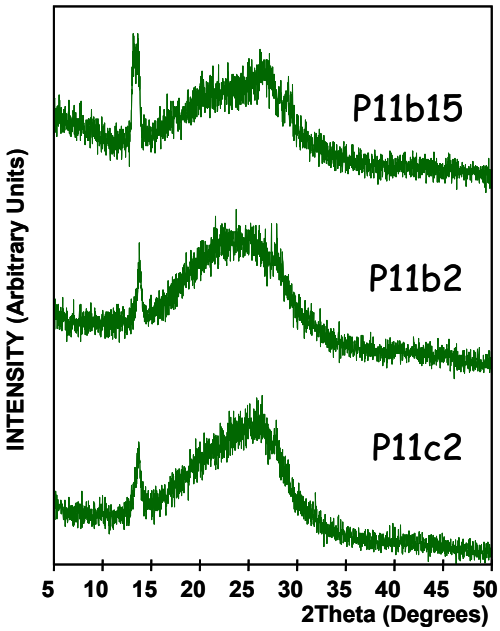

Figure 7.14.- Powder XRD of PPy/$VOPO_4$ hybrid samples, optimized according to the acid molar ratio.

7.3.4.3. *Electrochemical Characterization*

In figure 7.15 we show the first charge-discharge cycle in lithium cells carried out for all our three new powder samples, and sample PVP11B for comparison, (30% carbon super-P and 70% hybrid material) using a charge-discharge current density of I=10 mA/g, between a voltage range of 2.1 V and 3.8 V. The initial specific charge values for the new samples are more or less similar (85 Ah/Kg for P11b15, 80 Ah/Kg for P11b2, and 79 Ah/Kg for P11c2), but they are lower than the value for sample PVP11B (with a molar ratio for Py:$VOPO_4.2H_2O$:$HClO_4$ of 1:1:1). The cyclability properties for sample P11b15 were relatively good between the potential range used. On the other hand, the other two samples (P11b2 and P11c2) during the 2nd. recharge cycle, could not reach the 3.8 V (only up to 3.5V), which was not surprising considering that by

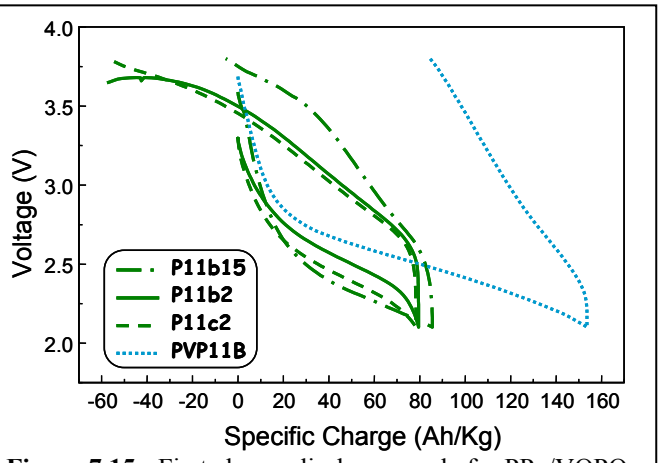

Figure 7.15.- First charge-discharge cycle for PPy/$VOPO_4$ hybrid samples, synthesized by changing the acid molar ratio. We include PVP11B sample for comparison.

using more acid in the synthesis, PPy was not well formed. Although, in these set of new samples, P11b15 was the one that could cycle between the voltage range applied, this optimization (based on the acid molar ratio) did not represent an improvement. By increasing the molar ratio of the acid from 1 to 1.5 and to 2, PPy is over-oxidized or not formed.

Therefore, sample PVP11B (obtained from the optimization of the addition order of the reagents) with higher initial specific charge was the one selected for the next optimization step based on the amount of nominal pyrrole in the reaction mixture.

7.3.5. Optimization of the pyrrole to vanadyl phosphate ratio

In this section, we present our results for the optimization based on the pyrrole: vanadyl phosphate nominal ratio used during the synthesis. We study how this optimization step influences the total amount of PPy in the hybrid, and also on their performance in Li cells. As we have just mentioned, sample PVP11B chemically synthesized using a molar ratio for $HClO_4$:Py of (1:1), adding first the protonated pyrrole solution to the $VOPO_4{\cdot}2H_2O$ suspension, was the one selected for the optimization of the amount of nominal pyrrole.

7.3.5.1. Synthesis

We have carried out four experiments varying the nominal amount of pyrrole used in the synthesis (together with the corresponding amount of acid), keeping constant the following factors: the acidic solution of pyrrole (0.5 ml of pyrrole risen with a solution of 0.62 ml of $HClO_4$ risen to 50 ml volume with deionized water) was added during 3 minutes to the suspension of $VOPO_4{\cdot}2H_2O$ (amount of table VII:III in 50 ml), using an ice bath with magnetic stirring at 500 rpm, and a reaction time of 1 hour. The samples that we synthesized are shown in table VII.III. After the reaction time was completed we filtered off the solids, washed them with deionized water, and dried them under vacuum for 3 days.

Table VII.III.- PPy/$VOPO_4$ hybrids synthesized using different molar ratios.

Sample	Molar ratio (Py:$VOPO_4.2H_2O$:$HClO_4$)	$VOPO_4.2H_2O$ amount in 50 ml suspension
PVP14	(4:1:4)	0.355 g
PVP13	(3:1:3)	0.4734 g
PVP12	(2:1:2)	0.71 g
PVP1-5	(0.5:1:0.5)	2.84 g

7.3.5.2. Basic characterization

FTIR spectra for these samples are presented in figure 7.16, were we include the spectrum of sample PVP11B (molar ratio of 1:1:1) for comparison. In general, we can observe that they all present the vibrational modes of polypyrrole (782-793 cm^{-1}, 1046-1049 cm^{-1}, 1172-1179 cm^{-1}, 1313-1317 cm^{-1}, 1378-1382 cm^{-1}, 1465-1468 cm^{-1}, and at 1548-1551 cm^{-1}) and to $VOPO_4$ (1089-1093 cm^{-1}, 898-905 cm^{-1}, 963-9666 cm^{-1}, 674 cm^{-1}, and at 601-608 cm^{-1}). On the other hand, we cannot rule out the existence of a band at 1700 cm^{-1} belonging to C=O formation in all samples, indicating an over-oxidation of PPy. In addition, the presence of water can be detected in the spectra (3427-3434 cm^{-1} and 1627-1635 cm^{-1})

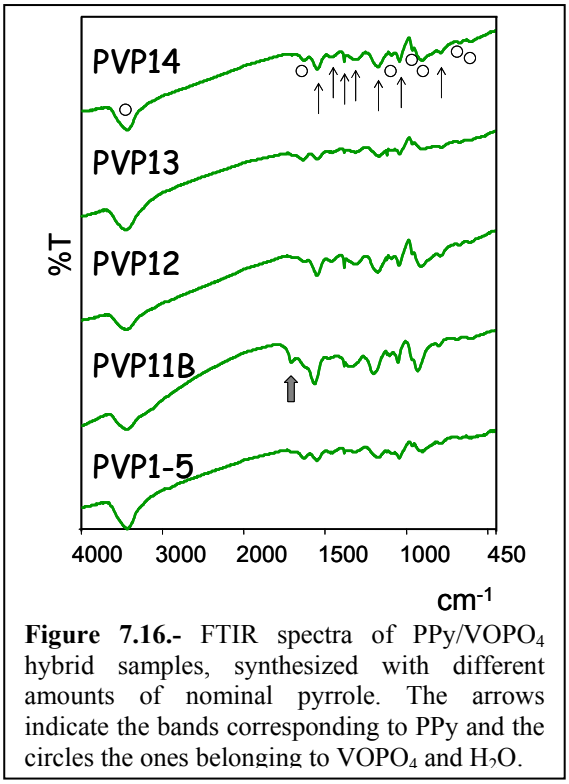

Figure 7.16.- FTIR spectra of PPy/$VOPO_4$ hybrid samples, synthesized with different amounts of nominal pyrrole. The arrows indicate the bands corresponding to PPy and the circles the ones belonging to $VOPO_4$ and H_2O.

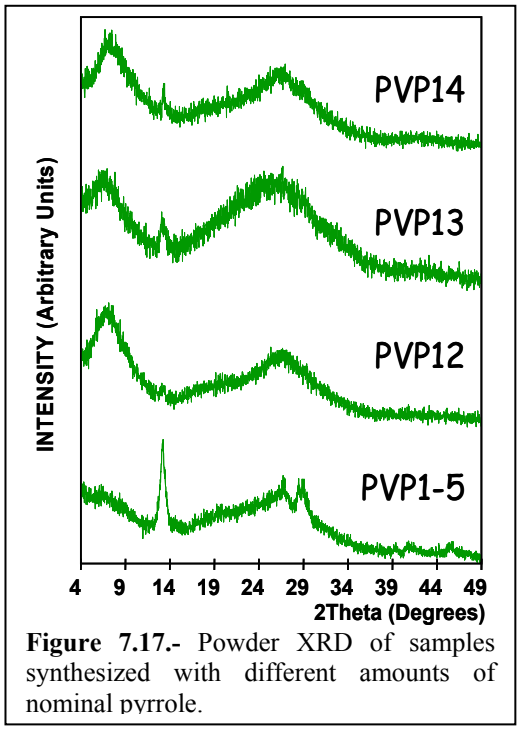

Figure 7.17.- Powder XRD of samples synthesized with different amounts of nominal pyrrole.

In figure 7.17 we show the diffraction patterns of these four samples. All samples are essentially amorphous, but a wide peak can be detected at low angles at $2\theta=6.66^{o}$-7.26^{o} (12.16-13.26 Å), depending on the sample, indicating the insertion of polypyrrole. In addition, variable small amounts of α_{II}-$VOPO_4 \cdot H_2O$ phase can be detected as impurities in some samples, most notably in sample PVP1-5 (2θ= 13.28^{o}, 6.66 Å for PVP14, 13.12^{o}, 6.74 Å for PVP13, and $2\theta=13.16^{o}$, 6.72 Å for PVP1-5).

7.3.5.3 Physical-chemical Characterization

In order to characterize in more detail our hybrid samples, we will present in this section an extended study by using physical-chemical characterization methods. These methods are Scanning Electron Microscopy (SEM), and ambient resistivity measurements by the Van der Pauw method.

7.3.5.3.1. Scanning Electron Microscopy (SEM)

We have carried out SEM photographs of samples synthesized with different amounts of pyrrole (PVP14, PVP13, PVP12, PVP11B, and PVP1-5). In figure 7.18 we show the series of photographs carried out at the same magnification. We should note that higher magnifications were attempted but charging of the sample took place and it was not possible to get sharp images at higher resolution.

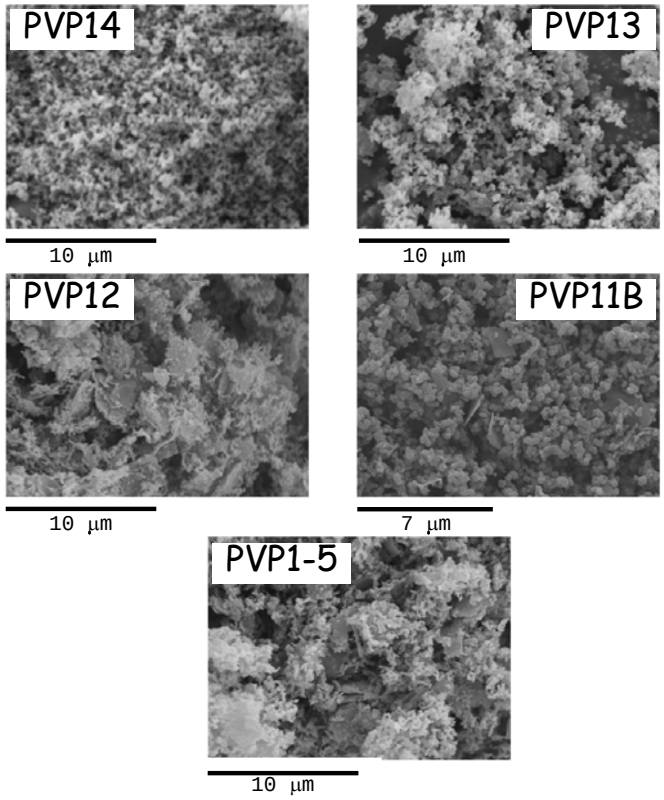

Figure 7.18.- SEM photographs of the samples synthesized with different amount of nominal pyrrole. We also include sample PVP11B.

Without trying to do a quantitative analysis or a correlation with their basic characterization for the different SEM images, we can only say that in all cases we can detect the presence of two phases. These two phases show very different

morphologies, there are some very flat plates, mixed among predominating smaller globular particles. The plates conform to the well known morphology of $VOPO_4$ and therefore correspond most likely to the crystalline vanadyl phosphate imputirities with no intercalated PPy which were also detected by XRD.

7.3.5.3.2. Resistivity Measurements

We carried out resistivity measurements at room temperature by using the Van der Pauw method for all these hybrid samples (PVP14, PVP13, PVP12, PVP11B, PVP1-5), in order to estimate their conductivity. In table VII.IV we show the conductivity values obtained for each sample.

Table VII.IV.- Values of the conductivity calculated from the resistivity measurements made at room temperature.

Sample	Py:$VOPO_4$	Conductivity σ (S/cm)
PVP14	(4:1)	$3.14x10^{-4}$
PVP13	(3:1)	$2.07x10^{-3}$
PVP12	(2:1)	$1.12x10^{-6}$
PVP11B	(1:1)	$9.05x10^{-5}$
PVP1-5	(0.5:1)	$3.34x10^{-3}$

We could not detect any obvious correlation between the conductivity values obtained for the different samples and their synthetic parameters. This seems to point out to the existence of some additional factors affecting the microstructure and the conductivities of these materials in addition to the ones controlled in our experiments. We haven't been able either to correlate these values with the possible overoxidation of the corresponding samples. Furthermore, the conductivity values are small in comparison with conventional PPy samples indicating that it might be the vanadyl phosphate the component limiting the conductivity in the hybrid.

7.3.5.4. Stoichiometry determination

We carried out different chemical analyses in order to establish the stoichiometry of our hybrid samples. These analyses were: TGA to have a general idea of the hybrid composition, elemental analysis to determine the organic matter, and ICP to determine the amounts of V and P in the hybrid samples.

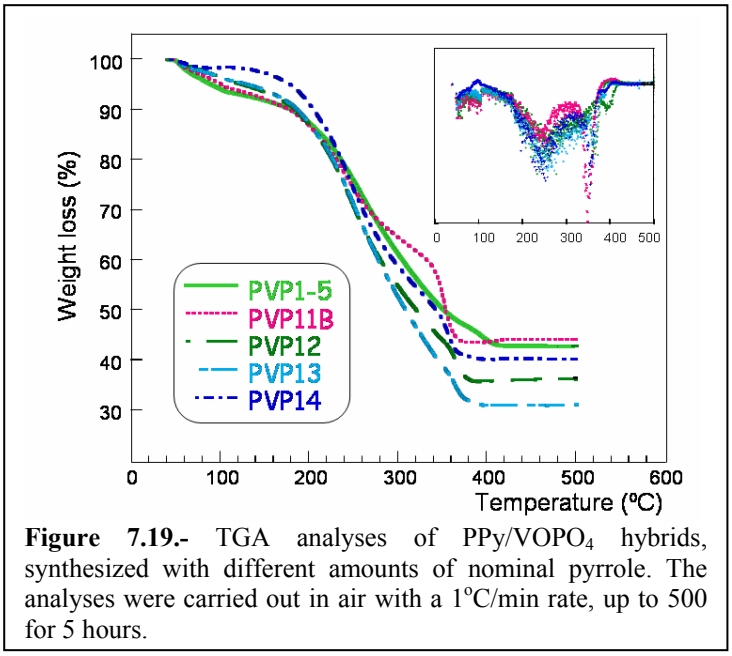

Figure 7.19.- TGA analyses of $PPy/VOPO_4$ hybrids, synthesized with different amounts of nominal pyrrole. The analyses were carried out in air with a 1°C/min rate, up to 500 for 5 hours.

Thermogravimetric analyses (TGA) were carried out to determine the amount of residual inorganic mater, and to have an idea of the organic mater and hydration water present in each hybrid sample. In figure 7.19 we can observe the TGA analyses corresponding to $PPy/VOPO_4{\cdot}2H_2O$ hybrid samples synthesized by using different amounts of pyrrole. The analyses were carried out in air by heating with a 1 °C/min rate up to 500 °C keeping this temperature for 5 hours. We can observe three weight losses (see inset): a small one between 80-100 °C corresponding to loosely bound hydration water, at 250 °C, corresponding to the combustion of the polymer, and at 350 °C corresponding to the decomposition of the inorganic phase. The remaining weight percent corresponds to residual V_2O_5 crystalline phase, which was verified by XRD (not presented here). For each sample these vanadium pentoxide residues were different: 43% for PVP1-5, 44.2% for PVP11B, 36.5% for PVP12, 31.2% for PVP13, and 40.3% for PVP14. At first glance there is not a proportional increase in organic matter lost during heating in comparison with the nominal amount of pyrrole used during synthesis. Thus, the possibility that by adding more pyrrole in the synthesis we could get more polypyrrole in the hybrids, is not confirmed by the TGA data.

The proposed stoichiometries of these $PPy/VOPO_4{\cdot}2H_2O$ hybrid samples were calculated based on elemental analyses and ICP. In table VII.V we present the summarized data of these analyses and the proposed formulas.

Table VII.V.- Summarized data of the chemical analysis and tentative formulas of each PPy/$VOPO_4{\cdot}2H_2O$ hybrid samples.

	Py: $VOPO_4$	%C	%N	%H	%V	%P	$\%V_2O_5$	Formula[(1)]	sample
Exp	(0.5:1)	26.96	7.75	2.60	13.89	5.70		$PPy(VOPO_4)_{0.33}(V_2O_5)_{0.08}2.6H_2O$	**PVP1-5**
Cal		26.70	7.78	4.59	13.87	5.68	8.08	FW=179.89	
Exp	(1:1)	29.20	8.50	2.40	19.61	1.70		$PPy(VOPO_4)_{0.09}(V_2O_5)_{0.27}1.96H_2O$	**PVP11B**
Cal		29.28	8.53	4.25	19.56	1.69	29.93	FW=164.06	
Exp	(2:1)	34.33	9.87	2.79	15.22	1.58		$PPy(VOPO_4)_{0.08}(V_2O_5)_{0.18}1.85H_2O$	**PVP12**
Cal		33.34	9.72	4.68	15.55	1.71	22.72	FW=144.09	
Exp	(3:1)	37.23	10.69	3.00	11.93	2.22		$PPy(VOPO_4)_{0.09}(V_2O_5)_{0.11}1.75H_2O$	**PVP13**
Cal		36.62	10.67	4.99	12.03	2.12	15.25	FW=131.17	
Exp	(4:1)	34.28	9.81	2.66	15.36	1.45		$PPy(VOPO_4)_{0.07}(V_2O_5)_{0.18}1.87H_2O$	**PVP14**
Cal		33.63	9.80	4.75	15.33	1.51	22.92	FW=142.83	

(1) V_2O_5 stoichiometries indicate just formal contents, do not imply the presence of V_2O_5 as crystallographic phases (see text)

It should be noted that in the proposed formulas we have included variable amounts of V_2O_5 impurities. This was decided to account for the possible partial decomposition of vanadyl phosphate which was indicated by certain low values of phosphorus contents. This decomposition makes sense if we take into account that vanadyl phosphate is formed and is stable under acidic pH which could have been perturbed by the addition of pyrrole, in excess in several cases. In good agreement with this hypothesis, sample PVP1-5 synthesized by using the lowest amount of pyrrole, results in a lower decomposition degree of vanadyl phosphate. On the other hand, in figure 7.16 which shows the FTIR spectra for these samples, it is hard to detect bands associated to V_2O_5 (1020 cm^{-1} V=O, 760 cm^{-1} and 510 cm^{-1} for V-O-V). Therefore, we are including V_2O_5 coefficients merely as a way to indicate formal V contents (in V_2O_5 equivalents) coming from $VOPO_4$ decomposition. As it will be shown below, these impurities must correspond to undetermined cluster species which can be eliminated by washing with organic solvents.

7.3.5.5. Electrochemical Characterization

In figure 7.20, we show the first charge-discharge cycle carried out for all samples (30% carbon super-P, 70% hybrid) in lithium cells, including sample PVP11B (1:1 of Py:$VOPO_4{\cdot}2H_2O$) for comparison, analyzed by using a charge-discharge current density of I = 10 mA/g, between a voltage range of 2.1 V and 3.8 V. We have obtained different initial specific charge values, were the highest value was obtained

for sample PVP11B (157.23 Ah/Kg). The remaining samples resulted in specific charge values of 130 Ah/Kg for PVP14, 113 Ah/Kg for sample PVP13, 108 Ah/Kg for PVP12, and finally 100Ah/Kg for sample PVP1-5. In addition, we can detect again an irreversible capacity in all samples (observed in the recharge profile line that does not go back to the starting point), which is larger in the case of sample PVP11B. On the other hand, their cyclability properties after this initial cycle resulted in stabilized values after 10 cycles of 65 Ah/Kg for sample PVP14, 50 Ah/Kg for PVP13, 75 Ah/Kg for PVP12, 70Ah/Kg for sample PVP11B, whereas sample PVP1-5, could not reach the 3.8V during the second cycle recharge. In this last sample, the successive charge-discharge cycles were carried out by modifying the voltage range to 2.1-3.25V giving a stabilized value of specific charge of 50 Ah/Kg.

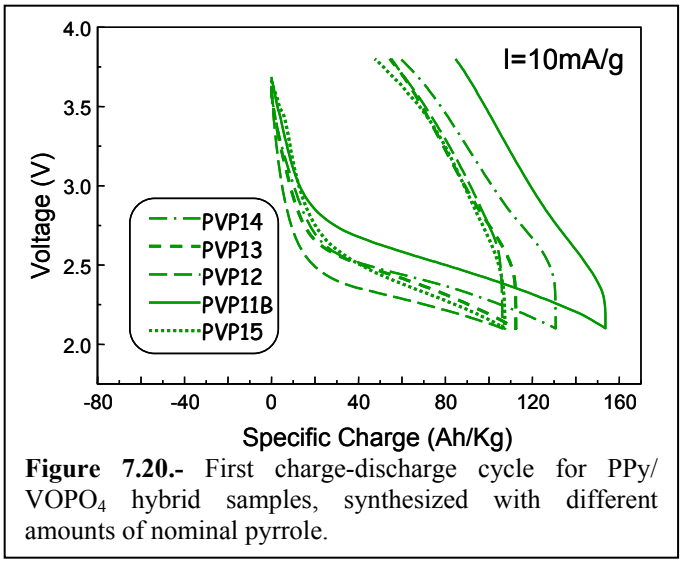

Figure 7.20.- First charge-discharge cycle for PPy/ $VOPO_4$ hybrid samples, synthesized with different amounts of nominal pyrrole.

Our hypothesis for the origin of this irreversible capacity rested on the possible presence of oxidation by-products which could be reduced in a first discharge process but were not reversible. Based on this hypothesis, we carried out the final optimization step over sample PVP11B (157 Ah/Kg), by applying successive washings with different organic solvents, to try to eliminate possible oxidation by-products.

7.3.6. Final Optimization and purification of PPy/$VOPO_4$ (sample PVP11B)

In this section we present the final optimization step carried out over sample PVP11B, chosen because it presented the best initial specific charge value and lower loss of its specific charge through cycling. We carried out the synthesis as previously explained in section 7.3.3.1., but after filtering off the solid and washing with deionized water, we washed with ethanol, acetone and with ethyl ether. We synthesized three samples: PVP11B2S with the additional washing with organic solvents, PVP11B (same sample of section 7.3.3.1) for comparison, and PVP11B2H synthesized with exactly the same conditions as for PVP11B to test its reproducibility. PVP11B2S (new

sample) was analyzed by FTIR obtaining the characteristic bands of polypyrrole (776 cm^{-1}, 1037 cm^{-1}, 1170 cm^{-1}, 1303 cm^{-1}, 1382 cm^{-1}, 1465 cm^{-1}, and 1546 cm^{-1}) with no indication of overoxidation, bands of $VOPO_4$ (1089 cm^{-1}, 964 cm^{-1}, 901 cm^{-1}, 673 cm^{-1}), and bands corresponding to hydration water (3431 cm^{-1}, 1631 cm^{-1}).

The X-ray diffraction pattern of this sample showed diffuse scattering typical of amorphous solids with only one sharp 001 peak at $2\theta=13.6^{o}$ (6.5Å), indicating the presence of α_{II}-$VOPO_4 \cdot H_2O$ phase as impurity, thus implying polypyrrole segregation instead of insertion between the slabs of the inorganic matrix.

We have carried out elemental analysis and ICP analysis in order to calculate the formula weight of sample PVP11B2S. The results for these analyses are shown in table VII.VI.

Table VII.VI.- chemical analysis and formula of the new PPy/$VOPO_4$ hybrid.

	Py: $VOPO_4$: $HClO_4$	%C	%N	%H	%V	%P	Formula[a]	Sample
Exp.	(1:1:1)	44.57	13.03	3.26	5.51	3.80	$PPy(VOPO_4)_{0.13} \cdot 1.1H_2O$	PVP11B2S
Calc.		44.92	13.09	5.84	6.19	3.76		

We measured the resistivity of these samples (PVP11B2H and PVP11B2S) by the Van der Pauw method, in order to estimate their corresponding conductivities, leading to values of 9.05 $x10^{-5}$ S/cm and 1.15 $x10^{-4}$ S/cm, respectively. Therefore the additional washings with organic solvents result in a slightly higher conductivity value.

But the most interesting aspect of this washed material comes from the fact that their V/P rate agrees well with the expected for $VOPO_4$ (Table VII.VI), that is, the washing procedure has removed the vanadium decomposition products that we expressed in terms of V_2O_5 equivalents in Table VII.V . This solubility in turn confirms the hypothesis that these impurities could be of a molecular or nanometric colloidal nature.

Finally, we carried out the testing of these three samples (30% carbon super-P and 70% of hybrid) in Li cells by applying 2 different current densities (10 mA/g and 20 mA/g) between a voltage range of 3.8-2.1V. In figure 7.21 we show the successive charge-discharge cycles for sample PVP11B and PVP11B2H (washed with deionized water), and sample PVP11B2S (washed with organic solvents). First, we can note that the irreversible capacity is indicated by the difference between the specific charge

values (Y axis) of the first 2 cycles. This irreversible capacity was significantly decreased in the case of sample PVP11B2S, indicating that by washing with organic solvents we probably eliminate oxidation by-products as anticipated. In addition this leads to a higher specific charge after stabilization, leading to a sustained value of 90-100 Ah/Kg (between cycles 13 and 35). Finally, we tested the effect of applying different charge-discharge rates. Thus, the vertical line in figure 7.20 marks a change from 10 to 20mA/g (I=10 mA/g for the first 5 cycles, and I=20 mA/g for the rest of the cycles). Interestingly there is no major effect upon this doubling, which indicates good intercalation kinetics for the novel $PPy(VOPO_4)_{0.13}\cdot 1.1H_2O$

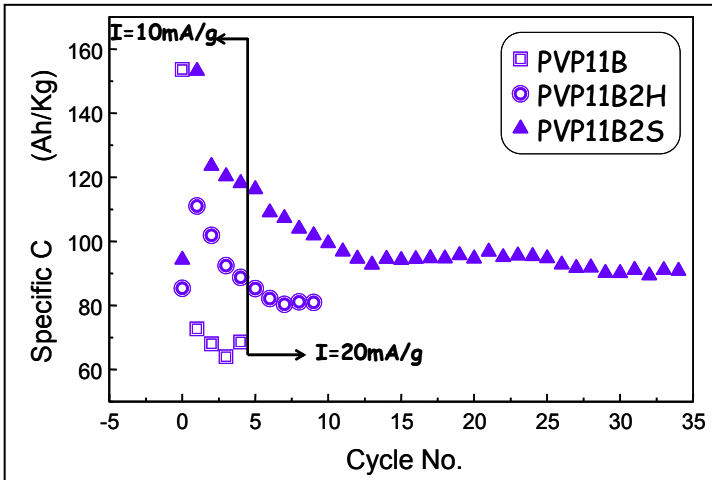

Figure 7.21.- Electrochemical characterization of $PPy/VOPO_4$ hybrid samples, optimized based on PVP11B. The vertical line marks a change in the constant current used for charge-discharge.

7.4. PAni/$VOPO_4\cdot$HYBRIDS

Hybrid materials based on polyaniline and $VOPO_4\cdot 2H_2O$, have been previously synthesized by de Farias et al [19] from a basic point of view with no electrochemical application. This group reports a bulk hybrid material of formula $(C_6H_4N)_{1.1}VOPO_4$ (which was only determined from elemental analysis), in which XRD data seem to indicate the intercalation of PAni into $VOPO_4$.

In this section we will explore different synthetic methods for the preparation of PAni-$VOPO_4$ materials similarly to the case of polypyrrole-vanadyl phosphate hybrids. The main objective and control parameter for the design of these PAni/$VOPO_4$ hybrid materials and for the optimization of their synthesis will be essentially their electrochemical performance as insertion cathodes in rechargeable Li cells.

First, we will discuss the synthetic methods applied initially for the formation of PAni/$VOPO_4$ hybrids, followed by successive optimization procedures based on

different synthesis parameters. Also, we will present the corresponding basic characterization, in some cases their physical-chemical characterization, as well as their electrochemical characterization as cathode material for lithium insertion batteries.

7.4.1. Comparative analysis of Synthetic Methods

In order to determine the best synthetic route, we explored three different syntheses procedures. In all cases the $VOPO_4 \cdot 2H_2O$ used was prepared by ultrasound treatment: 1) sonochemical method, using pre-formed $VOPO_4 \cdot 2H_2O$ to react with aniline in an ultrasound bath; 2) an in-situ sonochemical method (addition of aniline during the formation of $VOPO_4 \cdot 2H_2O$); and 3) chemical method in an ice bath.

7.4.1.1. Synthesis

First of all, we carried out method (1) above by using the same ultrasound bath set-up, as mention in section (7.2.1.). The synthesis procedure was carried out as follows: 1 ml of aniline and 5 ml of water were mixed in a beaker with 0.7242 g of $VOPO_4 \cdot 2H_2O$ resulting in a molar ratio of Ani:$VOPO_4 \cdot 2H_2O$ of (3:1), and was treated with ultrasounds for a period of 3 hours. We observed a color change from green to black, during the synthesis. The fine black solid (E1AVP) was filtered off through a Millipore filter, washed with deionized water, collected and dried under vacuum for 3 days.

Subsequently, we carried out the in-situ sonochemical method (2), which consisted in the formation of the hybrid during the formation of $VOPO_4 \cdot 2H_2O$ (0.8324 g of V_2O_5, 12.9 ml of H_3PO_4 with 42 ml of deionized water). We followed the same procedure of section 7.1.1., adding the aniline solution (1 ml risen to 25 ml with deionized water) 30 minutes after the $VOPO_4 \cdot 2H_2O$ synthesis had begun, and letting it react for 2.5 hours more. The molar ratio used of Ani:$VOPO_4 \cdot 2H_2O$ was (3:1). As in the case of the reaction with pyrrole, before the addition of the aniline solution we observed a color change to light yellow, indicating the formation of $VOPO_4 \cdot 2H_2O$. Instantly after the addition of aniline solution, we observed a color change to dark green. The very fine dark green solid (E2AVP) was filtered off with a Millipore filter, washed with deionized water, and dried under vacuum for 3 days.

Finally, the chemical method was carried out as follows: we suspended 0.7242 g of $VOPO_4 \cdot 2H_2O$ in a 50 ml $HClO_4$ solution (0.31 ml conc. 70% $HClO_4$ risen to 50 ml

with deionized water), followed by the addition of aniline solution (1 ml risen to 50 ml with deionized water) during 3 minutes, letting react for 5 days with magnetic stirring at 500 rpm in an ice bath. The molar ratio used of Ani:$VOPO_4{\cdot}2H_2O$:$HClO_4$ was 3:1:1. We observed a color change from light yellow to blue, then to pale green, and finally to black, when aniline was added during the synthesis. The dark solid obtained (E3AVP0^o) was filtered off, washed with deionized water, and dried under vacuum for 3 days.

7.4.1.2. Basic Characterization

As part of our basic characterization we carried out FTIR analyses in order to detect the formation of each of the components that constitute the hybrid material. In figure 7.22 we show the FTIR spectra for the different PAni/$VOPO_4$ samples obtained by different synthetic routes. First of all, observing the spectra for samples synthesized by the sonochemical method (E1AVP and E2AVP), we could not detect the infrared fingerprint of polyaniline, indicating its absence. Although, in sample E2AVP (in-situ $VOPO_4{\cdot}2H_2O$ formation) we can observe peaks (1400-1500 cm^{-1}) which could indicate some initial PAni formation.

On the other hand, in sample E3AVP0^o synthesized by the chemical method the presence of polyaniline was confirmed. These polyaniline bands are present at 1579 cm^{-1} (assigned to C-C ring stretchings, quinone and benzene groups), at 1493 cm^{-1} (for aromatic C=C stretchings), at 1305 cm^{-1} (assigned to C=N of an arylic secondary amine), and at 1147 cm^{-1} (corresponding to C-H ring deformations).

In addition the vibrational modes of the inorganic matrix are present at 1060 cm^{-1} (weak shoulder, ν_3 asymmetric stretching for P-O), at 942 cm^{-1} (for V=O stretchings, V-OH, V-OH,

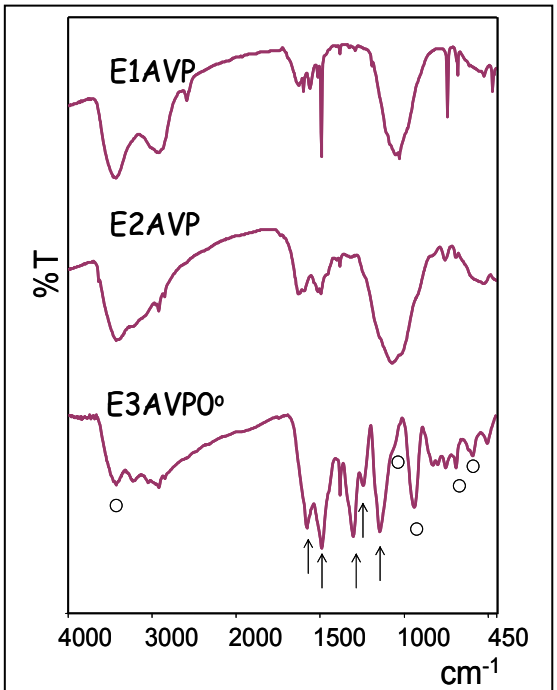

Figure 7.22.- FTIR analyses of PAni/VOPO4 hybrid samples, synthesized by different methods. The arrows indicate peaks from PAni, and the circles the ones assigned to $VOPO_4$.

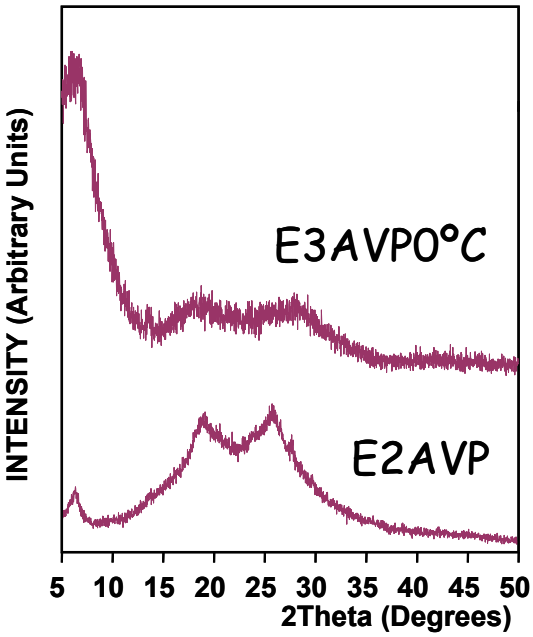

Figure 7.23.- Powder XRD of PAni/$VOPO_4$ hybrids samples, synthesized with different methods.

and ν_1 symmetric stretching for P-O, are overlapped), at 669 cm^{-1} (V-OH and P-OH), and the bending mode related to O-P-O at 595 cm^{-1} is weak and not clearly detected here. Also, hydration water can be detected at 3434 cm-1, and at 1650 cm-1.

Also as part of the basic characterization we carried out powder XRD analyses in order to get some structural information. With this analysis we can determine the formation or presence of specific $VOPO_4$ phases, or amorphous materials, and their intercalation properties. In figure 7.23 we show the diffraction patterns of samples E2AVP and E3AVP0°. Although both samples present very poor crystallinity we can detect at first glance a substantial difference between both. Thus, the diffraction pattern from sample E3AVP0° shows a 001 peak at low angles (2θ=6°, 14.6 Å), indicating the insertion of polyaniline into $VOPO_4$. On the other hand, for sample E2AVP (with no formation of polyaniline) a minor peak is still present at approximately the same angle but with a much lower intensity

Based on these two basic characterization techniques, we can conclude that the chemical method worked more efficiently for the formation and incorporation of PAni into $VOPO_4$ – based materials.

7.4.1.3. Electrochemical Characterization

We carried out the electrochemical characterization in rechargeable Li cells, for only the sample synthesized with the chemical method (E3AVP0°) where PAni was formed, and of sample E2AVP for comparison. The powder composite cathodes were fabricated by thoroughly mixing 30% weight of super-P carbon with 70% of our samples. Thorough grinding was avoided in order to prevent the decomposition of vanadyl phosphate. The cells were assembled in the dry box and tested by using a charge-discharge current density of I=3.5 mA/g, between a voltage range of 2.1 V and

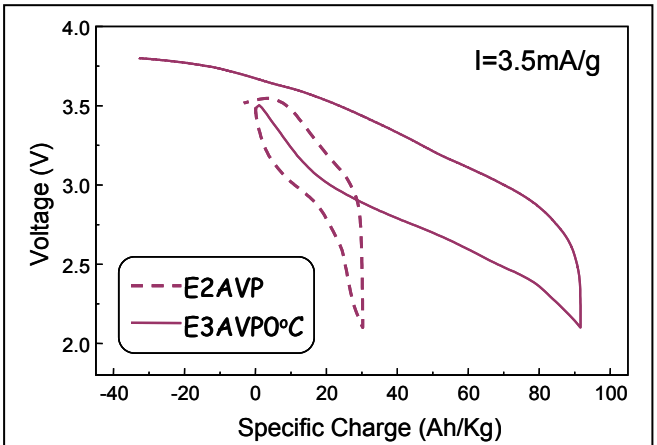

Figure 7.24.- First charge-discharge cycle for PAni/ $VOPO_4$ hybrids samples, made by 2 different methods.

3.8 V. In figure 7.24 we show the first charge-discharge cycle for both samples resulting in low specific charge values, especially for E2AVP. In the case of sample E3AVP0^o the specific charge value was 90 Ah/Kg, and for sample E2AVP, 30 Ah/Kg. This difference is not surprising due to the contribution of polyaniline only for sample E3AVP0^o. On the other hand, the cyclability was not good enough in sample E3AVP0^o. During the second recharge a plateau at 3.5 V appeared which turned out to be due to an irreversible oxidation process, resulting in a system that could not properly recharge up to 3.8V (only up to 3.3V) during the following cycles. Thus, sample E3AVP0^o synthesized by the chemical method at 0^{o}C corresponded to the best synthetic conditions for the formation of PAni/$VOPO_4$ hybrid with a moderate initial specific charge value, but with a cyclability that needs to be improved.

7.4.2. Optimization of the order of addition of the reagents.

As a first step of the several optimization procedures that we will describe in the following sections, we will focus in this section on the order of addition of the reagents. This optimization step has been carried out based on sample E3AVP0^o synthesized by the chemical method. Previously, in this chemical method we had performed the synthesis by first adding the aniline solution to the acidic ($HClO_4$)-$VOPO_4{\cdot}2H_2O$ suspension and had used an aniline:$VOPO_4$ ratio of 3:1.

7.4.2.1. Synthesis

We have carried out three experiments by the chemical method varying the order of addition of the reagents, keeping constant the following factors: molar ratio of aniline: $VOPO_4{\cdot}2H_2O$:$HClO_4$ (1:1:1), using magnetic stirring at 500 rpm in an ice bath during 5 days of synthesis. The three samples that we synthesized were: AVP11A, where aniline solution (0.5 ml risen up to 50 ml with deionized water) was added to the acidic suspension of $VOPO_4{\cdot}2H_2O$ (1.0815 g suspended in a solution of 0.47 ml of

conc. $HClO_4$, risen to 50 ml with deionized water), AVP11B, acidic aniline solution (0.5 ml of aniline risen to 50 ml with a solution consisting of 0.47 ml of conc. $HClO_4$ risen to 50 ml with deionized water) was added to the aqueous suspension of $VOPO_4{\cdot}2H_2O$ (1.0815 g in 50 ml of deionized water); and finally AVP11C, where in this case the acid was divided in two parts, one for the solution with aniline (0.5 ml of aniline risen to 50 ml with a solution consisting of, 0.235 ml of acid risen to 50 ml with deionized water), and the other for the suspension with $VOPO_4{\cdot}2H_2O$ (1.0815 g of vanadyl phosphate suspended in 50 ml of a solution of 0.23 ml of $HClO_4$ risen to 50 ml with deionized water). In this latter sample the acidic aniline solution was added to the acidic $VOPO_4{\cdot}2H_2O$ suspension. After the reaction time was completed, we filtered off the solids, washed them with deionized water, and dried them under vacuum for 3 days.

7.4.2.2. Basic Characterization

In figure 7.25 we show the FTIR spectra of the three new hybrid samples. We can detect bands corresponding to PAni formation (at 1566-1573 cm^{-1}, 1483-1486 cm^{-1}, 1306 cm^{-1}, and at 1122-1132 cm^{-1}), the vibrational modes of the inorganic matrix (around 1060 cm^{-1} overlapped with PAni modes, at 944 cm^{-1}, around 706 cm^{-1}, and at 587-590 cm^{-1}), and bands corresponding to hydration water (3442-3463 cm^{-1} and at 1627-1613 cm^{-1}).

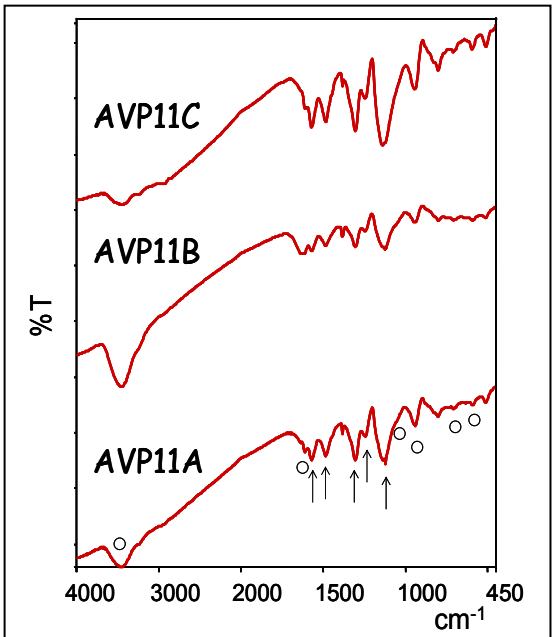

Figure 7.25.- FTIR spectra of PAni/$VOPO_4$ hybrid samples, synthesized by changing the addition order of the reagents. The arrows indicate the bands of polyaniline and the circles the ones belonging to $VOPO_4$ and H_2O.

In figure 7.26 we show the diffraction patterns of our PAni/$VOPO_4$ samples, where we can observe that all samples show a similar profile. The 001 plane of the inorganic matrix is present at $2\theta=7.24^o$ (12.19 Å) in sample AVP11A (synthesized by adding the aniline solution to the acidic $VOPO_4{\cdot}2H_2O$ solution), at $2\theta=7.12^o$ (12.39 Å) in AVP11B (synthesized by adding the acidic aniline solution to $VOPO_4{\cdot}2H_2O$ solution) and in sample AVP11C (synthesized by adding the half acidic

solution of aniline to the half acidic $VOPO_4 \cdot 2H_2O$ solution) at $2\theta=7.25^o$ (12.17 Å). The displacement of the peak to lower angles in all samples results in a spacing reveling the intercalation of PAni between the layers of the inorganic matrix.

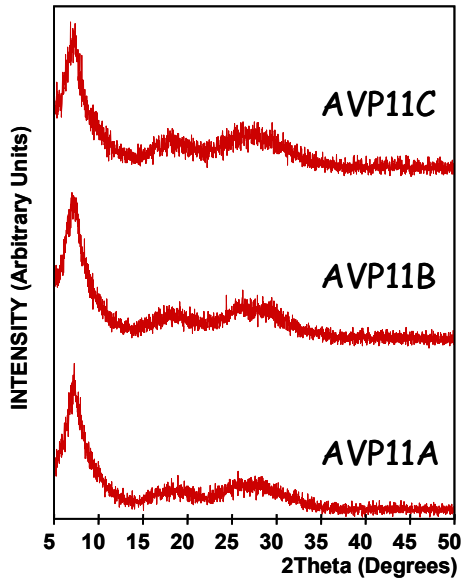

Figure 7.26.- Powder XRD of PAni/$VOPO_4$ hybrids samples, made by changing the order of addition of the reagents.

7.4.2.3. *Electrochemical Characterization*

In figure 7.27 we show the first charge-discharge cycle carried out for all samples (30% carbon super-P, 70% hybrid) using a charge-discharge current density of I=10 mA/g, between a voltage range of 2.1 V and 3.8 V. The initial specific charge values obtained for all samples were more or less similar (145 Ah/Kg for AVP11A, 127 Ah/Kg for AVP11B, and 140 Ah/Kg for AVP11C). During the recharge of the cells, the specific charge values do not return to their starting point, indicating the presence of an irreversible capacity very similar to the behavior observed for PPy/$VOPO_4$. Indeed, this similarity points out to a possible effect due to $VOPO_4$ which seems to be affecting the cells of an unusual polarization. In any event, this partial irreversibility, leads to effectively decreased specific charge values for all samples in the successive cycles, values which eventually tend to get stabilized around 87 Ah/Kg for AVP11A and AVP11C, and around 72 Ah/Kg for sample AVP11B.

Finally, concerning the order of addition of reagents, and contrary to what happened in the case of PPy, we have detected here very minor effects on the performance of these materials. We can conclude that by adding the aniline solution to the acidic suspension of vanadyl phosphate (AVP11A) or with

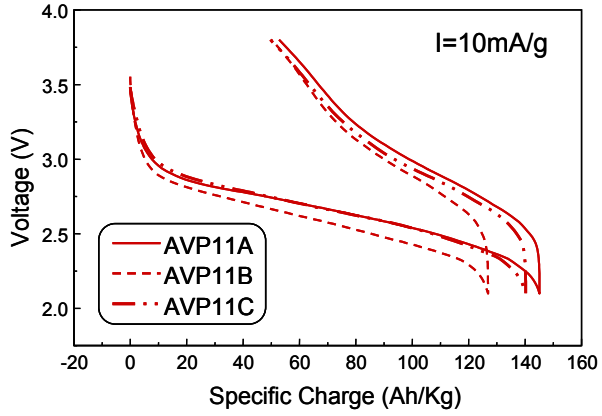

Figure 7.27.- First charge-discharge cycle for PAni/$VOPO_4$ hybrid samples, synthesized by changing the order of addition of the reagents.

aniline in a low protonated state (AVP11C), results in a higher value of specific charge. However, sample AVP11A showing the highest specific charge (145 Ah/Kg) was the chosen one for the next optimization step.

7.4.3. Optimization of the $HClO_4$ molar ratio.

In this section we have carried out the optimization based on the amount of acid used. The chemical synthesis carried out in this optimization step was based on the same parameters used for sample AVP11A.

7.4.3.1. Synthesis

We carried out three experiments based on sample AVP11A by varying the molar ratio of $HClO_4$ with respect to aniline and $VOPO_4{\cdot}2H_2O$ (see table VII.VII). We followed the synthesis by keeping constant the following parameters: the addition order was the aniline solution (0.5 ml risen to 50 ml with deionized water) to the $VOPO_4{\cdot}2H_2O$ acidic suspension (1.0815g suspended in the corresponding 50 ml acidic solution) using an ice bath with magnetic stirring at 500 rpm during 5 days of synthesis. For samples C20 and A20 the same overall molar ratios were used, but the acid was added differently. Thus, for sample C20 the total amount of acid was divided in two (as in sample AVP11C) one part for the aniline solution (0.47 ml of $HClO_4$) and the other part for the $VOPO_4{\cdot}2H_2O$ suspension (0.47ml of $HClO_4$). This sample was synthesized only for comparison, due to the resulting properties that were similar to those of sample AVP11A. After the reaction time was completed, we filtered off the solids, washed them with deionized water, and dried them under vacuum for 3 days.

Table VII.VII.- Experiments to synthesize PAni/$VOPO_4$ hybrids with different $HClO_4$ quantities.

Sample	Molar ratio (Py:$VOPO_4.2H_2O$:$HClO_4$)	$HClO_4$ ml in 50 ml solution
A15	(1:1:1.5)	0.71 ml
A20	(1:1:2)	0.94 ml
C20	(1:1:2)	0.94 ml

7.4.3.2. Basic Characterization

In figure 7.28 we show FTIR spectra for the 3 samples (A15, A20, C20). We can detect polyaniline formation by its characteristic peaks (at 1572-1576 cm^{-1}, 1491 cm^{-1}, at 1299-1303 cm^{-1}, and at 1122-1129 cm^{-1}), the bands corresponding to the inorganic matrix (the band at 1088 cm^{-1} overlapped with PAni, a weak shoulder at 934-941 cm^{-1}, around 691 cm^{-1}, and finally at 591-506 cm^{-1}).

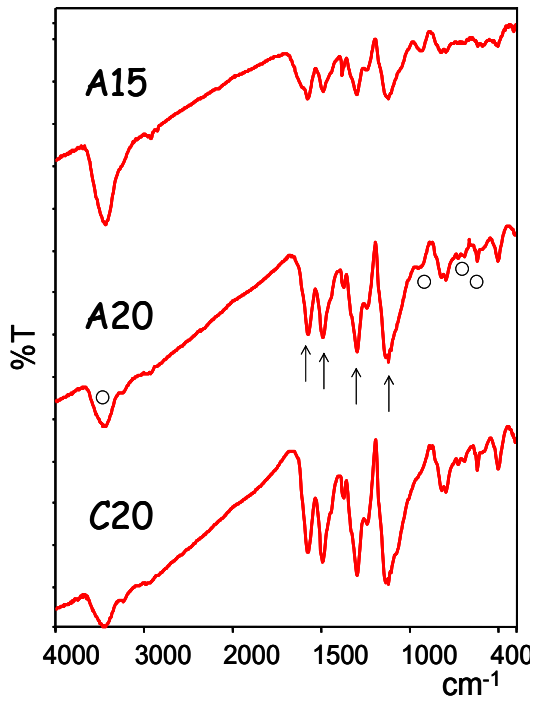

Figure 7.28.- FTIR spectra for PAni/$VOPO_4$ hybrids samples, synthesized with different amounts of acid. The arrows indicate the stretching modes of polyaniline and the circles the ones for $VOPO_4$.

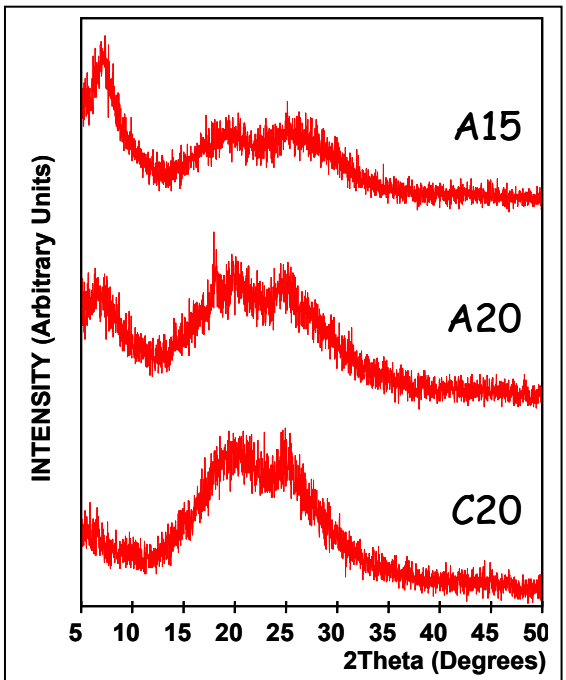

Figure 7.29.- Diffraction patterns of PAni/$VOPO_4$ hybrids samples, with variable amounts of acid used in their synthesis.

In figure 7.29 we show the diffraction patterns of these samples. All samples are more or less amorphous and they present some revealing differences. Samples A15 and A20, present a very broad basal peak at lower angles at $2\theta=7.4^{o}$ (11.9 Å) and at $2\theta=6.6^{o}$ (13.3 Å) respectively, corresponding to a spacing which indicates the intercalation of polyaniline between the layers of the inorganic matrix resulting in a inserted-PAni/$VOPO_4$ hybrid. Comparing sample A20 and C20 (splitting the acid), we can observe that it did had an influence on the crystalline arrangement of the material. In this case, the only sample in which PAni is previously protonated (C20) leads to the hybrid with the polymer not inserted into $VOPO_4$.

7.4.3.3. Electrochemical Characterization

In figure 7.30, we show the first charge-discharge cycle carried out for all composite samples (30% carbon super-P, 70% hybrid) by using a charge-discharge current density of I=10 mA/g, between a voltage range of 2.1 V and 3.8 V. The highest specific charge was obtained for sample A15 with 131 Ah/Kg, followed by sample A20 with 104 Ah/Kg, and the lowest was for sample C20 with 93.76 Ah/Kg. From these results it seems that lower acid amounts result in somewhat higher specific charges.

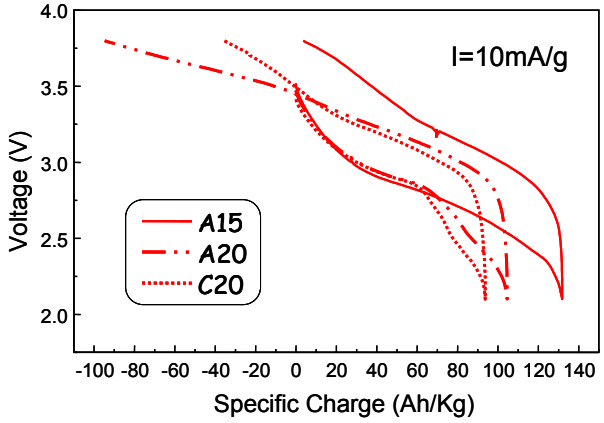

Figure 7.30.- First charge-discharge cycle for PAni/$VOPO_4$ hybrid samples, synthesized by changing the acid molar ratio.

On the other hand, the cyclability properties resulted in stabilized values of 90-110 Ah/Kg for samples A20 and C20.

Sample A15, as the best of this series not only presents a higher specific charge but also doesn't show the irreversible capacity found for the previous series.

7.4.3.4 Resistivity measurements

We carried out resistivity measurements by the 4 probe Van der Pauw method, in order to calculate the corresponding conductivity values for each PAni/$VOPO_4$ hybrid samples. In table VII.VIII we show the values obtained for each sample. Sample A15 presents a conductivity which is one order of magnitude better than the other samples. The lower conductivity values for samples A20 and C20 indicates that using a higher content of acid is detrimental for the electronic transport. Furthermore these results are in good agreement with the better performance of hybrid sample A15 in lithium cells.

Table VII.VIII.- Values of the conductivity calculated from the resistivity measurements made at room temperature.

Sample	PAni:$VOPO_4$:$HClO_4$	Conductivity σ (S/cm)
A15	(1:1:1.5)	2.46×10^{-5}
A20	(1:1:2)	6.38×10^{-6}
C20	(1:1:2)	1.8×10^{-6}

7.4.4. Optimization of the aniline to vanadyl phosphate ratio

In this section, we present our results for the optimization based on the aniline to vanadyl phosphate nominal ratio used during the synthesis, how it affects the final PAni contents in the hybrid materials, and on their performance in Li cells. As we have mentioned in the last optimization section, sample A15 chemically synthesized using a

molar ratio Ani:$VOPO_4$:$HClO_4$: of (1:1:1.5), adding the aniline solution to the acidic $VOPO_4{\cdot}2H_2O$ suspension, was the one chosen for the optimization of the amount of nominal aniline.

7.4.4.1. Synthesis

We have carried out four experiments varying the nominal amount of aniline used in the synthesis as seen in table VII.IX, keeping constant the following factors: the aniline solution (amount on table VII.IX) was added to the acidic suspension of $VOPO_4{\cdot}2H_2O$, a molar ratio of aniline:$HClO_4$ of (1:1), using an ice bath with magnetic stirring at 500 rpm, and a reaction time of 5 days. After the reaction time was completed, we filtered off the solids, washed them with deionized water, and dried them under vacuum for 3 days.

Table VII.IX.- PAni/$VOPO_4$ hybrids synthesized using different molar ratios.

Sample	Molar ratio (Ani:$VOPO_4.2H_2O$:$HClO_4$)	ml aniline risen to 50ml	$VOPO_4.2H_2O$ amount/ $HClO_4$ ml in 50 ml suspension
A154	(4:1:6)	1 ml	0.5407 g / 1.41ml
A153	(3:1:4.5)	1ml	0.721 g / 1.41 ml
A152	(2:1:3)	1 ml	1.0815 g / 1.41 ml
A15-5	(0.5:1:0.75)	0.5 ml	2.163 g / 0.708 ml

7.4.4.2. Basic characterization

In figure 7.31 we show the FTIR spectra for the four samples, including the spectrum of sample A15 for comparison. At first glance, PAni bands are better defined on samples A15-5 and A15, synthesized with less amount of aniline, indicating a better formation of the polymer (at 1568-1579 cm^{-1}, at 1491-1494 cm^{-1}, at 1295-1306 cm^{-1}, and at 1111-1133 cm^{-1}). The PAni spectra shows a peak around 1299 cm^{-1} that belongs to C=N, which decreases as the amount of aniline increases in the synthesis. In general, the vibrational modes of polyaniline are less defined as the nominal amount of aniline increases.

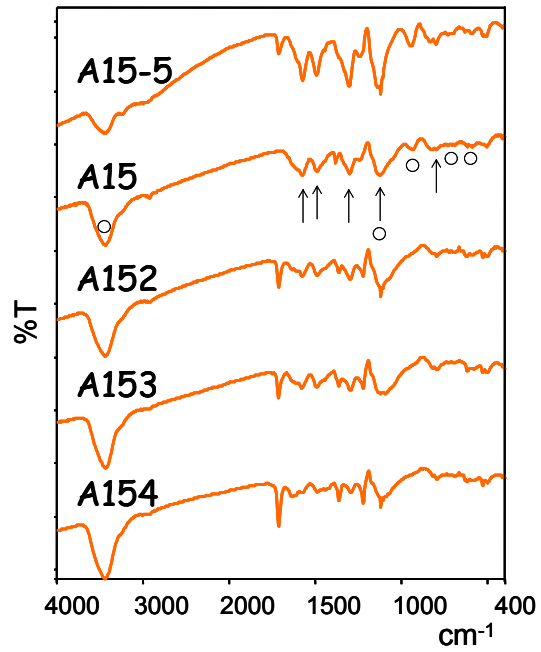

Figure 7.31.- FTIR spectra of PAni/VOPO4 hybrid samples, synthesized with different amounts of aniline. The arrows indicate the bands of polyaniline and the circles of $VOPO_4$.

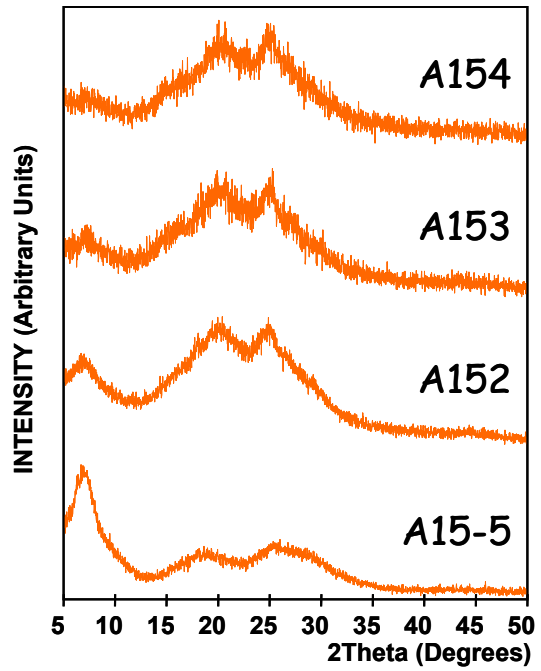

Figure 7.32.- diffraction patterns of samples synthesized with different amounts of nominal aniline.

On the other hand, the bands assigned to the inorganic phase are presented (overlapped with PAni band at 1111-1133 cm^{-1}, at 945 cm^{-1}, around 693-710 cm^{-1}), as well as bands corresponding to hydration water (at 3431-3439 cm^{-1} for H-O stretching).

In figure 7.32 we show the diffraction patterns of these four samples. As for all other hybrids of this family, none of these materials is highly crystalline, however there are obvious differences in crystallinity as we change the nominal Ani:$VOPO_4$ ratio. As this ratio is increased, the samples resulted in a more amorphous material. Furthermore the peak corresponding to the 001 plane at lower angles is present in all samples but its definition and intensity gets drastically decreased for higher Ani:$VOPO_4$ ratios (at $2\theta=7.3^o$ with 12.0 Å for A154, at $2\theta=7.2^o$ with 12.2 Å for A153, at $2\theta=6.8^o$ with 12.9 Å for A152, and for A15-5 at $2\theta=6.9^o$ with 12.8 Å). The spacings of these peaks confirms the insertion of polyaniline between the slabs of the inorganic matrix, but this insertion leads to a more ordered and crystallized materials for lower amounts of aniline used in the reaction mixture.

7.4.4.3. Physicochemical Characterization

In order to characterize in more detail our hybrid samples, we will present in this section an extended study by using physical-chemical characterization methods, such as: Scanning Electron Microscopy (SEM), and ambient resistivity measurements by the Van der Pauw method.

7.4.4.3.1. Resistivity Measurements

We carried out resistivity measurements at room temperature by using the Van der Pauw method for all these PAni/$VOPO_4$ hybrid samples (A154, A153, A152, A15, A15-5) in order to estimate their conductivity. In table VII.X we show the conductivity values obtained for each sample. We could not detect any obvious tendency between the conductivity values, obtained for the different samples and their synthetic parameters. As in the case of hybrids with polypyrrole, this fact seems to point out the existence of some additional factors affecting the microstructure and the conductivities of these materials in addition to the ones controlled in our experiments. This additional factor might be related to the partial decomposition of vanadyl phosphate by the additional excess of nominal aniline used, limiting the conductivity in the hybrid.

Table VII.X.- Values of the conductivity calculated from the resistivity measurements made at room temperature.

Sample	PAni:$VOPO_4$	Conductivity σ (S/cm)
A154	(4:1)	$2.46x10^{-6}$
A153	(3:1)	$2.39x10^{-5}$
A152	(2:1)	$1.77x10^{-7}$
A15	(1:1)	$2.46x10^{-5}$
A15-5	(0.5:1)	$1.96x10^{-7}$

Nevertheless, sample A15 that was synthesized with a molar ratio for aniline:$VOPO_4{\cdot}2H_2O$:$HClO_4$ of (1:1:1.5) had one of the highest conductivity value.

7.4.4.3.2. Scanning Electron Microscopy (SEM)

We have carried out SEM photographs of samples synthesized with different amounts of aniline (A154, A153, A152, A15, and A15-5). In figure 7.33 we show the series of photographs carried out at the same magnification. Higher magnifications were also applied (up to 18k), but the photos presented here (5k) were more suitable for the microstructure analyses.

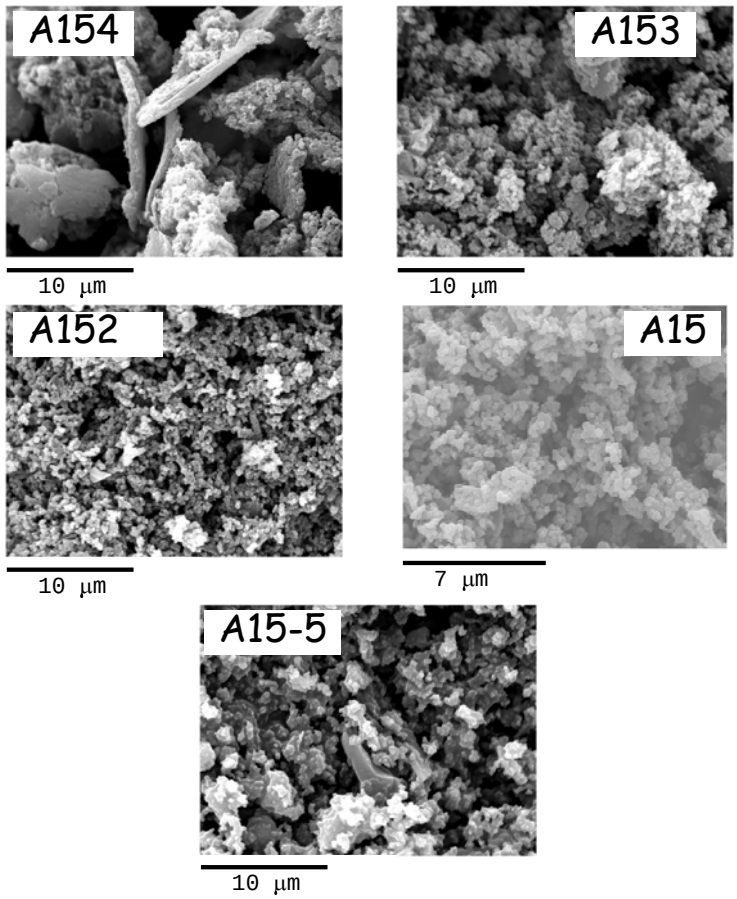

Figure 7.33.- .- SEM photographs of the samples synthesized with different amount of aniline. We also include sample A15. 5k magnification.

In addition to the globular porous microstructure this series of photographs allowed us to detect the presence of two grains with different morphologies for samples A154, A153 and A15-5. The first two show some very flat plates, mixed among predominating smaller globular particles, although the plates are not rectangular crystals. On the other hanf sample A15-5 with the lower Ani amount shows few isolated rectangular plates which conform to the well known morphology of $VOPO_4$. On the other hand, samples A152 and A15 present a homogeneous phase composed of globular particles.

7.4.4.4. Stoichiometry determination

We carried out different chemical analyses in order to establish the stoichiometry of our PAni/$VOPO_4$ hybrid samples. These analyses were: TGA to have a general

idea of the hybrids composition, elemental analysis to determine the organic matter, and ICP to determine the amounts of V and P in the hybrid samples.

Thermogravimetric analysis (TGA) were carried out to determine the amount of residual inorganic matter, and to estimate the organic mater and hydration water present in each sample. In figure 7.34 we can observe the TGA analyses carried out for our PAni/$VOPO_4 \cdot xH_2O$ hybrids, synthesized by using different amounts of nominal aniline. The analyses were carried out in air by heating at a 1°C/min rate up to 500 °C, keeping this temperature for 5 hours. We can observe three weight losses in samples A15, A152, A153, A154 (see inset): a small one between 50-80 °C corresponding to loosely bound water, a second small weight loss around 180 °C corresponding also to water, and between 250-350 °C, correspondent to the combustion of the organic part. Sample A15-5 also presents three different weight looses: the same small loss between 50-80 °C corresponding to loosely bound water, a second between 200-300 °C corresponding to the combustion of the organic part, and a sharper third loss at 340 °C corresponding to the decomposition of the inorganic phase (resolved in this case probably due to the smaller PAni amounts in the hybrid). The remaining weight percent corresponds to residual V_2O_5 crystalline phase, which was verified by XRD (not presented here). For each sample these vanadium pentoxide residues were different: 39.59% for A15-5, 27.53% for A15, 14.15% for A152, 9.40% for A153, and 7.5% for A154. We can observe a good correlation between the amount of nominal aniline in the reaction mixture. By adding more aniline per $VOPO_4$ in the synthesis, resulted in more amount of organic mater in the resulting hybrids. We should note the exception of samples A153 and A154, richer in aniline, for which the difference is very small in comparison with the change in nominal Ani:$VOPO_4$ ratio.

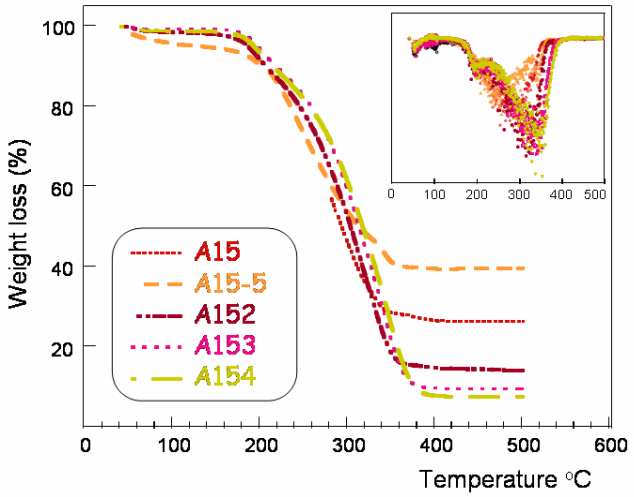

Figure 7.34.- TGA analyses of PAni/$VOPO_4$ hybrids, synthesized with different amounts of aniline. The analyses were carried out with a 1 °C/min rate, upto 500 °C for 5 hours

The proposed stoichiometries of these samples were calculated based on elemental analysis (C, N, H) and ICP (V, P). In table VII.XI we present the summarized data for these analyses and the proposed formulas.

Table VII.XI.- Summarized data of the chemical analysis to determine the respective stoichiometry of each PAni/$VOPO_4$·$2H_2O$ hybrid samples.

	Ani: $VOPO_4$	%C	%N	%H	%V	%P	%$VOPO_4$	Formula (1)	sample
Exp	(0.5:1)	51.54	9.75	3.65	18.60	1.37	6.68	$C_6H_4N(VOPO_4)_{0.06}(V_2O_5)_{0.23}0.2H_2O$	**A15-5**
Cal		49.61	9.64	3.05	18.23	1.27		FW=145.25	
Exp	(1:1)	46.05	8.71	3.43	12.94	0.80	4.14	$C_6H_4N(VOPO_4)_{0.04}(V_2O_5)_{0.18}1.5H_2O$	**A15**
Cal		46.09	8.95	4.51	13.03	0.79		FW=156.34	
Exp	(2:1)	53.58	9.71	3.84	6.03	0.34	2.24	$C_6H_4N(VOPO_4)_{0.02}(V_2O_5)_{0.08}2H_2O$	**A152**
Cal		50.07	9.73	5.60	6.37	0.43		FW=143.92	
Exp	(3:1)	55.92	10.67	3.95	3.79	0.12	1.23	$C_6H_4N(VOPO_4)_{0.01}(V_2O_5)_{0.05}1.7H_2O$	**A153**
Cal		54.82	10.65	5.67	4.26	0.23		FW=131.44	
Exp	(4:1)	55.57	10.56	3.83	3.41	0.11	1.23	$C_6H_4N(VOPO_4)_{0.01}(V_2O_5)_{0.04}1.8H_2O$	**A154**
Cal		54.83	10.65	5.82	3.48	0.23		FW=131.42	

(1) From P and V contents we have estimated the amounts of V_2O_5 derived from the decomposition of $VOPO_4$. In these cases weak bands assignable to V_2O_5 can be detected in the FTIR spectra.

The first striking observation is the low P contents which point out to the partial decomposition of vanadyl phosphate and or to the presence of spurious organic matter not corresponding to PAni. This low P contents are lower as the Ani:$VOPO_4$ nominal ratios increase. In order to distinguish between possible organic by-products and $VOPO_4$ decomposition we can use the V and P analysis combined or more specifically, the ratios between estimated V_2O_5 impurities and $VOPO_4$ contents. Interestingly, these ratios are approximately constant within the whole series, oscillating between 4 and 5 V_2O_5 per $VOPO_4$. The decrease in P % (parallel to an increase in C%) should therefore be assigned to the presence of aniline oxidation by-products.

7.4.4.5. Electrochemical Characterization

In figure 7.35, we show three successive charge-discharge cycles carried out for all these samples (30% carbon super-P and 70% hybrid) using a charge-discharge current density of I=10 mA/g for the first five cycles and I=20 mA/g for the rest of the

cycles, between a voltage range of 2.1 V and 3.8 V. In general, we can observe a stabilization value of the specific charge between 90 and 100 Ah/Kg for all samples. Also, increments of the specific charge for samples (A4H, A3H, A2H) where the molar ratio used of nominal aniline was equal or higher than two, respect to $VOPO_4 \cdot 2H_2O$. This increment appears and disappears in a small number of cycles, and it is due to a new low-voltage plateau attributed to an unknown phase that appears during the discharge at 2.35V. In samples A15 and A15-5 with less amount of nominal aniline (molar ratio of aniline:$VOPO_4 \cdot 2H_2O$ is 1:1 and 0.5:1), this increment of the specific charge did not take place. However, sample A15 resulted in a more stabilized value of specific charge (90 Ah/Kg). Since this abnormal increments take place for the samples with higher aniline contents we propose that this temporary increase could be due to reactions involving the excess organic products.

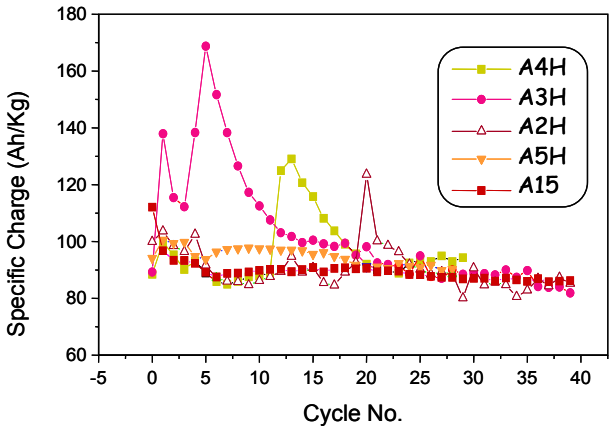

Figure 7.35.- Electrochemical characterization of samples synthesized with different amounts of aniline, where we can se the specific charge values through successive charge-discharge cycles. For the first 5 cycles the I=10mA/g, and the rest of them with I=20mA/g

7.4.5. Electrochemical studies on sample A15

We carried out different electrochemical studies over sample A15 (the best one, with an initial specific charge value of 113 Ah/Kg and a stabilized value through cycling of 90Ah/Kg), which did not present the abnormal increment of the specific charge.

In figure 7.37 we present the electrochemical studies of composite cathodes of sample A15 tested in different voltage ranges: 1.5-3.8V (A15c) and 2.1-3.8V (A15a, A15b). Also we have applied different current densities to study their effect on their intercalation kinetics. It appears that by increasing the voltage window from 3.8-2.1V (A15a) to 3.8-1.5V (A15c) using the same current, did not represent an important increase of the specific charge. On the other hand, if we use from the start a current density of I=20 mA/g (A15b) instead of I=10 mA/g (A15a and A15c), we observe that

the specific charge gets stabilized more rapidly and, remarkably, at a higher value of 100 Ah/Kg.

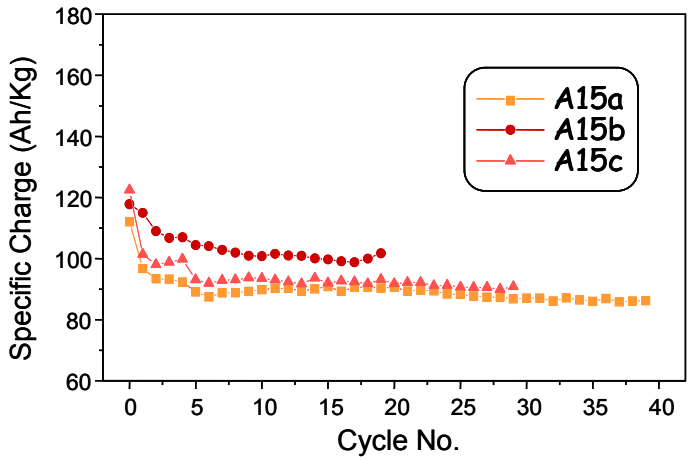

Figure 7.36.- Electrochemical experiments over sample A15 in lithium reversible cells, where we can see the specific charge values through successive charge-discharge cycles. First 5 cycles at I=10mA/g, and the rest of them at I=20mA/g for samples A15a (3.8-2.1V) and A15c (3.8-1.5V). For samples A15b (3.8-2.1V) at I=20mA/g.

So, we can conclude that by using a higher intensity (20 mA/g) from the start, the PAni/$VOPO_4$ hybrid responds better in reversible lithium cells, which gives a clue of the good intercalation kinetics that this system has.

This is in common with the PPy/$VOPO_4$ system, both have good kinetics and do not show the typical marked decrease of performance upon increasing the current density used for charge-discharge. This makes us hope these materials might be promising if the problems related with the partial decomposition of the inorganic matrix can be solved.

REFERENCES

[1] Lim, S.C.; Vaughey, J.T.; Harrison, W.T.A.; Dussack, L.L.; Jacobson, A.J.; Jonson, J.W.; *Solid State Ionics* **1996**(84), 219.
[2] Benabdelouahab, F.; Volta, J.C.; Olier, R.; *J. Catálisis* **1994**(148), 334.
[3] Kerr, T.A.; Gaubicher, J.; Nazar, L.F.; *Electrochem. And Solid State Lett.* **2000**(3), 460.
[4] Azmi, B.M.; Ishihara, T.; Nishiguchi, H.; Takita, Y.; *Electrochim. Acta* **2002**(48), 165.
[5] Capková, P.; Trchová, M.; Zima, V.; Schenk, H.; *J. Solid State Chem.* **2000**(150), 356.
[6] R'Kha, C.; Vandenborre, M.T.; Livage, J.; Prost, R.; Huard, E.; *J. Solid State Chem.* **1986**(63), 202.
[7] Park, N.G;. Kim, K.M; Chang, S.H.; *Electrochem. Commun*. **2001**(3), 553.
[8] Thackeray, M.; *Nature* **2002**(1), 81.
[9] Dupre, N.; Gaubicher, J.; Le Mercier, T.; Wallez, G.; Angenault, J.; Quarton, M.; *Solid State Ionics* **2001**(140), 209.
[10] Chauvel, B.; Bondot, P.; de Roy, M.; Besse, J.P.; *Solid State Ionics* **1993**(63-65), 494.
[11] Tachez, M.; Theobald, E.; Bordes, E.; *J. Solid State Chem.* **1981**(40), 280.
[12] Bagnasco, G.; Banes, L.; Galli, P.; Massumli, M.A.; Patrono, P.; Turco, M.; Zima, V.; *J. Therm. Anal.* **1998**(52), 615.
[13] Zima, V.; Benes, L.; Sisková, R.; Fatena, P.; Votinsky, J.; *Solid State Ionics* **1994**(67), 277.
[14] Ladwing, G.; Anorg, Z.; *Allg. Chem.* **1965**(338), 266.
[15] Kinomura, N.; Toyama, T.; Kumada, N.; *Solid State Ionics* **1995**(78), 281.
[16] Nakajima, H.; Matsubayashi, G.; *Chem. Lett.* **1993**, 423.
[17] De Stefanis, A.; Foglia, S.; Tomlinson, A.A.G.; *J. Mater. Chem.***1995**(5), 475.
[18] Nakato, T.; Furumi, Y.; Terao, N.; Okuhara, T.; *J. Mater. Chem.* **2000**(10), 737.
[19] De Farias, R.F.; Airobli, C.; *Solid State Sci.* **2003**(5), 611.
[20] Christensen, P.A.; Hamnett, A.; *Electrochim. Acta* **1991**(36), 1263.

Chapter 8

Molecular Hybrids for Electrochemical Supercapacitors

Abstract:

Molecular hybrid materials formed by polyoxometalates dispersed in conducting polymers are interesting concept materials for energy storage but showed a very poor cyclability in lithium cells. The work we present here constitutes the first practical realization of electrodes based on these materials for energy storage, in particular in electrochemical supercapacitors. The molecular hybrids PAni/SiW12 PAni/PW12, PAni/PMo12, have been prepared electrochemically on carbon substrates, with the latter as a prototype example. This hybrid displays the combined activity of its organic and inorganic components to store and release charge in solid state electrochemical capacitor cells, leading to promising values of 120 F/g and good cyclabilities of at least 10^3 cycles.

8.1. INTRODUCTION

Polyoxometalates (POMs) are ideal models for quantum-sized oxides and perfect candidates for the design of molecular electrochemical supercapacitors. They resemble clusters of metal oxides both from the structural and electronic point of view; they are formed by a small number of metal centers (typically 6-18 W or Mo) coordinated by bridging oxygen atoms, they present well-known, stable structures and undergo reversible multielectron reduction processes, in clusters in which all the metal centers are at the interface with an electrolyte. Nevertheless, it has been precisely their zero-dimensionality and solubility, derived from their molecular nature that has prevented their application as active compounds for electrodes or for any kind of material where collective properties were needed.

POMs have been extensively studied from a chemical point of view and have been used in catalysis and photocatalysis, either as homogeneous catalyst or supported onto polymers. Some examples are known of POMs doping conducting organic polymers such as polyaniline for application in catalysis and in energy storage. [1]

The similarities between POMs and oxides are not limited to their composition and topologies. Their electrochemical and photochemical behaviors are also parallel. Thus, POMs can be electrochemically or photochemical reduced to form blue species. These reduced species are chemically and spectroscopically equivalent to tungsten or molybdenum bronzes in the form of colloidal semiconducting quantum dots, with the added advantage in POMs of a well-known structure that is stable in solution [2,3].

On the other hand, COPs have been extensively studied as promising novel materials, most frequently as catalysts, but also in other applications related to their electrochemical activity. The combination of conducting polymers and electroactive molecular, cluster or extended inorganic species to form nanocomposite hybrid materials represents an opportunity for the design of concept materials with improved properties and enhanced energy storage capabilities in comparison with conducting polymers alone. Indeed the anchoring of POMs within the network of COPs such as PAni leads to the fabrication of hybrid materials in which the inorganic clusters keep their integrity and activity while benefiting from the conducting properties and polymeric nature of the hybrid structure. Some of these hybrid materials have been studied in non-aqueous solvents as lithium inserting electrodes for their potential use

in lithium batteries. However, under such conditions, the electroactivity of POMs could not be harnessed for too many charge-discharge cycles. Indeed, the electroactivity of these inorganic clusters integrated in a hybrid material is dependent upon the electrolyte used. Thus, the use of aqueous acidic electrolytes facilitates the protonation of the cluster upon reduction, leading to quick and reversible redox chemistry. As we have mentioned, POMs clusters provide an ultimate degree of dispersion for an oxide phase since all twelve MO_6 moieties are at the surface of the cluster. Thus, the POMs species could act as ideal active materials for electrochemical supercapacitors when combined with acidic electrolytes [4,5]. Contrary to COPs, POMs have not been widely exploited as electrodic materials for electrochemical supercapacitors. Aside from their use as electrolyte components reported in several patents [6,7] to the best of our knowledge dealing with the use of POMs as active materials for electrochemical supercapacitors [4], a single report describing the device consisting of pure phosphomolybdic acid in one electrode vs. widely used RuO_2 in the other have been published so far [8].

We present in this chapter the use of molecular hybrid materials formed by polyaniline (PAni) and, $H_4SiW_{12}O_{40}$ (SiW12), $H_3PW_{12}O_{40}$ (PW12), or $H_3PMo_{12}O_{40}$ (PMo12) as electrodes for solid state electrochemical supercapacitors.

8.2. SYNTHESIS BACKGROUND

We carried out the syntheses of PAni/POMs hybrids by an electrochemical method using a cyclic voltammetry technique (CV), with a three electrode cell using as reference electrode Ag/AgCl. CV was used as the synthesis technique because PAni is deposited more homogeneously [9] onto the surface of the working electrode.

From past publications [8,10-12] we know that PAni has been electrochemically synthesized by a CV technique between the range potential -0.2V and 0.9V vs. Ag/AgCl, and that has a selectivity for high molecular weight dopands [10]. Above 0.9 V degradation of PAni takes place, with a consequent loss of electroactivity, due to formation of phenazine rings and/or to soluble species like benzoquinone and hydroquinone. Below -0.2 V PAni is not conducting.

On the other hand, when we have POMs in solution and we carry out their CVs we can observe all their different characteristic redox peaks. In figure 8.1 we show CVs for different POMs (SiW12, PW12, and PMo12) carried out at 20 mV/s and cycled inside the PAni redox limits mentioned above. Some of the POMs are more difficult to reduce and can be seen from the displacement of redox waves to more negative potentials, the order from the more oxidazing to the less oxidazing is PMo12>PW12>SiW12.

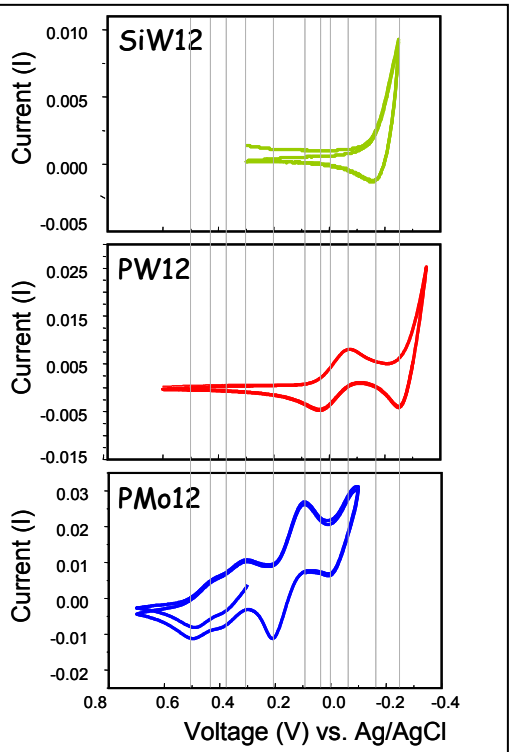

Figure 8.1. Cyclic Voltamograms (20mV/s) of the heteropolyacids (0.02M aq.) vs. Ag/AgCl. SiW12 $[SiW_{12}O_{40}]^{4-}$, PW12 $[PW_{12}O_{40}]^{3-}$, PMo12 $[PMo_{12}O_{40}]^{3-}$.

A work reported earlier [13], shows the CV of POMs in acidic solution at 20 mV/s, where the voltage limits used were: from 0.0V to -0.75V for SiW12, and from 0.6V to -0.6V for PMo12. In other publication regarding PAni/POMs hybrids, the voltage range used for the CV synthesis of PAni/PMo12 was from -0.1V to 0.9V [1], for PAni/SiW12 from -0.25V to 1.5V vs. Pt and for PPy/PW12 -0.25V to 0.3V vs. Pt. [14]

8.3. PAni/SiW12 HYBRIDS

8.3.1. Synthesis of PAni/SiW12 hybrids

We carried out the electrochemical synthesis of the PAni/SiW12 hybrid using the suspension made by mixing 5.23g of silicontungstic acid ($H_4O_{40}SiW_{12}{\cdot}xH_2O$, FW: 2878.29) with 1 ml of aniline, and then adding 100 ml of water. The cell was setup with a graphite plate working electrode, Pt counterelectrode and Ag/AgCl reference. Common details for these syntheses were given in Chapter 2. The specific conditions used for each experiment are given in table VIII.I.

Table VIII.I.- Electrochemical conditions of CV for the syntheses of different PAni/SiW12 hybrids

Sample	Voltagerange	Scan rate (mV/s)	Nº of cycles	Observations
SW1	-0.25/0.9V	10 mV/s	40	
SW2	-0.25/0.9V	5 mV/s	40	Dark bluish thin layer
SW3	-0.25/0.9V	2.5 mV/s	40	Dark bluish thin layer
SW4	-0.25/0.9V	5 mV/s	60	Dark bluish thin layer

We varied the scan rate in order to try to deposit the greater amount of hybrid material in a homogeneous layer. The best results were obtained for a rate of 5 mV/s (SW2) and consequently we repeated that experiment with more cycles (SW4). In figure 8.2 we show the CV of PAni/SiW12 of sample SW2, which is representative of the rest of the samples. We can observe the first and fortieth cycle, were we can detect a decrease of the intensity through cycling, indicating a possible conductivity loss of the working electrode. This fact could be attributed to the deposition of SiW12 cluster on the surface of the electrode making it less conducting.

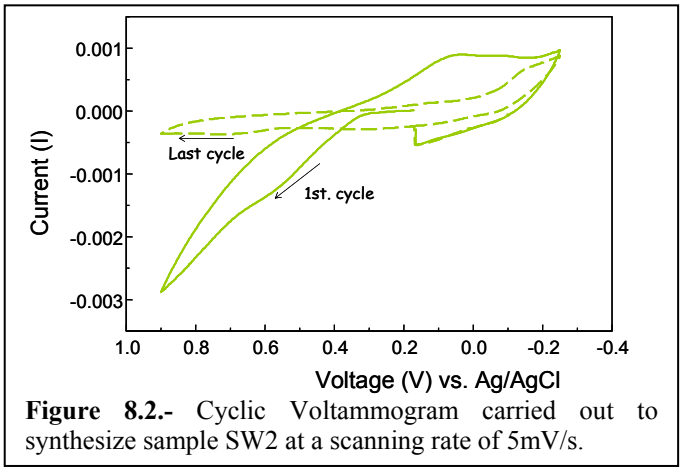

Figure 8.2.- Cyclic Voltammogram carried out to synthesize sample SW2 at a scanning rate of 5mV/s.

8.3.2. Characterization of PAni/SiW12

First we carried out the electrochemical characterization of the PAni/SiW12 hybrid electrode by cyclic voltammetry, using a three electrode cell vs. Ag/AgCl as reference electrode, in a solution of $HClO_4$ 1M at a scanning rate of 20 mV/s. In figure 8.3 we show the CV corresponding to the electrochemical characterization, where we can detect the redox waves for this material. Most of them belong to polyaniline except the oxidation shoulder at -0.15 V, which can be assigned to the SiW12 polyanion by comparison with its own CV. As it could be anticipated from the different voltage activity windows from SiW12 and PAni this anion is not the best to be combined with PAni although we have tried the synthesis of their hybrid for comparative purposes.

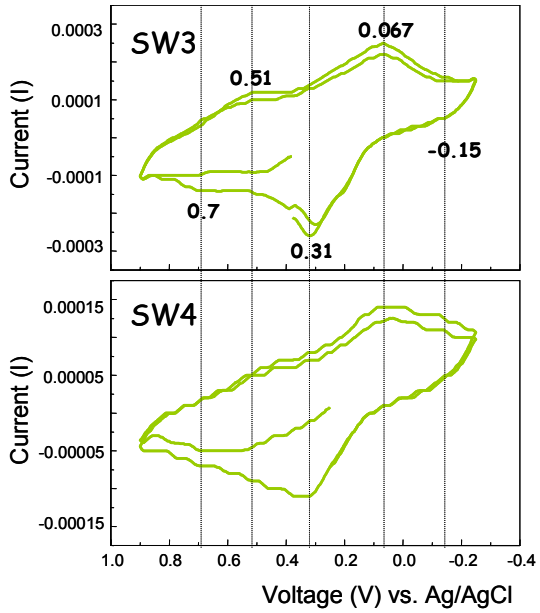

Figure 8.3.- CV of SW3 and SW4 electrodes, carried out in a 1M HClO4 solution at 20mV/s.

We carried out SEM photographs as part of the characterization procedure with the corresponding microanalyses, and W composition analysis for each sample. In figure 8.4 we show the corresponding SEM photos at x300 and at x5000 magnification. We see a compact deposit for sample SW2, on top of which further agglomerates grow in the case of samples SW3 and SW4 (fig. 8.4b and 8.4c, respectively). Samples SW2 and SW4 were made using similar conditions (5 mV/s) and the only difference was that for sample SW4 60 cycles were carried out instead of 40 cycles for sample SW2. This explains the presence of more material in SW4. EDX (Energy Dispersive X-Ray) Microanalyses carried out in the three samples showed the presence of Si and W, confirming the presence of the SiW12 polyanion and its integration within the polymer. Finally, a mapping composition analysis confirmed a greater concentration of W in the agglomerate particles (fig. 8.4b and c).

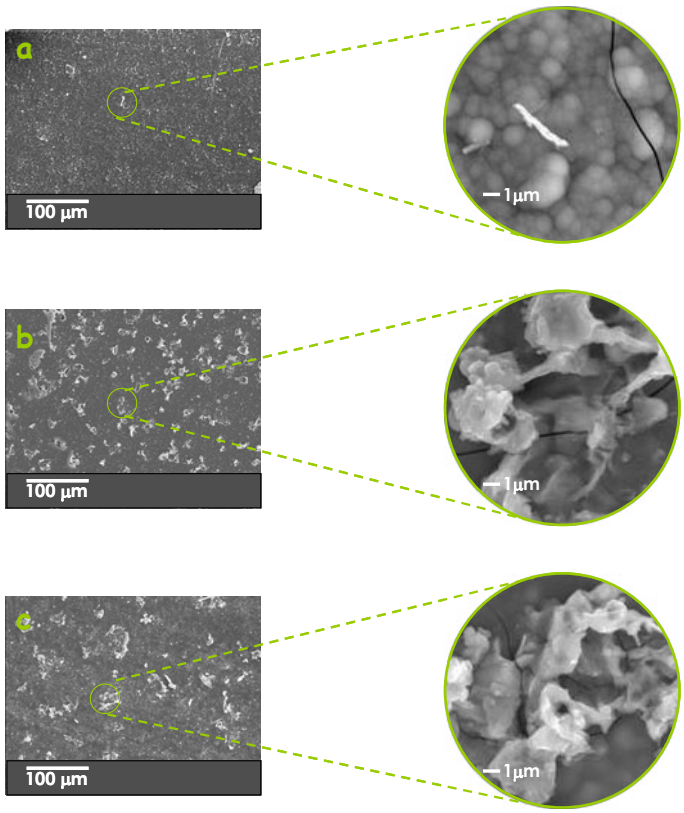

Figure 8.4.- SEM photographs made at x300 for the square photos and x5000 for the circles. a)SW2, b)SW3, and c)SW4.

8.3.3. PAni/SiW12 Electrochemical Supercapacitors

We assembled the solid state electrochemical supercapacitors in swagelok cells, using two PAni/SiW12 electrodes separated by Nafion impregnated in 1M H_2SO_4 (proton conductor membrane). In figure 8.5 we show the capacitance obtained for each hybrid sample at different current densities between a voltage range of 0-1V. In

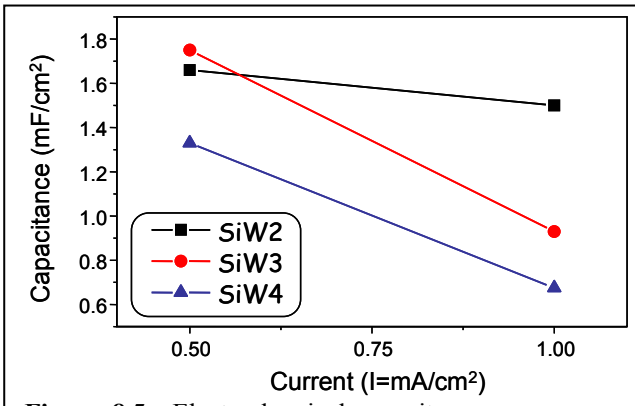

Figure 8.5.- Electrochemical capacitors response over PAni/SiW12 hybrid samples with different current densities. Current density normalized per effective electrode area.

seems that all hybrid samples behave similarly at all current densities, except when using I=0.5 mA/cm^2. Sample SW3 synthesized using a slower rate (2.5 mV/s) was the one that resulted in a higher capacitance value (4.5 mF/cm^2).

8.4. PAni/PW12 HYBRIDS

8.4.1. Synthesis of PAni/PW12 hybrids

We carried out the electrochemical synthesis of PAni/PW12 hybrids using two types of suspensions: 1) mixing 7.89g of phosphotungstic ($H_3PW_{12}O_{40}\cdot xH_2O$, FW: 2880.17) acid with 1 ml of aniline and adding 100 ml of water (series PW1), and 2) dissolving 3.94g of phosphotugstic acid in 100ml water and adding 0.5 ml of aniline (series PW2), thus leading to the same reagents ratio but half concentration. The conditions used for each experiment are presented on table VIII.II.

Table VIII.II.- Electrochemical conditions of CV for the syntheses of different PAni/PW hybrid samples.

sample	Series	Voltage range	scaning rate (mV/s)	number cycles	observations
PW1A	PW1	0.7V→ -0.35V	5mV/s	5	Dark blue iridescent thin layer
PW1C	PW1	0.9V→ -0.35V	50mV/s 20mV/s	3 3	Almost no deposit. Thin dark blue layer
PW1D	PW1	0.9V→ -0.35V	10mV/s	40	Dark blue-greenish thin layer
PW1E	PW1	0.9V→ -0.35V	10mV/s	60	Dark blue-greenish thin layer and light yellow particles.
PW1F	PW1	0.9V→ -0.35V	10mV/s	80	Dark blue-greenish thin layer and light yellow particles.
PW1G	PW1	0.9V→ -0.35V	10mV/s	100	Dark blue-greenish thin layer and light yellow particles.
PW2A	PW2	0.9V→ -0.35V	10mV/s	10	Dark blue iridescent thin layer
PW2B	PW2	0.9V→ -0.35V	3mV/s 10mV/s	3 5	Iridescent (yellow-green-violet-blue) thin layer.

We carried out different experiments with different scan rates and number of cycles to try to deposit homogeneously the greater amount of hybrid. The scanning rate that worked better in this sense was 10 mV/s with 40 cycles (PW1D). In figure 8.6 we show the CV of PAni/PW12 of sample PW1E, which is representative of the rest of the samples. We can compare the first and sixtieth cycle.

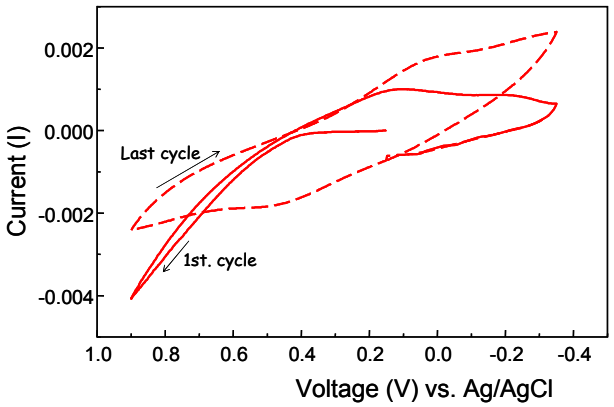

Figure 8.6.- Cyclic Voltamogram carried out to synthesize sample PW1E at a scanning rate of 10mV/s.

8.4.2. Characterization of PAni/PW12

First we carried out the electrochemical characterization of the PAni/PW12 hybrid electrodes using a three electrode cell vs. Ag/AgCl as reference electrode, in a solution of $HClO_4$ 1M at a scanning rate of 20 mV/s. In figure 8.7 we show the CV corresponding to the electrochemical characterization of some samples, where we can detect and have marked the characteristic redox waves. The couple 0.5/0.75V is assigned to polyaniline whereas the bands and shoulders around -0.22/-0.1V and -0.31 are assigned to PW12. The main features at 0.11/0.2V could actually correspond to some overlap between PAni and PW12 electroactivity. With the exception of sample PW1A, the intensity increases through cycling indicating an increase of the conductivity which could be associated to the progressive impregnation of the hybrid electrodes

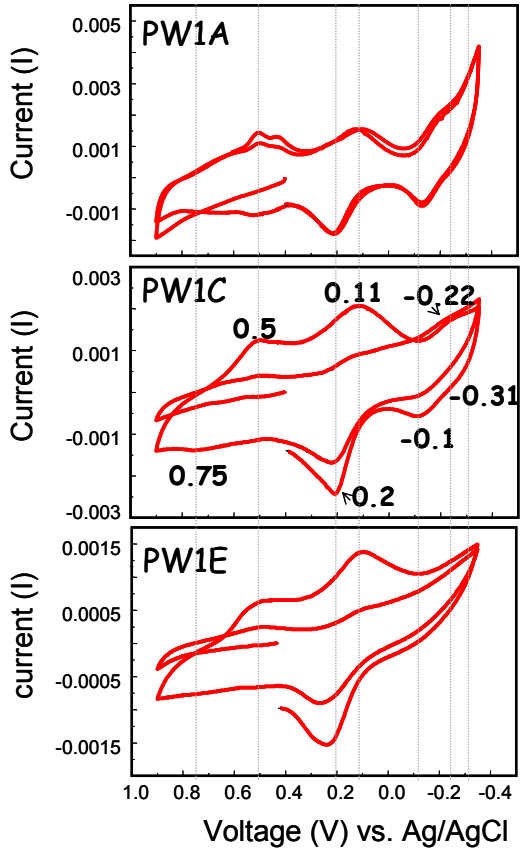

Figure 8.7.- CV of PW1A, PW1C and PW1E electrodes, carried out in a 1M $HClO_4$ solution at 20 mV/s

with electrolyte as successive redox cycles with the corresponding cyclic swelling of PAni take place.

We carried out SEM photographs as part of the characterization procedure with the correspondent microanalyses for each sample, and composition analysis (EDX W,P,C). In figure 8.8 we show the corresponding SEM photos at x318 and at x5000 magnification of PW1 series of samples, and in figure 8.9 the samples of series PW2.

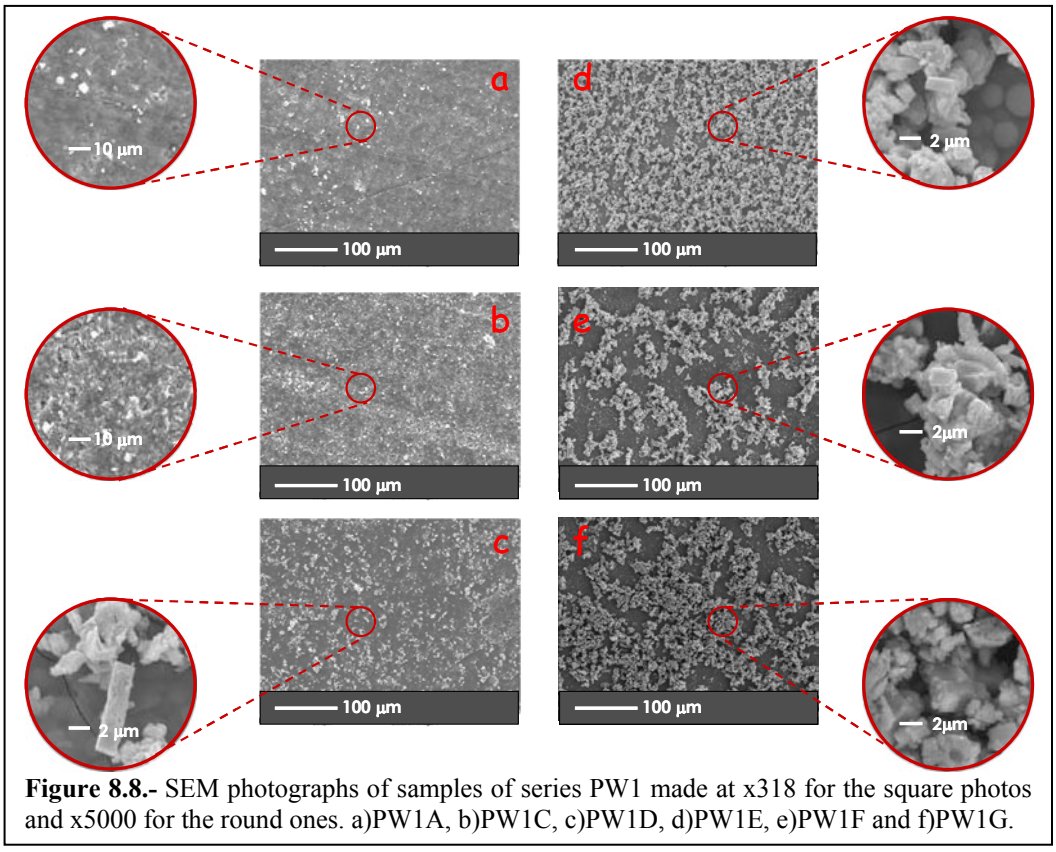

Figure 8.8.- SEM photographs of samples of series PW1 made at x318 for the square photos and x5000 for the round ones. a)PW1A, b)PW1C, c)PW1D, d)PW1E, e)PW1F and f)PW1G.

Looking at the photos of series PW1 of samples PW1A, PW1C and PW1D (fig. 8.8a, b, c), we can observe that by using a 10mV/s rate (PW1D), the particles deposited are bigger. Comparing samples PW1D, PW1E, PW1F, PW1G (fig. 8.8c, d, e, f) synthesized with the same scanning rate (10mV/s) and by varying the number of cycles, we can observe that the optimum number of cycles in order to have the most homogeneous layer was up to 60 (PW1E). When we increase the number of cycles to 80 (PW1F) or 100 (PW1G), the layer gets more heterogeneous. We carried out EDX analyses (W,P,C) of samples PW1D and PW1G, resulting in general in a homogeneous distribution of the analysed elements, observing nevertheless slight

local concentrations of W and P in prismatic crystals (thus from PW12) and C from the polymer in the rounder particles for sample PW1D.

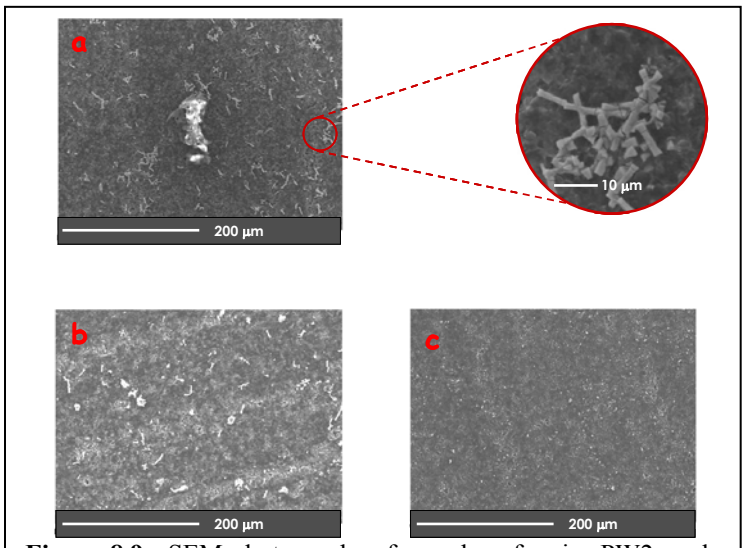

Figure 8.9.- SEM photographs of samples of series PW2 made at x300 for the square photos and x5000 for the round ones. a)PW2A, b)PW2B, c)rigid graphite electrode.

Looking at samples from series PW2 on figure 8.9, both samples have small particles as in some samples of series 1 (PW1A and PW1C). There is also a photo of the rigid graphite electrode (fig. 8.9c) which confirms that only small particles were electrodeposited on samples PW2A and PW2B electrodes. Only EDX microanalyses (not mapping) were carried out on these series of samples (series 2) and they showed the presence of P and W, confirming the presence of the PW12 polyanion.

8.4.3. PAni/PW12 Electrochemical Supercapacitors

We assembled the solid state electrochemical supercapacitor devices using two PAni/PW12 electrodes of the same sample separated by Nafion impregnated with 1M H_2SO_4, in a voltage range of 0-1V. In figure 8.10 we show the capacitance obtained at different current densities, for samples of

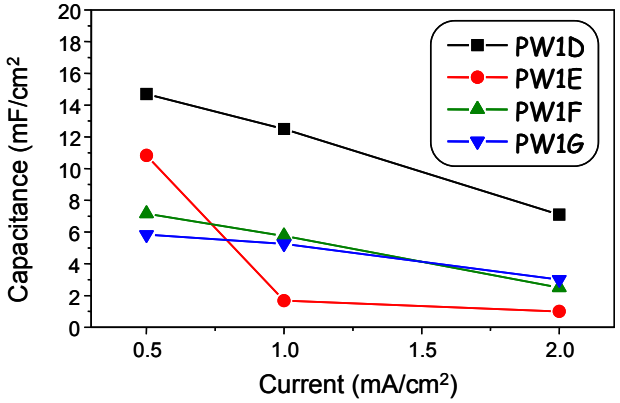

Figure 8.10. Electrochemical capacitors response for PAni/PW12 hybrid samples with different current densities.

series PW1 synthesized with a 10 mV/s rate and where the only difference between them is the number of cycles applied in the CV (PW1D with 40 cycles, PW1E with 60, PW1G with 80, and PW1F with 100cycles). The sample PW1D (40 cycles) has the highest capacitance values for all current densities applied, and the same as all other samples when using I=10 mA/cm^2.

8.5. PAni/PMo12 HYBRIDS

8.5.1. Synthesis of PAni/PMo12 hybrids

We carried out the electrochemical synthesis of PAni/PMo12 hybrid using a suspension made by thoroughly mixing 5g of phosphomolibdic acid with 1 ml of aniline in a mortar until a powdery solid was obtained, and then adding 100 ml of water in a beaker. The conditions used for each experiment are shown in table VIII.III, where we used the same voltage range -0.1→0.9V vs. Ag/AgCl.

Table VIII.III.- Electrochemical conditions of CV for the syntheses of different PAni/PMo12 hybrids

Sample	Counter electrode	scaning rate (mV/s)	Number of cycles
PMoA	Pt wire fold in a zig zag form	0.5 mV/s	5
		2.5mV/s	2
PMoB	Pt plate of same dimensions	0.5 mV/s	5
	as the working electrode	1.5 mV/s	2

Earlier work by our group in the electrochemical synthesis of this hybrid[1] showed that when using higher scan rates during the electrochemical synthesis the deposition of PMo12 polyanion competes with and hinders the formation of PAni. As the scan rate used is increased, the polyanion is first electrodeposited onto the surface of the working electrode, insulating the electrode resulting in an electrode with no polyaniline formation. In this sense we used first a slower rate to deposit PAni and then a higher velocity to increase the amount of PMo12 clusters onto the surface of the electrode, increasing also the porosity, which plays an important role in electrochemical supercapacitors as described in the introduction of chapter 1.

In figure 8.11 we show the CV of PAni/PMo12 hybrid which is representative of both samples. We compare the last cycles of each rate used for the electrodeposition, which allow us to detect an increase of the intensity in the last procedure (1.5 mV/s) compared to the first one (0.5 mV/s). This behaviour is a positive indication that conductive polyaniline is being grown on the surface of the graphite working electrode.

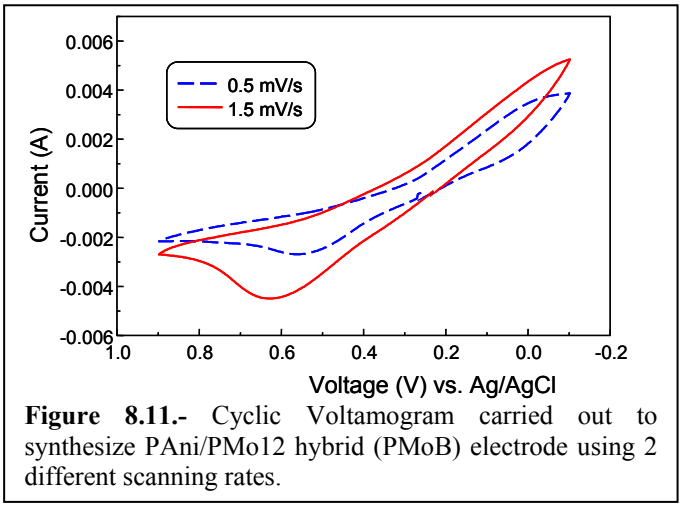

Figure 8.11.- Cyclic Voltamogram carried out to synthesize PAni/PMo12 hybrid (PMoB) electrode using 2 different scanning rates.

8.5.2. Characterization of PAni/PMo12

First we carried out the electrochemical characterization of the PAni/PMo12 hybrid electrode using the same set-up as for the other two types of hybrids, in a 1M solution of $HClO_4$ at a scanning rate of 20 mV/s. In figure 8.12 we show the CV correspondent to the electrochemical characterization, where we can detect the redox peaks of each procedure. We can detect two very well defined redox waves at 0.25/0.42V and at 0.10/0.32V characteristic of the PMo12 polyanion. Two additional redox waves corresponding to PAni can be detected as shoulders at 0.46/0.65V and -0.08/0.1V.

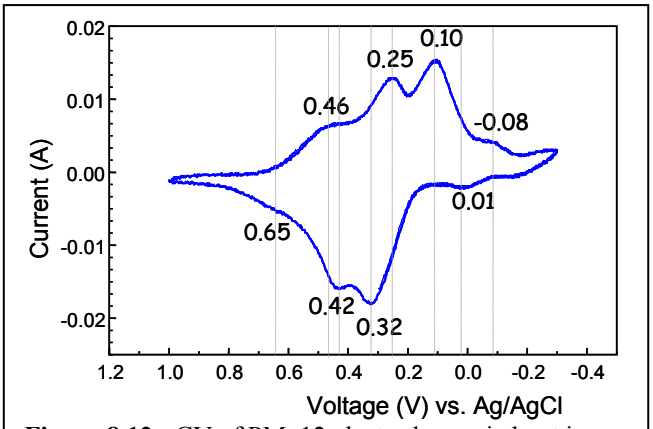

Figure 8.12.- CV of PMo12 electrode, carried out in a 1M $HClO_4$ solution at 20 mV/s.

We carried out SEM photographs, with EDX microanalyses included for each sample (no mapping). In figure 8.13 we show the corresponding SEM photos at x318 and at x5000 magnification, where we can observe a more homogeneous deposit over the graphite electrode in sample PMoB (fig. 8.13b). Microanalyses confirmed the

presence of P and Mo in both samples. Samples PMoA and PMoB were made by using very similar conditions, the difference was the rate of the second procedure and the counter electrode used. In addition, in the case of sample PMoA the solid hybrid fell off the graphite substrate very easily.

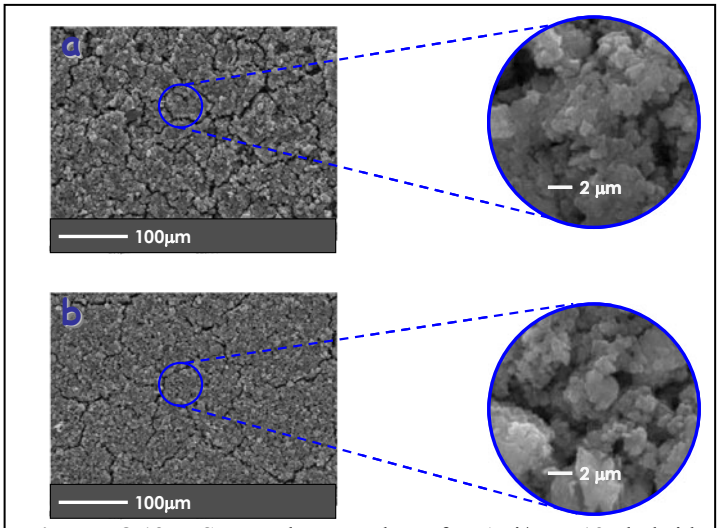

Figure 8.13.- SEM photographs of PAni/PMo12 hybrid electrode samples made at x318 for the square photos and x5000 for the circles. a)PMoA, and b)PMoB.

We carried out FTIR analysis of sample PMoB to confirm the presence of PAni and the phosphomolybdate anion in the hybrid electrode. The analysis was carried out by carefully scraping off the material from the surface of the graphite working electrode and diluting it in KBr pellets. In figure 8.14 we show the FTIR spectrum of this hybrid, where we can detect the characteristic bands of PAni, and bands assigned to the phosphomolybdate anion. The peak at 1577 cm^{-1} is assigned to a deformation mode of benzene rings, the one at 1486 cm^{-1} to a deformation of benzene or quinoide rings, the ones at 1248 cm^{-1} and 1147 cm^{-1} to a C=N stretching of a secondary amine, at 1060 cm^{-1} to a P-O bond, at 955 cm^{-1} to a Mo=O

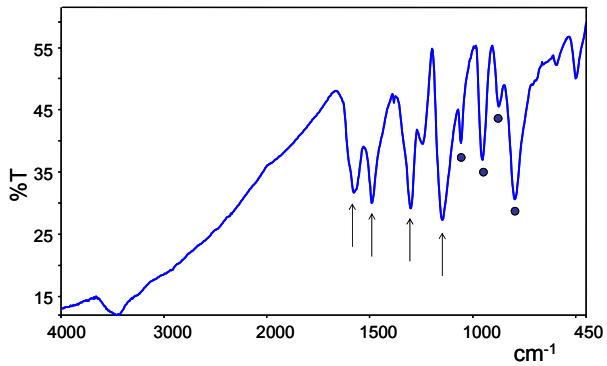

Figure 8.14.- FTIR spectrum of PAni/PMo12 hybrid sample (PMo12), where the arrows indicate the stretching modes of polyaniline and the circles the ones belonging to phosphomolibdic anion.

terminal bond, at 876 cm^{-1} to a vertex Mo-O bond, and finally at 800 cm^{-1} to an edge Mo-O bond.

We carried out elemental analysis (%C, %H, %N) and ICP (%Mo) of PMoB hybrid sample synthesized on a Pt working electrode that was scrapped off (see section 8.5.3), in order to obtain the stoichiometric formula for this hybrid. For the analyses we used the material synthesized on Pt to avoid errors in the %C. In table VIII.IV we show the experimental data and calculated composition for the proposed formula.

Table VIII.IV.- Summarized data obtained from chemical analyses, and calculated values obtained for the proposed formula weight.

	%C	%N	%H	%Mo	formula
Exp.	23.13	4.30	1.74	15.1	$C_6H_5N(PMo_{12}O_{40})_{0.042}.8.5H_2O$
Calc.	22.46	4.36	6.91	15.09	FW=320.7 g/mol

We can see a clear disagreement between experimental and calculated H % for this formula. Indeed 8.5 water molecules per formula are too many (exp. H/N ratio indicates some 1.5 H_2O molecules). The most plausible explanation is the presence of some undetected impurity (not containing C, N, H, nor Mo), possibly metallic platinum scrapped off the electrode. Aside from this impurity, all the experimental molar ratios between C, H, Mo and N confirm indeed the formula $C_6H_5N(PMo_{12}O_{40})_{0.042}.1.5H_2O$

8.5.3. PAni/PMo12 Electrochemical Supercapacitors

We assembled the solid state electrochemical supercapacitor device, using two PAni/PMo12 electrodes (PMoB) separated by "Nafion" impregnated in 1M H_2SO_4 as electrolyte. We have carried out all the following analyses on supercapacitor cells only for sample PMoB. In figure 8.15 (upper graph) we show how the values of capacitance (normalized per effective electrode area) of our symmetrical cell vary as a function of current densities applied, in cycling between 0V and 1V. Each set of points for each current density is an average of the capacitance of four successive charge-discharge cycles. At it should be expected, the discharge capacitance values are higher at low current densities. However, it should be noted that the decrease in capacitance with increasing current density is relatively small, amounting to a 35% decrease (from 140 to 90 mF/cm^2) upon one order of magnitude decrease in current density (from 1 to 10mA/cm^2). At I=0.5 mA/cm^2 a mismatch of the charge and discharge values can be observed.

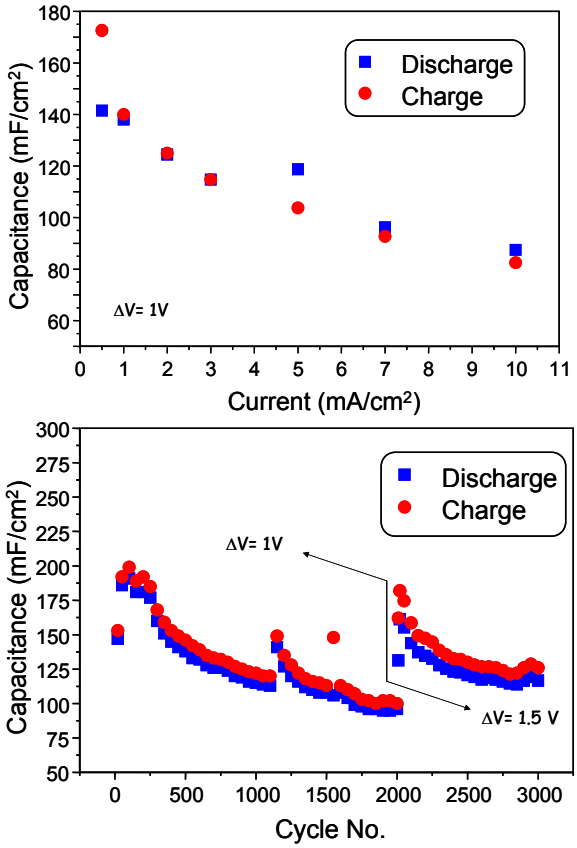

Figure 8.15.- Electrochemical Supercapacitor studies of PAni/PMo12 (sample PMoB). Capacitances are normalized per effective electrode area. Upper graph (a) shows capacitances under different current densities at ΔV=1V. Lower graph (b) shows the successive charge-discharge cycles at I=1mA/cm^2, where the first 2000 cycles are carried out with a voltage window of ΔV=1V and the following 1000 cycles using a voltage window of ΔV=1.5V

In the bottom graph of figure 8.15b we show the evolution of capacitance in successive charge-discharge cycles using a 1 mA/cm^2 current density. The first 2000 cycles were carried out between 0V and 1V, and the following 1000 cycles between 0V and 1.5V. In the first 2000 cycles, we observe that the capacitance declines from a starting value of 200 mF/cm^2 to a value of around 110 mF/cm^2. We note two instances in which the continuity of the cycling activity is accidentally disturbed and the system was able to relax (around cycles 1200 and 1600). In the following 1000 cycles, another jump of the capacitance to higher values (up to 165 mF/cm^2) was induced by a controlled change of cycling regime involving the increase of the voltage range (ΔV=1.5V). The capancitance decreases thereof down to values stabilized around 120 mF/cm^2 (30% loss in 1000 cycles), remarkably, a better stabilization and at a slightly higher capacitance than that reached after the first 1000 cycles under the 1volt regime.

Up to this point, we have discussed capacitance values normalized per effective surface area of our electrodes (mF/cm^2). However, from a technological point of view, material science studies in this field rely upon measurements in terms of Farads per gram, that is with the capacitance normalized per unit mass of active material.

In order to calculate the capacitance by active mass, we have carried out successive electrochemical syntheses of PMoB hybrid sample onto a Pt foil working electrode. After each synthesis, the material was collected by scrapping off the working electrode. The greenish solid obtained was washed with deionized water, until all blue coloration disappeared (elimination of excess phosphomolybdic acid), and was dried under vacuum for 3 days. This hybrid material presented the same FTIR spectrum as the hybrid deposited onto graphite and its formula is given in section 8.5.2. After weighing the active hybrid material we proceeded to fabricate a film following the procedure described in chapter 2 (section 2.4.3.1.).

In figure 8.16a we show the capacitance per active mass obtained for PMo2B hybrid sample at different current densities, always cycled between 0V-1V. Each set of points for each current applied was an average of the capacitance in four successive charge-discharge cycles. Again, at lower current densities the capacitance is higher and with a larger mismatch between charge and discharge, confirming that the device has better performance at higher current densities. In addition, there are two extra points at I=125 mA/cm^2 (a charge point and a discharge) belonging to an extra four cycle average, which was carried out after recollecting the data for each current density applied. These extra points were measured to confirm its reproducibility.

Figure 8.16 a also includes data for electrodes fabricated with just PMo12 (without PAni) as the active material in film electrodes prepared as above. We have included the performance of a symmetrical cell based on just the polyoxometalate for comparison purposes. The capacitance obtained for this device was smaller than for the hybrid material, confirming the synergic effect in the performance of the PAni/PMo12 hybrid electrodes.

In figure 8.16b we compare the successive charge-discharge cycles of two supercapacitor devices using new, and used electrodes (same capacitor of figure 8.16a), applying a current density of 125 mA/g. We can see how the capacitance values stabilize in both cells around close values of 50-60 F/g. However the initial behaviour of both cells is quite different. For the device assembled with used

electrodes, we observe a higher initial capacitance value of 75 F/g. On the other hand, when using new electrodes the supercapacitor performance seems to require an electrochemical activation of the electrodes through initial cycling. The starting value of the capacitance for the new electrodes was 40 F/g (lower than with the used electrodes), increasing during the first 300 cycles (electro-activation) to eventually reach the same stabilized value mentioned above.

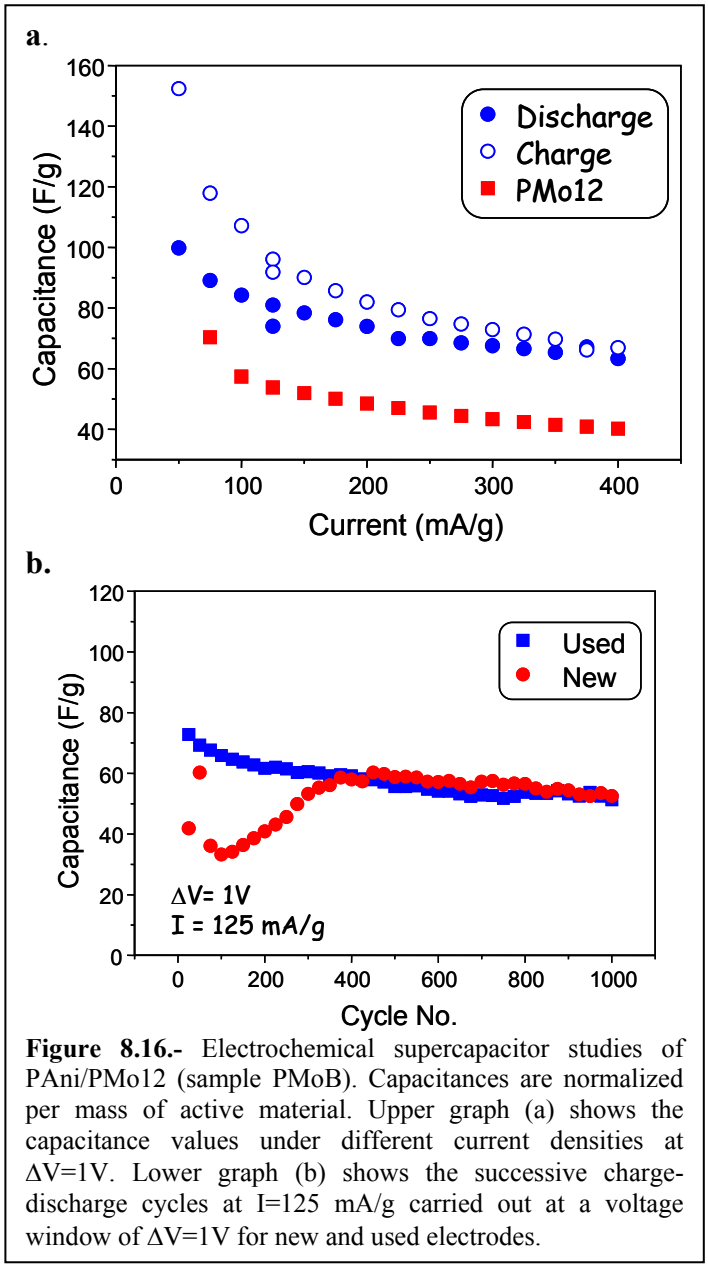

Figure 8.16.- Electrochemical supercapacitor studies of PAni/PMo12 (sample PMoB). Capacitances are normalized per mass of active material. Upper graph (a) shows the capacitance values under different current densities at ΔV=1V. Lower graph (b) shows the successive charge-discharge cycles at I=125 mA/g carried out at a voltage window of ΔV=1V for new and used electrodes.

The fact that this electro-activation process takes place only for self-standing composite films but not for the electrochemically prepared deposits indicates a kinetic

origin of the phenomenon, probably more related to the microstructural engineering of the films than to intrinsic materials properties

We carried out experiments increasing the voltage range up to 1.5V, as we had done for electrochemical deposits, but in this case during recharge we could not reach the cutting voltage of 1.5V. This behavior could be understood based on the fabrication differences of the electrodes. In table VIII.V we show the different fabrication procedures for these two types of electrodes.

Table VIII.V.- Fabrication procedures for devices assembled with active area electrodes, and active mass electrodes.

	capacitance	maximum voltage window	synthesis	electrochemical capacitor
Electroactive area electrode	mF/cm^2	1.5V	Electrochemical synthesis over rigid graphite, washed by submerging in water and air dried.	Electrodes made by cutting the graphite with the deposited material
Electroactive mass electrode	F/g	1.2V	Electrochemical synthesis over Pt plate, washed by submerging in water and air dried. Then collecting by scraping off the electrode, and washed with water and vacuum dried. NO polyanion excess	Electrodes made by adding carbon, binder (Kinar flex) and acetone to fabricate the electrode film.

We carried out more studies for the active mass electrodes in supercacitor cells by decreasing the maximum voltage to 1.2V. In figure 8.17a we show the capacitance values obtained for PMoB hybrid sample at different current densities(each set of points of each current applied was an average of the capacitance of four successive charge-discharge cycles). Surprisingly, the behaviour here was opposite to the observed until this moment. When the current density applied increases the capacitance value obtained also increases. This could be assigned to the increase of the voltage window, or to the electro-activation process, but will need more studies to confirm its attribution. However, the higher mismatch of the charge and discharge capacitance values are also observed in lower intensities.

In figure 8.17b we show the successive charge-discharge cycles using a 400 mA/g current density (less degree of mismatch in charge vs. discharge capacitance values) over the same device of figure 8.17a. We observe an increase of the capacitance value from 65 F/g (same value obtained at 400 mA/g in figure 8.17a) up to 110-120 F/g. In addition, during the first 300 cycles the capacitance value increases

gradually, indicating an electro-activation process of the electrodes at the given conditions (ΔV=1.2V, I=400mA/g). Finally, we can observe no mismatch between the charge and discharge values, indicating excellent reversibility of the overall polarization process.

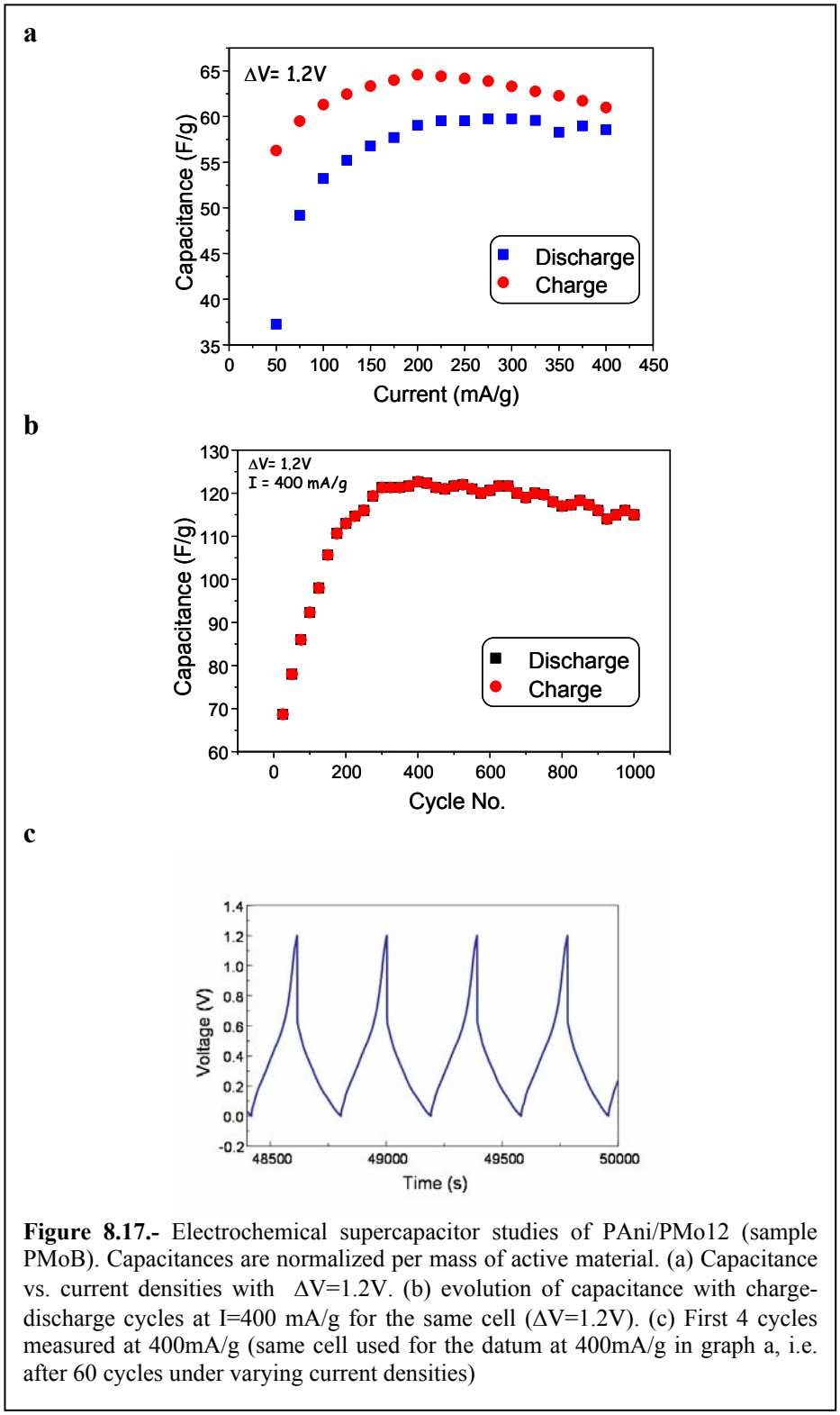

Figure 8.17.- Electrochemical supercapacitor studies of PAni/PMo12 (sample PMoB). Capacitances are normalized per mass of active material. (a) Capacitance vs. current densities with ΔV=1.2V. (b) evolution of capacitance with charge-discharge cycles at I=400 mA/g for the same cell (ΔV=1.2V). (c) First 4 cycles measured at 400mA/g (same cell used for the datum at 400mA/g in graph a, i.e. after 60 cycles under varying current densities)

In figure 8.17c we show the charge-discharge profiles measured at 400 mA/g for the same device of figure 8.17a.

We carried out more electrochemical studies, using new electrodes with different current densities cycling between 0V-1V in order to try to understand the factors that influence the electro-activation process described. In figure 8.18 we show the results of this study. First, we use a high current of I=400 mA/g for the first 2000 cycles, obtaining very low capacitance values between 3-10 F/g. Then a slower current density of I=125mA/g was applied for 300 cycles, to activate the electrode (conditions extracted from the experiments of Figure 8.16b), resulting in a rapid increase of the capacitance up to 100 F/g, marking the electro-activation process. Finally, we carried out 2000 cycles more again at a higher current density of I=400 mA/g, observing a decrease of the capacitance down to 60 F/g in the first cycle, then a continuous increase and then detecting a jump improvement in cycle 3300 (cycle 1000 of the 2000 with I=400 mA/g) from 75 F/g to 110 F/g. This value of 110 F/g did evolve slowly decreasing down to 75 F/g at the end of the experiment, after more than 4000 cycles.

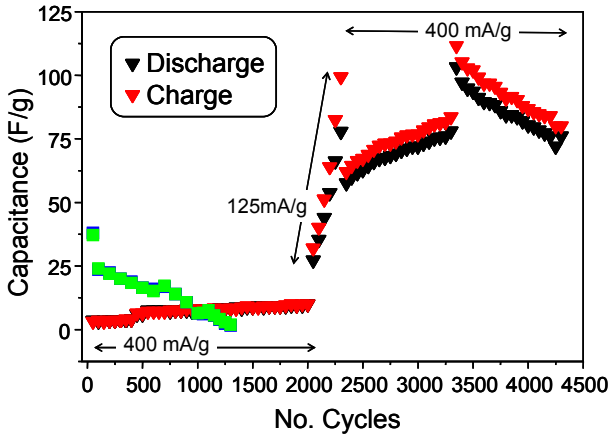

Figure 8.18.- Electrochemical studies over supercapacitors with new electrodes between a voltage range of ΔV= 0→1V. For the PAni/PMo12 hybrid, the first 2000 cycles we applied a 400 mA/g, the next 300 cycles at 125 mA/g and finally the next 2000 cycles at 400 mA/g. For comparison we show the performance of electrodes based on PMo12 (■),the first 1000 cyles we applied a 400mA/g, the next 300 cyles at 125mA/g.

Furthermore, we have included the performance of a symmetrical supercapacitor with PMo12 (polyanion in a film composite) electrodes to determine if an electro-activation process can be detected. The analysis was carried out by applying a fast charge–discharge rate (I=400 mA/g) for the first 1000 cycles, and then in the following 300 cycles the same slower current density (I=125 mA/g) to detect if an electro-activation process is detected. During the first 1000 cycles we observed a decrease of the capacitance from 38 F/g to 6.4 F/g. In the following 300 cycles the decrease of the capacitance continued to a value of 1.9F/g, thus no electro-activation process was detected.

In conclusion we have found that new PAni/PMo12 electrodic novel hybrids used to assemble an electrochemical supercapacitor has the necessity of an electro-activation process at low current densities, independently of the voltage window used. This electro-activation process in the hybrid can not be attributed to the inorganic component of the molecular hybrid material, but most probably to the swelling of the conducting organic polymer, as has been previously detected in other molecular hybrids [14]. In the electrochemical deposits this electroactivation seems to be easier (Figure 8.15b) as it could be expected for a thinner film deposit with a larger interface with the electrolyte.

Despite this electroactivation, the hybrid materials described in this chapter, and very particularly the PAni/PMo12, where the electroactivity of both components is better matched, constitute very promising novel systems for energy storage as electrochemical supercapacitors.

REFERENCES

[1] Lira-Cantú, M.; Gómez-Romero, P.; *Chem. Mater.* **1998**(10), 698.
[2] Lapkowski, M.; Bidan, G.; Fournier, M.; *Synt. Met.* **1991**(41-43), 407.
[3] Gómez-Romero, P.; Lira-Cantú, M.; *Adv. Mat.* **1997**(9), 144.
[4] Torres-Gómez, G.; Lira-Cantú, M.; Gómez-Romero, P.; *J. New Electrochem. Syst.* **1999**(2), 145.
[5] Kuleza, P.J.; Malik, M.A.; Karwowska, B.; Miecznikowski, K.; Dzwolak, W.; Wolkiewicz, A.; Gursynska, A.; Grzybowsa; in: Delnick, F:M; Ingersoll, D.; Andrieu, X.; Naoi, K.; (Eds.), *Electrochemical Capacitors, Proc.***1997**(96-25), 89. Electrochemical Society, Pennington.
[6] Li, C.; Reuss, R.H.; Chason, M.; *US Patent 5847920* **1999** (16 Nov), 4.
[7] Li, C.; Reuss, R.H.; *US Patent 5986878 A* **1999** (16 Nov), 4.
[8] Yamada, A.; Goodenough, J.B.; *J. Electrochem. Soc.* **1998**(145), 737.
[9] Geniès, E.M.; Boyle, A.; Lapkowski, M.; Tsintavis, C.; *Synth. Met.* **1990**(36), 139.
[10] Zhang, A.Q.; Cui, C.Q.; Lee, J.L.; *Synth. Met.* **1995**(72), 217.
[11] Syed, A.A.; Dinesan, M.K.; *Talanta* **1991**(38), 815.
[12] Pud, A.A.; *Synth. Met.* **1994**(66), 1.
[13] Gómez-Romero, P.; Casañ-Pastor, N.; *J. Phys. Chem.* **1996**(100), 12448.
[14] Torres-Gómez, G.; *Materials Hibrids Funcionals de Tipus Molecular. Hexacianoferrat integrat en Polímers Conductors com a Elèctrodes en Bateries Recarregables de Liti.*; Universitat Autonoma de Barcelona, Barcelona, **2001**,pp 166.

Chapter 9

Conclusions

CONCLUSIONS

V_2O_5 and V_2O_5 hybrid materials

- We have prepared and optimized V_2O_5 xerogels for their use as cathodes in reversible Li cells as well as reference materials for comparison with the corresponding hybrids. We carried out an aging study of V_2O_5 hydrogels through time, during a one year period, detecting a tendency to increase the amount of V(V) through time. We carried out two types of aging procedure for the V_2O_5 hydrogel: a static method used for the aging study of the gel through time, and a dynamic (stirring) used to synthesize the xerogels. We have proved that the dynamic aging gives way to a higher V(V) concentration for the same period of time.

- Xerogels were prepared from V_2O_5 gel dynamically aged submitting them to diverse thermal treatments in different atmospheres (Ar, O_2, Air), and performed their electrochemical characterization in Li rechargeable cells. We observed that as the temperature of treatment increases, the xerogels presented a higher initial specific charge, but a poorer cyclability due to increased crystallinity. Our cyclability studies showed that crystalline V_2O_5 presents worse reversibility than the amorphous xerogels. We have also shown that thermal treatment of these materials has a double and opposite effect, the higher the temperature, the lower the water contents (and better initial specific charge) but higher presence of crystralline phase (and worse cyclability). We have therefore determined the optimal treatment temperature for each atmosphere

- We have studied and optimized the synthesis of PAni/V_2O_5 hybrids concerning the effect of synthesis conditions (especially stirring procedures), on the microstructure, porosity and by consequence on the electrochemical performance as insertion electrodes for lithium cells. In this sense, we have prepared materials with higher porosity leading to higher values of specific charge for a given cycling rate (280 Ah/Kg at a C/6 rate) compared to earlier results for this PAni/V_2O_5 hybrid system,

- From a structural point of view, the work carried out in PAni/V_2O_5 hybrid system has also provided new data on the PAni insertion into V_2O_5 gels. The materials

obtained contain higher amounts of polyaniline per V_2O_5 unit (1:1), compared to previous hybrids obtained using the same amount of aniline in the reaction mixture and resulted in a moderate interlayer spacing expansion of the gel (corresponding to a polymer monolayer insertion). In addition the new synthetic procedures avoided the need of thermal treatment of the materials under O_2 in order to optimize their electrochemical properties.

- We have studied successive charge-discharge cycles for these capacity-enhanced PAni/V_2O_5 materials. We observed that in every sample analyzed during 100 cycles, there is a continuous loss of charge that gets eventually stabilized at ca. 50 Ah/Kg, a value which turns out to be common for all samples analyzed regardless of their synthesis procedure. The charge fading is associated with a qualitative change from fradaic, potential-specific redox processes characteristic of batteries to non-faradaic, potential-independent energy storage cycles characteristic of capacitors. Some of our experiments seem to indicate that this charge fading is not associated to the decomposition of our hybrid material, but possibly to its passivation or to other cell factors.

- Comparing the electrochemical properties of PAni/V_2O_5 hybrids and the correspondent xerogels, we can conclude that the hybrids present better specific charges but in both cases the cyclability needs to be improved.

Novel hybrid materials

- We have carried out attempts to synthesized PAni/MnO_2 hybrid materials. The synthesis approach we used led to the formation of p-doped polyaniline with a low concentration of HSO_4^- anions, instead of the formation of the desired PAni/MnO_2 hybrid.

- On the other hand, we have carried out successfully the syntheses of Polypyrrole/MnO_2 hybrids. The only precedents for this type of material were based on previously formed MnO_2. In our case we have developed an “in situ” simultaneous synthesis, where the oxidative polymerization of pyrrole takes place at the same time as the MnO_4^- anion is reduced to MnO_2 . We prepared hybrids with

varying PPy:MnO_2 ratios and found out that those with higher MnO_2 contents led to a detrimental overoxidation of pyrrole.

- We have tested PPy/MnO_2 hybrid samples as cathodes in lithium rechargeable cells, obtaining moderate specific charge values (40-140 Ah/Kg), where their performance depends on the MnO_2 amount. As the content of MnO_2 increases in the hybrid composition we obtained higher initial specific charge values (120-140 Ah/Kg) but a worse cyclability. In contrast the hybrids with less content of MnO_2 resulted in lower specific charge values but with better cyclability.

- We have carried out the syntheses of PPy/HCF/V_2O_5 and PAni/HCF/V_2O_5 triple hybrids, confirming by FTIR and chemical analyses the presence of the three components in the hybrids. On the other hand, XRD patterns present a shoulder at 2θ=4-5^o in some samples which suggest a large expansion between the layers of V_2O_5 (of an otherwise very poorly crystalline material). All these analyses indicate the formation of a new type of hybrid material in which hexacyanoferrate dopes the conducting polymer which is in turn inserted into V_2O_5. Further work with other characterization techniques will be needed for confirmation of these results.

- Concerning the electrochemical performance of novel PPy/HCF/V_2O_5 triple hybrid materials in lithium rechargeable cells, we obtained high initial specific charge values of 160 Ah/Kg, giving a greater value than for PPy/HCF system (69Ah/Kg), and PPy/V_2O_5 system (120Ah/Kg). However; its cyclability was poor. This might have more to do with the choice of voltage limit values during recharge, since in all samples synthesized the voltage could not reach the 3.8V on recharge or to the effect of C=O groups formed by overoxidation of polypyrrole.

- We have explored the synthesis of new hybrid materials based on the insertion of PAni and/or PPy between the layers of vanadyl phosphate. We obtained hybrid materials containing molecular or colloidal vanadium species soluble in organic solvents, in addition to the expected $VOPO_4$ plus conducting polymers. After purification we were able to isolate a material of formula $PPy(VOPO_4)_{0.13}\cdot 1.1H_2O$.

- These complex nanocomposite hybrid materials based on $VOPO_4$ and COPs were successfully tested for the first time in lithium rechargeable cells. The electrochemical properties of PPy/$VOPO_4$ hybrids revealed an initial irreversible capacity that was reduced through the successive optimizations. The performance of $PPy(VOPO_4)_{0.13}\cdot 1.1H_2O$ in Li rechargeable cells resulted in a stabilized specific charge values of 90-100 Ah/Kg through 35 cycles (current density of I=20 mA/g), with good intercalation kinetics.

  The electrochemical behavior of PAni/$VOPO_4$ in lithium cells resulted in initial specific charge values of 118 Ah/Kg (I=10 mA/g) that got stabilized at 100-110 Ah/Kg and maintained for 20 cycles. Under higher current densities (20 mA/g), the PAni/$VOPO_4$ hybrid responded even better, a behaviour which indicates the good intercalation kinetics of this system.

Molecular hybrid materials

- We have pursued the synthesis and further study of molecular hybrids based on polyaniline and polyoxometalates for their possible application in energy-storage devices other than Li batteries. In particular, we have targeted their use and optimization as novel hybrid electrodes in electrochemical supercapacitors. Thus, we have successfully prepared by electrochemical methods deposits of the hybrid PAni/PMo12 on graphite and have used these materials to set up symmetrical cells with H_2SO_4-impregnated Nafion as electrolyte.

- These cells can be repeatedly cycled for thousands of cycles (at least 4000) with only a small loss of capacity. Values of 120 F/g can be reached. These results constitute very positive preliminary performance and open the door for a possible improvement and application of this type of hybrid materials in electrochemical supercapacitors cells.

- We have detected a characteristic behavior concerning the activity of these molecular hybrids, which need an electro-activation process in order to reach their optimal performance. This activation is due to kinetic aspects probably related with

the characteristic swelling behavior of conducting polymers, resulting in a progressive impregnation with electrolyte during the first cycles.

- We have also prepared electrodes with PAni/SiW12 and PAni/PW12 as active materials, although the cells based on those electrodes led to poorer preliminary results than those based on PAni/PMo12 both concerning capacities (1-14 mF/cm^2) and number of cycles.